T H E U N I V E R S I T Y O F M I C H I G A N

COLLEGE OF ENGINEERING
Department of Mechanical Engineering

LUNAR MODULE CASK SUPPORT STRUCTURE: A CASE STUDY AT BENDIX AEROSPACE, ANN ARBOR, MICHIGAN

James Benes
Ralph Dalessandro
John Kemme

Paul F. Youngdahl
Faculty Advisor

ORA Project 31230

administered through:

OFFICE OF RESEARCH ADMINISTRATION ANN ARBOR

December 1970

UM/0298

PREFACE

There are several ways to approach a design course. The student can choose to design some mechanical system of his own choice or an assigned project. In this design project, the student actually takes his engineering background, studies the design problem, and formulates a final solution to that problem, making his own decisions along the way.

Another approach is to study the development of a design project in industry. In this case, the student must follow the steps professional engineers take to complete their design. He is able to learn the technical aspects of the design as well as the decision-making processes of a corporation. The problem may be more complicated and involved, as time-consuming research and development have been carried out. This second approach is presented here in the form of a case study. The authors present a design problem faced by the Bendix Aerospace Systems Division of the Bendix Corporation at Ann Arbor, Michigan, in connection with the Apollo Space Program.

We would like to acknowledge the complete cooperation of the staff at Bendix Aerospace in providing the necessary information and personnel for our study. Particular thanks are due to William Durrant, who volunteered his time for our interviews, providing us with most of the technical information for the study, and to Professor Paul F. Youngdahl for his guidance and assistance throughout the project.

TABLE OF CONTENTS

TABLE OF CONTENTS (Concluded)

LIST OF ILLUSTRATIONS

LIST OF ILLUSTRATIONS (Continued)

LIST OF ILLUSTRATIONS (Continued)

LIST OF ILLUSTRATIONS (Concluded)

LIST OF ABBREVIATIONS

ALSEP - Apollo Lunar Surface Experiments Package

LM - Lunar Module

SLA - Spacecraft LM Adaptor

GLFC - Graphite LM Fuel Cask

GAEC - Grumman Aircraft Engineering Corporation

NASA-MSC - National Aeronautics and Space Administration Manned Spacecraft Center

AEC - Atomic Energy Commission

CG - Center of Gravity

FCA - Fuel Capsule Assembly

ACA - ALSEP Cask Assembly

GE - General Electric

T/C - Thermocouples

EFCS - Electric Fuel Capsule Simulator

GHT - Ground Handling Tool

FHT - Flight Handling Tool

BxA - Bendix Aerospace

SIT - Spontaneous Ignition Temperature

IU - Instrumentation Unit

MMH - Monomethyl Hydrazine

GN_2 - Gaseous Nitrogen

RTG - Radioisotope Thermoelectric Generator

1. INTRODUCTION

1.1 ALSEP PACKAGE

The Aerospace Systems Division of The Bendix Corporation (BxA), Ann Arbor, Michigan, was awarded a contract by the National Aeronautics and Space Administration (NASA) to design an experiment package for the Apollo 12 moon flight. This package included a passive and active seismic experiment, a super thermal ion detector, a magnetometer, a heat flow experiment, a dust detector, a gauge to measure the electronic particles of the solar wind, and a machine to measure the ionosphere encircling the moon near the ground. To transmit the data from the experiments to the earth and provide power for the experiments, a central station was used. Power for the central station was supplied by a radioisotope thermoelectric generator (RTG). The fuel capsule for the RTG was radioactive and had a temperature of 1400° F. NASA felt that under these conditions, it was necessary to place the element in a protective container, somewhere on the outside of the Lunar Module (LM).

Although General Electric (GE) developed the radioactive fuel element and was responsible for designing the containment cask, the task of designing the support structure to attach the cask to the LM was awarded to BxA in the early part of 1966, as an extension of the total Apollo Lunar Surface Experiments Package (ALSEP) program. In addition, BxA was responsible for the removal of the fuel element from its container and deployment in the RTG. This case study deals with the overall design problem faced by BxA of attaching the cask to the outside of the LM.

1.2 DESIGN CRITERIA

Of primary importance to NASA was the safe reentry of the radioactive fuel element through the earth's atmosphere in case of an aborted mission. Should that possibility occur, the containment cask would have to withstand high reentry temperatures. NASA felt that the cask would have a better chance of doing this if it separated from the LM during reentry. GE first considered a berylium cask, but it was felt berylium would melt away completely at the high reentry temperature. GE then decided to use graphite with its higher melting temperature for the cask. This meant that BxA had to design some means of holding the graphite cask so as not to crush it, and yet allow enough surface area exposed for adequate cooling both on the launching pad and in space. On the launching pad, the cask surface temperature could not exceed the self-ignition temperature of the rocket fuel; while in space, the cask could not leak more than 100 Btu/hr into the LM to keep from damaging any of its components.

The cask support structure had to withstand the loadings and vibrations during launch and while landing on the moon. Once on the moon, the support structure had to provide safe and easy access to the fuel element, to allow the astronaut to remove it and place it in the RTG. With only radiative cooling the support structure temperature on the moon would be higher. This meant that BxA had to consider the increased thermal expansion of the support structure and insure adequate clamping of the containment cask.

1.3 SECTION ASSIGNMENTS

After NASA awarded the support structure contract to BxA, the project was sent to the Department of Mechanical Engineering. Here, it was divided into sections and assigned to Project Engineers. William H. Durrant was assigned to the mechanical design section, and most of our interviewing and research efforts were with him. He received his primary and secondary education in Great Britain. After completing his education, he became an aircraft design draughtsman, and then moved into guided weapon systems, followed by satellite design. In 1966, Mr. Durrant came to the United States and began working for BxA. Other sections with their respective Project Engineer were:

(1) stress analysis (thermal and static), Dr. D. Dewhirst;

(2) dynamic analysis, Dr. H. P. Lee; and

(3) thermal analysis, J. McNaughton.

In the remainder of the paper, we will present a study of the design developments and problems associated with each of the above sections. A chronological development of the total project is presented after the main body of the paper as a summary.

Appendix I contains several photographs showing the cask and support structure, both before the lunar mission and during the deployment of the ALSEP package on the Apollo 12 moon landing.

2. MECHANICAL DESIGN

2.1 CASK ROTATION

Cask Position

From the beginning there were certain conditions governing the positioning of the fuel cask with which Bendix had to comply. First, because of the high temperature of the cask itself and its need for adequate heat transfer and its ready disposability in case of emergency, the cask had to be mounted on the outside of the LM vehicle. Secondly, there was a limitation of the cask's position due to the presence of a cone-shaped physical shroud which covered and protected the LM during launch and the exit through the atmosphere. This shroud, or SLA (Spacecraft LM Adaptor), so closely surrounded the LM that the longitudinal axis of the cask was forced to lie vertically and parallel to the LM's longitudinal surface. In this vertical position the cask was not readily accessible to a man standing on the lunar surface. Consequently, a releasing and rotating system had to be devised so that the radioactive capsule could be removed from the cask to furnish the power for the ALSEP experiments.

The removal of the fuel capsule from the graphite cask was the most dangerous task facing the astronaut. Because the astronauts' suits were designed to withstant a maximum temperature of 280°F, inadvertent contact with either the 800°F cask or the 1400°F capsule would probably result in death. To make the capsule's removal as safe as possible, NASA and the human-factors engineers suggested that the cask be rotated from its near-

vertical attitude at or above the astronauts' eye-level both downward and outward away from the LM. In its final position the cask-top would be toward the astronaut so that he could sight directly down the cask axis. The cask base would be supported by the lower trunnion of the original support structure around which it had been rotated.

The rotation mechanism had to take three factors into account. First, it had been anticipated that the longitudinal LM-axis could vary from the true-vertical a maximum of ±15° due to the uneven lunar terrain. This meant that the rotation mechanism had to be variable. Secondary, the rotation mechanism had to provide a means of locking the cask in its rotated position for stability during capsule-removal. Finally, the rotation had to be both mentally and physically simple for the astronaut.

Original Rotation Mechanism

A motor, or electrical actuator, was initially eliminated for several reasons. (1) The motor would have to withstand the high temperature of the cask and its structure. (2) It would have to run in a vacuum. However, since no "space-application-approved" motor was available from any manufacturer at that time, it would have been necessary for Bendix to entirely design and test a new product. Time and cost factors would not allow this, so they decided to use a simple mechanical mechanism.

In March, 1967, Bendix devised a simple rotating mechanism, a castellated ring or gear deployment mechanism, as shown in Figure 2.1. From a position beside the cask, the astronaut was to fit the open end of a

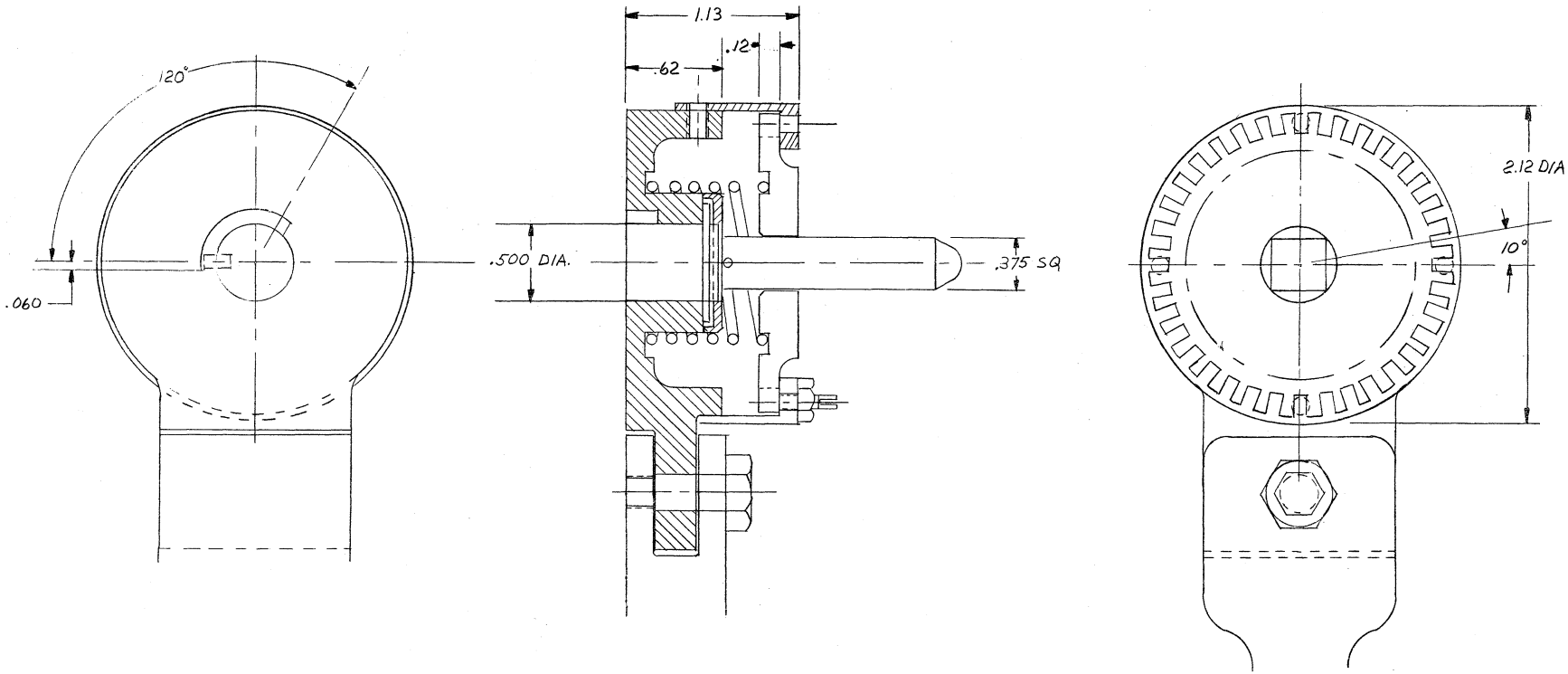

Figure 2.1. Original rotating mechanism.

T-handled tool (similar to a tire wrench) onto the square-ended extension of the lower trunnion shaft. Pressing the tool toward the hub disengaged the spring-locked gear from its four mating pins. The shaft was then free to rotate to the desired position. As the tool was withdrawn slowly, the astronaut felt for a pin-position between the gear teeth. The 36-tooth gear resulted in a limited number of usable positions at 10° increments. There was a built-in positive stop by means of a key at 120° to prevent accidental excess rotation. To slow the rotation and to facilitate correctional counter-rotations a counter-balance spring mechansim on the opposite lower trunnion was deployed (see Figure 2.1A).

By the end of March, Grumman (GAEC) notified Bendix that the cask would be mounted on the other side of the LM vehicle between the ALSEP compartment doors and the lunar landing foot. Now the mechanism could only be used by extending the T-tool through a hold in the open ALSEP compartment door. This limited the astronaut's clear view of the cask position.

Another complaint about this mechanism was voiced by NASA and the astronauts themselves. They could simulate and test the mechanism but not the astronauts' mental attitude. Previous experience with a space-walk showed that excitement and oxygen content might combine to produce erratic behavior in an astronaut. Thus, NASA did not know what to expect from the lunar astronauts. They feared the astronauts would become frustrated with the delicate positioning of the gear and requested the development of a mechanism with simple single-step sequences, fewer decisions, and a greater variability in positions. This mechanism would have to be operated from in front of the cask.

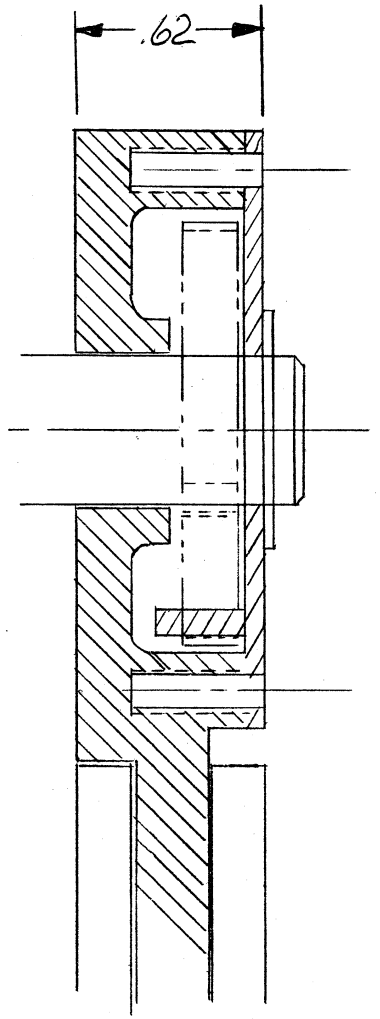

COVER REMOVED
FOR CLARITY

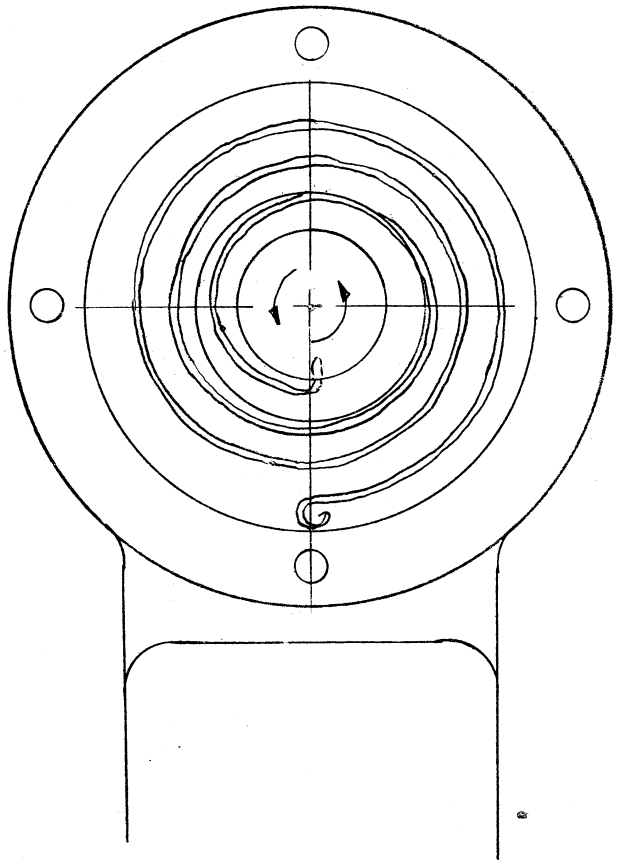

Figure 2.1A. Counterbalance spring mechanism.

Worm Gear Design

In the beginning of June, 1967, Bendix produced sketches of a worm gear mechanism which could be operated from in front of the cask and at a distance of several feet (as shown in Figure 2.2). Basically, the astronaut would pull a chain that would rotate a sprocket on a vertically oriented worm shaft engaged by a worm wheel. Originally this worm wheel's shaft formed the right-hand end of the lower trunnion. This mechanism thus provided a greater variety of positions than the castellated ring had. The high degree of friction and low efficiency of the worm gear provided a self-locking mechanism and prevented slipping caused by torque on the worm wheel.

It was calculated by human-factors engineers that due to the high center of gravity of the astronauts with their back-pack life support systems, the maximum force they could safely exert would be 20 lb, or 50 in./lb torque. This factor necessitated a gear box size that would accommodate both a gear and sprocket large enough to afford a mechanical advantage such that the astronaut could easily raise and lower the cask. On the other hand, the gear-box assembly had to be small and light. It had to be small enough to fit between the cask support structure and the ALSEP package door, and it had to be light enough to fit into the over-all weight limitations.

They began with a "ball-park" figure of a 1/4 in worm shaft for which test gears of standard materials would be readily available. With these they would construct dummy models to determine final gear size and a nominal pitch. Through routine calculations they could then determine whether resulting

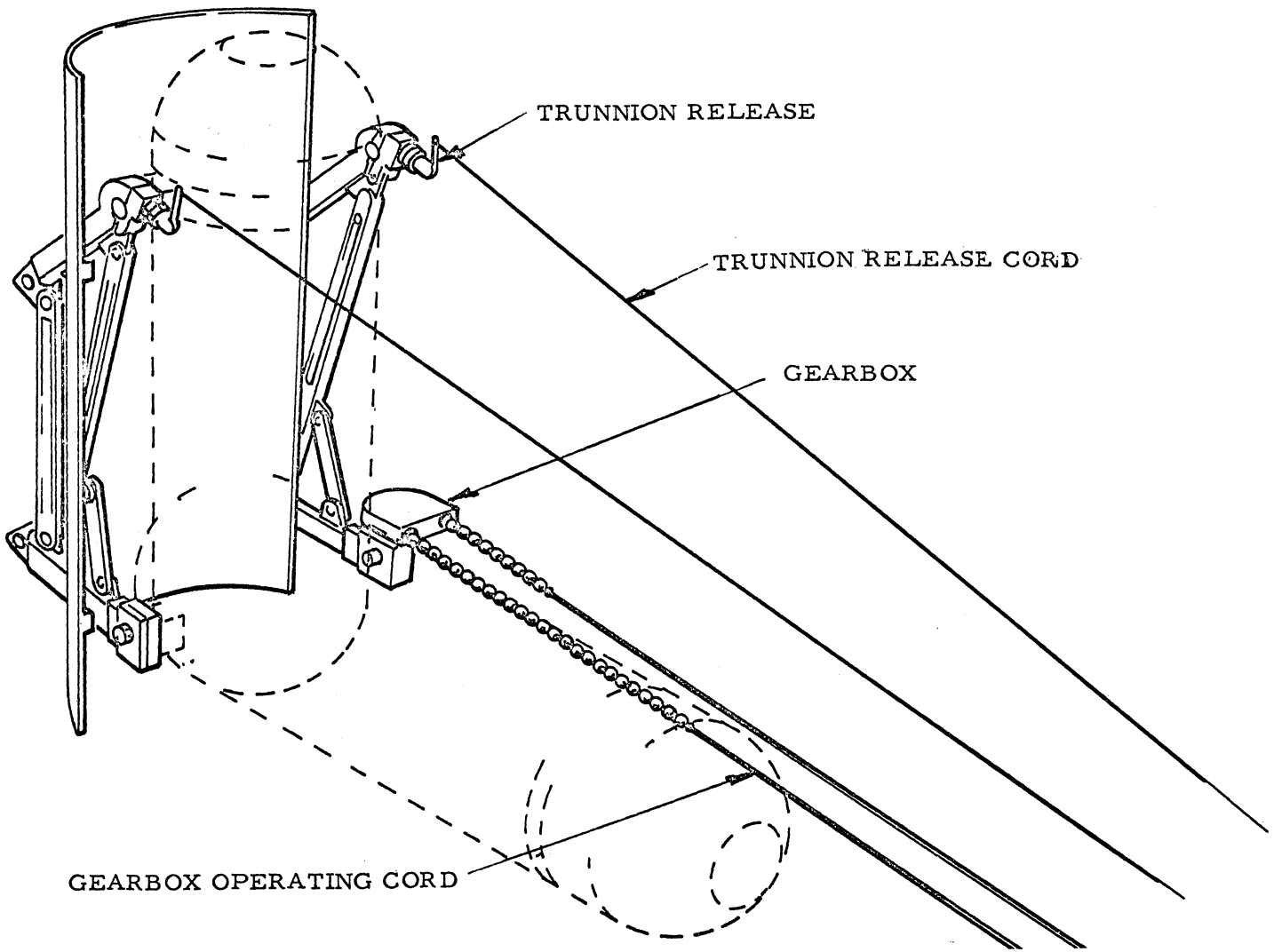

Figure 2.2. Cask rotation details.

tooth loads were acceptable. Example preliminary calculations from Bendix are shown in Exhibit 2.1.

A commonly-used safety factor in final calculations would be 1-1/4. However, in this case, the astronauts may have been unstable enough to apply their whole weight to the cord accidentally. A break thus caused to either the chain or gear system would have endangered the lives of the astronauts. Consequently, safety factors greater than 1-1/4 were necessary.

A final design consideration was to minimize secondary friction in the gearbox. The original consideration was to use plastic-impregnated sleeve bearings, but on July 12, 1967, the worm box was assessed at 800°F conditions and it was concluded that plastic sleeves would delaminate at these temperatures. Instead they decided to use self-aligning ball-bearings on the worm shaft and ball bearings on both the lower cask trunnions (see Figure 2.3)

A full year later, in September, 1968, Grumman changed the open position of the ALSEP package door adjacent to the cask. In its new position, the door interfered with the cord operation, so it became necessary to move the gearbox to the other side of the cask. Luckily, the same gearbox could be used in the inverted position, whereas any ratchet-type mechanism would have had to be redesigned.

Worm Gear Material Selection

It was known that in vacuum conditions similar materials under pressure would tend to cold weld. It was also known that generally coefficients of friction in vacuums are higher than in the atmosphere because of the lack of

B KING 9-11-67

I ANALYSIS OF 24 PITCH SINGLE THREAD WORM WHEEL AT LUNAR LOADS

FROM EQUATION (44) DESIGN OF MACHINE ELEMENTS BY MACMILLAN

(1) $F_s = \frac{s\,b\,Y}{P_d}$ [LEWIS EQUATION]

YIELDS THE MAX TOOTH STRESS

WITH GEAR PARAMETERS OF:

FORM FACTOR (Y) =	.318
DIAMETRAL PITCH (P_d) =	24
FACE WIDTH (b) =	.25"
MAX TORQUE TO ROTATE CASK (T)	60.5"#
PITCH DIAMETER (P)	1.25"

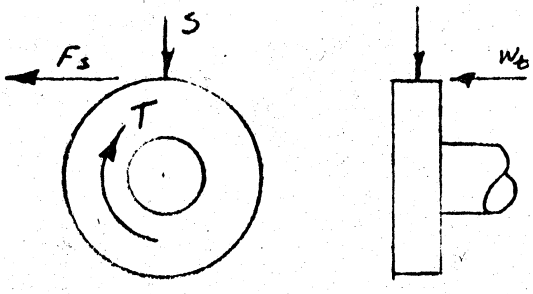

$$F_s = \frac{T}{P/2} = \frac{60.5}{.625} = \underline{\underline{96.8\#}}$$

SUBSTITUTING INTO (1) THE STRESS IS;

$$S = \sigma = \frac{P_d\,F_s}{b\,Y} = \frac{24 \times 96.8}{.25 \times .318} = \underline{\underline{29,200\ psi}}$$

II DESIGN CHECK OF WORM WHEEL KEY

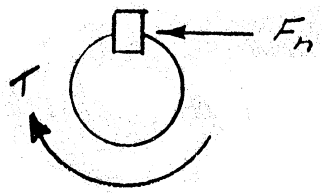

DIAMETER OF SHAFT = .50

KEY DIMENSIONS

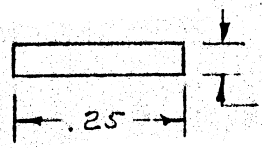

$$F_n = \frac{T}{D/2} = \frac{60.5}{.25} = \underline{242\ \#}$$

$$S_s = \frac{F_n}{b\,L} = \frac{242}{.125 \times .25} = \underline{7,740\ p.s.i}$$

$$S_c = \frac{2\,F_n}{t\,L} = \frac{2 \times 242}{.125 \times .25} = \underline{15,500\ p.s.i}$$

III ANALYSIS OF WORM GEAR SHAFT

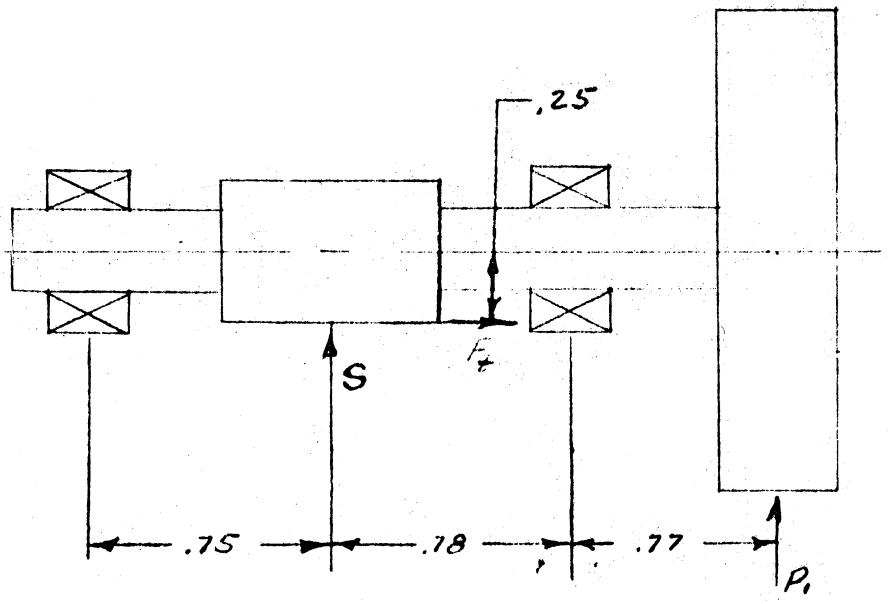

SEPARATING FORCE (S)

FROM PAGE 458 DESIGN OF MACH ELEMENTS

$$S = \frac{F_t \sin \phi_n}{\cos \phi_n \cos \lambda - f \sin \lambda} = \frac{96.8 \times .291}{.968 \times .9965 - .19 \times .083}$$

$S = \underline{\underline{2.54}}$ #

WORM CONSTANTS

24 PITCH SINGLE THREAD
LEAD .1309
PITCH DIAMETER .50
LEAD ANGLE λ 4°96'
PRESSURE ANGLE ϕ 14°30'

EFFICIENCY OF WORM MECHANISM

$$e = \tan\lambda \left[\frac{\cos\phi_n - f\tan\lambda}{\cos\phi_n \tan\lambda + f} \right]$$

FRICTION (f) ASSUMED TO BE .19

$$e = .0831 \left[\frac{.9684 - .19 \times .0833}{.9689 \times .0833 + .19} \right] = \underline{\underline{.292}}$$

AND FROM Pg #1 $F_s = F_t = 96.8$ #

DRIVING FORCE ON WORM (Wt)

FROM Pg 455 DESIGN OF MACH ELEMENTS

$$Wt = F_t \left[\frac{\cos\phi_n \sin\lambda + f\cos\lambda}{\cos\phi_n \cos\lambda - f\sin\lambda} \right] = \underline{\underline{13.8}} \text{ \#}$$

WORM IS SELF LOCKING IF THE COEFFICIENT OF FRICTION IS GREATER THAN THE TANGENT OF THE LEAD ANGLE λ (A LEAD ANGLE OF 6° OR LESS IS CONSIDERED SELF LOCKING.

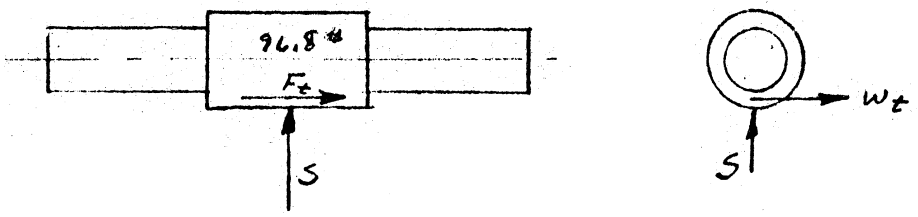

WORM SHAFT AND BEARING ANALYSIS

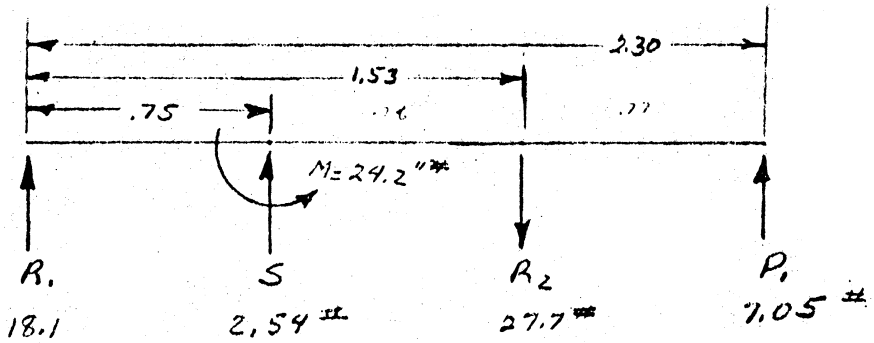

LOADS ON SHAFT

FORCE REQUIRED BY ASTRONAUT TO ROTATE CASK (P_1)

$P_1 \; e \; 2\pi$ = LEAD F_t

$$P_1 = \frac{.1309 \quad 96.8}{e \quad 2\pi} = \underline{7.05\ \#}$$

$\circlearrowleft^{+}$ THE BEARING LOADS ARE FOUND BY $\Sigma M @ R_1 = 0$

$$-.75S + 1.53 R_2 - 2.30 P_1 - .25 F_t = 0$$

$$R_2 = \frac{42.3}{1.53} = \underline{27.7\ \#}$$

$$R_1 = \underline{-18.1\ \#}.$$

MAX BEARING OPERATING LOAD

IS :: THRUST 96.8 #

RADIAL 27.7 #

SHAFT

M

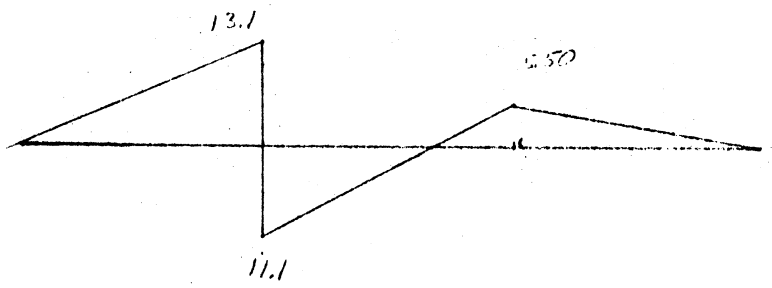

$$\sigma = \frac{M_{max}\, c}{I} = \frac{13.1 \times \frac{1}{8}}{.00149} = .86 \times 10^4 = 8{,}600\ psi$$

TORSION OF THE SHAFT AND DEFLECTION IS NEGLIGABLE WHEN CONSIDERING THE THE END PLAY OF .006 TO .010 END PLAY OF THE THRUST BEARING.

IF YOU CONSIDER A MAX CLEARENCE OF .025' BETWEEN THE WORM AND WORM GEAR, THE MAX UNCONTROLED ROTATION OF THE CASK WILL BE;

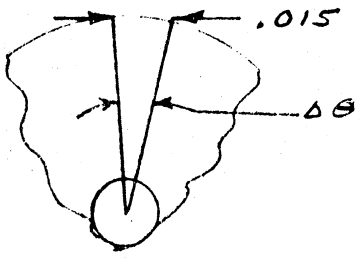

$$TAN^{-1}\,\Delta\theta = \frac{.015}{P/2} = \frac{.015}{.625} = .0234$$

$$\Delta\theta = 1^\circ 20'$$

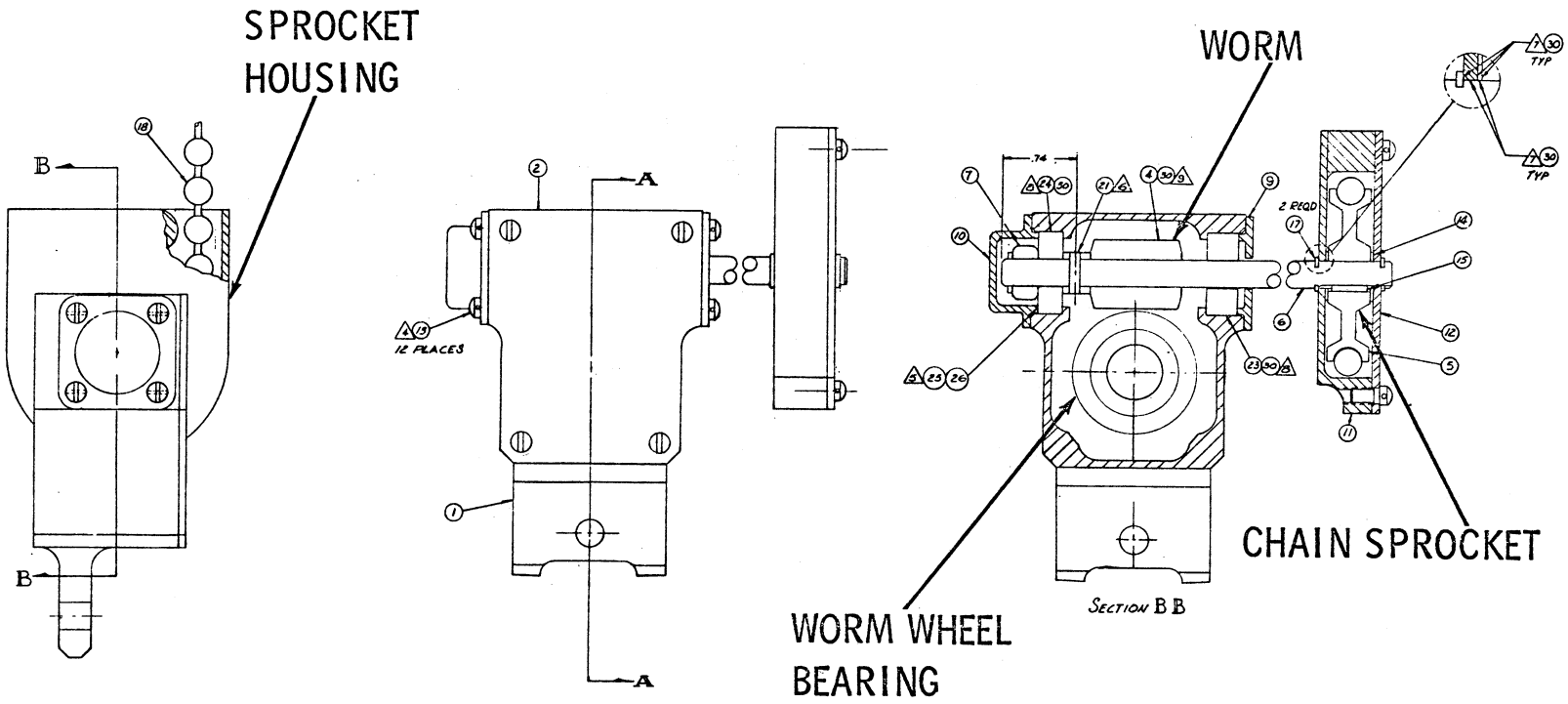

Figure 2.3. Tilt gearbox assembly.

an oxide layer. Finally, the project required that all materials be able to withstand high temperatures and be light-weight. The materials selected had to fit within these parameters.

Plastics were initially eliminated because their normal range of temperature tolerance would only extend to 150-200°F. Plastics might also outgas or sublime, but little information was available on their space performance. The temperature requirements necessitated the use of metals.

Titanium was selected to be the main material for the support structure and gear mechanism for three reasons. First, it has low density (.16 lb/cu in. compared with .29 lb/cu in. for steel) with an ultimate tensile strength approximately equal to that of the 300 series stainless steels. Second, it has a low coefficient of thermal expansion. Finally, it has high strength at elevated temperatures. Titanium was used in the worm wheel, and stainless steel was used in the worm. This avoided the cold welding found between similar materials. Aluminum had been discarded because of its greater loss of strength with increasing temperatures.

Titanium itself is difficult to machine and expensive. However, because of its physical properties and because so much was already being used in the structure, titanium was used for the worm wheel anyway.

Simulation and Testing of Rotation

Because of the importance of reliability in the gearbox for the control of this dangerous operation an extensive testing program was required to ensure success. Because of the difference in gravitational systems the terms

"simulation" and "duplication" could not be synonymous. It was impossible to duplicate lunar conditions, but simulation was possible through three different methods for the gearbox tests. First, it was possible to simulate the torque expected under lunar conditions and apply this to the specific apparatus. Second, they could make a cask 1/6 the weight of the actual cask by using lead weights to simulate the center of gravity. Finally, as it was necessary to test the actual flight model, it would be undesirable to overload the shaft with forces six times those on the moon as this would produce structural failure. Consequently, its lunar weight was represented by supporting 5/6 of the actual earth-weight with a spring compensating device. Designing the mechanism for lunar conditions by decreasing the weight and strength of the materials for rotation, resulted in a more sophisticated and costly testing program necessary in simulation and reliability determination.

There were a series of engineering models made for testing materials and assembles in a variety of contitions. For example, on July 21, 1967, the first gearbox model did not function properly due to faulty bearing alignment. This resulted in minor modifications before a qualification model could be made. Notes on the final qualification test follow:

Tests on Tilt Gearbox Assembly

Test Item

Gearbox Assembly-Dwg.

Purpose of Tests

To verify that the items under test will withstand the loads imposed by, and operate satisfactorily under, the following conditions:

- When the cask is supported (by the gearbox) with its major axis horizontal, i.e., position of maximum torque, at ambient local terrestrial conditions;
- With load as above but at maximum working temperature, i.e., 700°F ± 25°F;
- With load as above but at maximum working temperature (700°F ± 25°F) and a vacuum condition goal of 1×10^{-13} torr;

and to determine the maximum force required to operate the gearbox during normal cycling, and after repetitive cycling.

Test Procedure

The tests were conducted under Procedure No. ATP-D-96 in the following order:

- at ambient room temperature and atmospheric pressure;
- at 700°F ± 25°F and ambient atmospheric pressure; and
- at 700°F ± 25°F and at a vacuum of 1×10^{-7} torr. (1×10^{-13} could not be attained).

Success of the test was dependent upon all parts operating properly in the environments noted above. The load to operate the gearbox was not to exceed 20 lb, for a simulated torque load of 50 in.-lb.

Test Results

All parts did operate properly, even though the components were severely

overtested relative to number of operational cycles.

A maximum load of 11 lb was required to provide 50 in.-lb of torque at the gearbox output shaft for the normal test sequence. This load increased to 22 lb after cyclic testing that represented approximately 150 times the normal requirement.

2.2 LUBRICATION

Lubrication of all moving parts for the vacuum operations was necessary to lessen the raised coefficients of friction and the possibility of cold welding. Some special vacuum-application oils and greases, usually silicone products could have been used. However, at the high temperatures in space they might have sublimed. Also, the pressures on the gear teeth would probably have been too great. Consequently, a dry lubricant was necessary.

Molybdenum disulfide was ultimately used. The first dry lubricant (DL_1) tried had been accepted by both Boeing and NASA for space application. Bendix proceeded to have DL_1 applied to all bearings, chain pieces, gears, and the sprocket by a spraying process. During tests in high temperatures and vacuum conditions the gearbox did not operate as well as had been expected. When they looked inside the box they discovered considerable amounts of black particles, indicating that DL_1 had been worn off the worm gear faces. It was then concluded that the treatment, which had apparently been applied omitting the burnishing process, was unsatisfactory. At this point, it was discovered that DL_1 contained graphite, a substance not fit for vacuum application since it requires water vapor for its lubricating properties.

Because of improper application of the lubricant, one bearing from the manufacturer became so seized-up it could not be rotated. Bendix, well supplied with these DL_1-coated bearings, began a process of wearing-in the bearings in the gearboxes so that they would be operational. This was possible because the bearing loads in the gearbox were quite low and that the mechanical advantage of the astronaut through the chain and worm was capable of overcoming the increased coefficient of friction. However, the DL_1 coating could not be used on the guillotine release mechanism (to be discussed later.)

The second dry lubricant used on the guillotine was a molybdenum disulfide powder, not containing graphite which was applied by a burnishing process. The performance of the guillotine coated with DL_1 had been off by a factor of 3 due to the increased coefficient of friction. With DL_1 the final results were better than expected originally, the coefficient being lower.

2.3 UPPER TRUNNION RELEASE MECHANISMS

The Original Ball-Pin

Before the rotation could be accomplished it was necessary to release the cask from its upper trunnion cradle support. Before cask rotation the cask weight had been fully supported by the upper trunnion extensions of the circumferential bands. These trunnions had been supported by a stationary U-shaped member and a rotating lever which closed the U to form a cradle. In the original plan the cradle was held closed by a quick-release ball pin (see

Figure 2.4).

As in Figure 2.5, the ball pin consisted of an outer casing and an inner movable shaft. Through two holes in the outer casing protruded two balls that were normally forced outward by the inner shaft. These balls served to increase the casing's outside diameter at a point where it could not fit through the close tolerance hole in the restraining washer. The shaft was held in this locked position by spring tension. In order to release the pin the shaft was pulled forward by a cord against the spring tensioning. As it moved forward a groove in the shaft allowed the balls to drop from the protruding position inward, thus clearing the outer casing diameter. This would allow the pin (casing and shaft) to clear the restraining washer hole.

(A similar pin had also been considered. In it the interference was caused by a protruding U-shaped member. This provided the same type of locking except that it was unsymmetrical. The one-sided interference in a short pin would cause tipping of the pin in the hole and possible jamming. It was discarded for this reason.)

Though this ball pin was originally designed to be a shear pin, the manufacturer assured Bendix that they had been used as tension pins before successfully. In this case the outer casing was preloaded by tightening a nut to a predetermined torque. This then required that the collar or washer which interfered with the balls be hardened so that the balls could not be pulled through easily.

A series of tests were established to assess the suitability of the pin in vacuum conditions and at high and low temperatures. In addition the cask

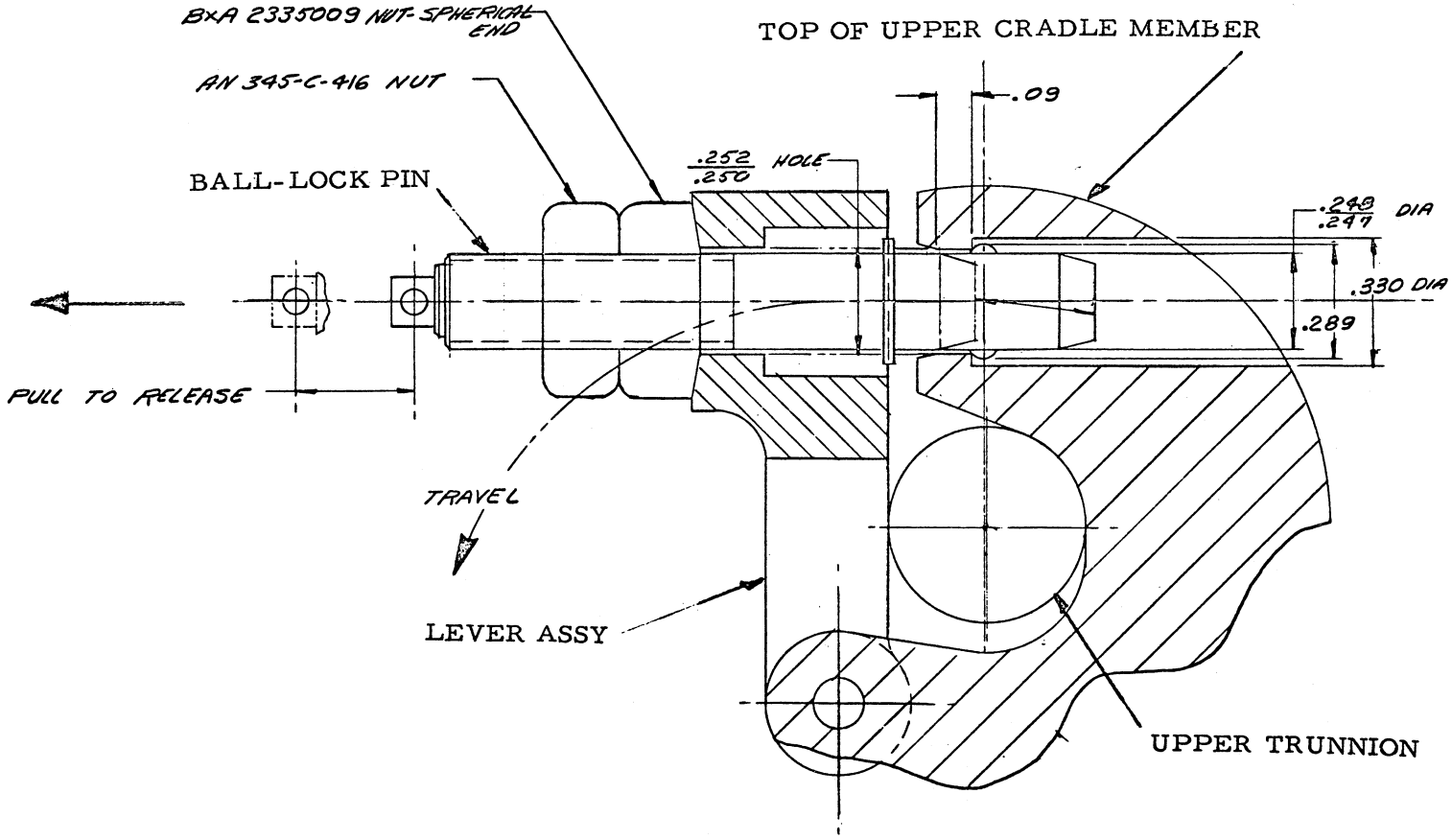

Figure 2.4. Upper trunnion release mechanism.

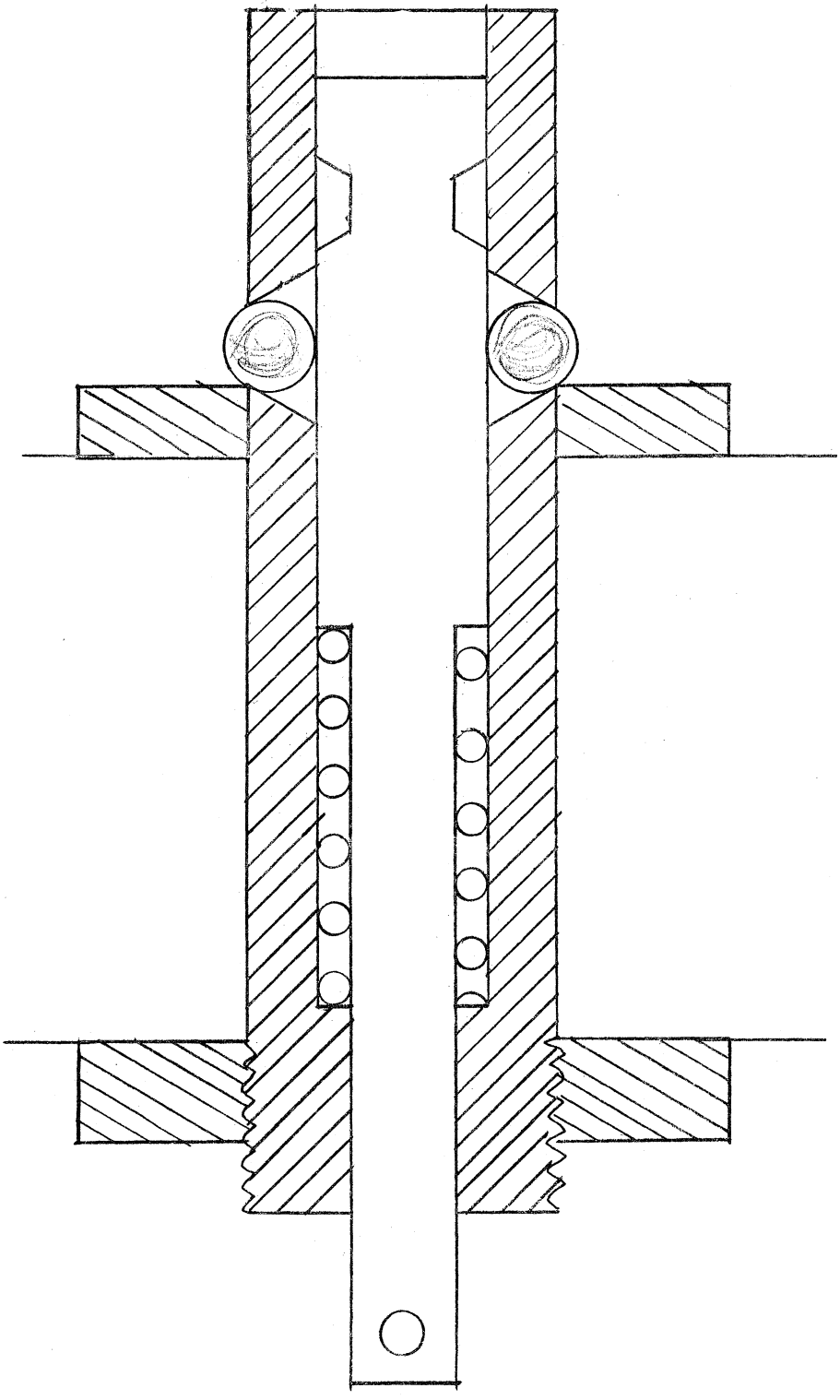

Figure 2.5. Quick release ball pin.

structure as a whole was to undergo extensive vibration testing. On July 30, 1968, one of the pins unlocked during a qualification model vibration test. It was found that the pin shaft had been manufactured so that it was short enough for the balls to be resting on the corner at the top of the ramp. The seating collar showed no signs of wear, but x-ray and microscopic examinations revealed that a Brinelling effect by the balls had worn down the corners of the ramp during the vibration test so that the preload caused the pin to pull out.

These short shafts were replaced in later runs by longer ones; however, with these there was a loss of preload and they would not unlock by any means. Because there was no assurance that this would not occur on the moon, this method was abandoned for a more positive method of releasing.

Three Alternate Mechanisms

One of the alternatives was a suitcase-like latch. This consisted of a spring-loaded hinge-bar with a loop and its interlocking pin. Upon removal of the pin the spring-loaded hinge would release itself.

The second alternative operated like a collet grip. This arrangement resembled the ball-pin assembly except that the pin would have been replaced by a titanium rod with an annular groove. Three collet jaws interlocked with the annular groove near the outside end of the rod and were held together by a surrounding sleeve. This locked the cradle members together until the sleeve would be pulled back. There was little chance of cold welding because of the low bearing pressure between the collet and the sleeve because all inter-

faces would be dry lubricated. Bendix calculations are shown in Exhibit 2.2.

The third method of release was similar in principle to the collet except that it required cutting through the locking rod. This guillotine method would actually require a smaller load from the astronaut to release the cask. Using the same cradle that had been assembled for the original ball-pin release they replaced the ball-pin with a titanium rod and replaced the ball-pin lever with a guillotine lever. The titanium rod, similarly shaped to a tensile test specimen, was positively held in the cradle end and extended through the lever and a threaded nut. Tightening of the nut pre-loaded the rod to a predetermined force.

Measurement of preload was accomplished through the use of Bellville washers. The amount of preload was determined by the extent of flattening the cup-shaped washer wedged between the nut and the lever assembly.

The cam lever and cutter cut the rod as shown in Figure 2.6. Pulling the cam lever notched the pretensioned rod. Before their use both the lever and cutter were held in place by shear wires that prevented inadvertent contact of the cutter and rod, an event which would have triggered early deployment and failure.

Preliminary calculations suggested that the ideal situation would be to have a preloaded pin such that a cut through 25% of the pin diameter would act like a necked tensile specimen and go to failure. A high preload would thus require little effort on the astronauts' part. However, the preload could not be so high that the imposed g-loadings of vibrations and launch might exceed either the yield or ultimate strengths. If the yield strength

AN 28

Exhibit 2.2. Collet Release Calculations.

PREPARED BY FBL
CHECKED BY
REVISED BY

ENGINEERING REPORT
Bendix Aerospace Systems Division

DATE 9-5-8 PAGE 1
REPORT No. 28
MODEL

CASE RELEASE PIN (#2 MECHANISM)

10:1 SCALE

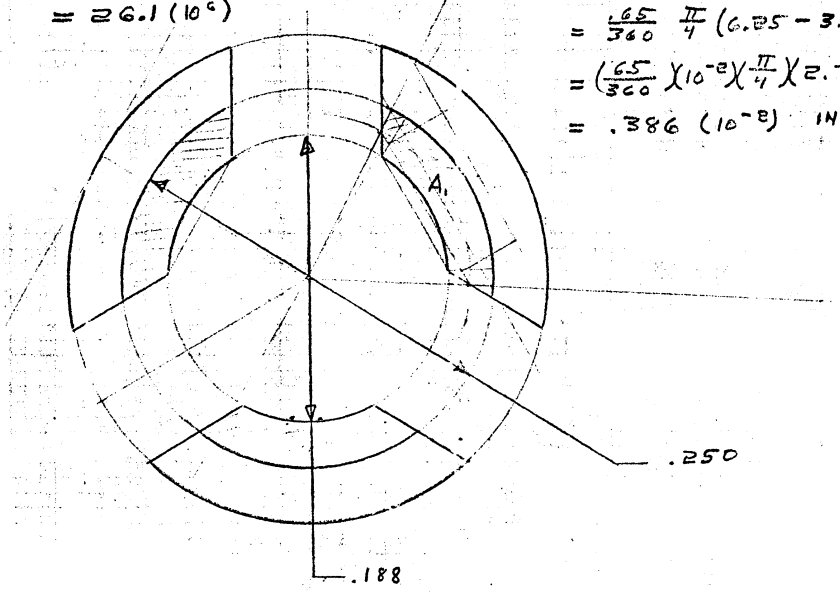

E @ 600° F $= (.90)E_{RT.} = (.9)(29)(10^6)$
$= 26.1\ (10^6)$

$A_1 = \left(\frac{65}{360}\right)\left(\frac{\pi}{4}\right)(d_o^2 - d_i^2)$
$= \frac{65}{360}\ \frac{\pi}{4}\ (2.5^2 - 1.28^2)\ (10^{-2})$
$= \frac{65}{360}\ \frac{\pi}{4}\ (6.25 - 3.53)$
$= \left(\frac{65}{360}\right)(10^{-2})\left(\frac{\pi}{4}\right)(2.72)$
$= .386\ (10^{-2})\ IN^2$

TO ARRIVE AT AN EQUIVALENT RECTANGLE FOR A_1, LET $A_1 = A_R$ AND LET PROPORTIONS BE SIMILAR.

$h = .04$

$A = .386\ (10^{-2}) = 4\ (10^{-2})\ W$

$W = .097$

$\therefore I = \frac{bh^3}{12} = \frac{.097\ (.04)^3}{12} = \frac{(9.7)(10^{-2})(64)(10^{-6})}{12}$
$= 51.7\ (10^{-8})$

$c = \frac{h}{2} = .02$

$I/c = 25.4\ (10^{-6})$

BxA 542

CASK RELEASE PIN

$E = 26.1 \times 10^6$ PSI

$I E = 13.5$

FOR $\delta = .035$, $\delta = \frac{1}{3}\frac{Wl^3}{EI}$

$3.5(10^{-2}) = \frac{1}{3}\frac{W(.80)^3}{13.5}$

$W = \frac{(3.5)(3)(13.5)}{.51}$

$= 2.78$ LB.

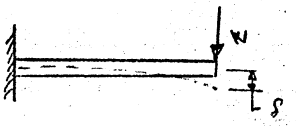

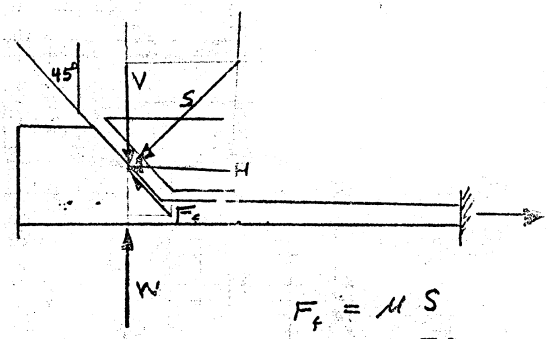

$F_f = \mu S$

$\mu = .20$

$\Sigma F_x = 0$: $L = H + .707 F_f$ (1)

$\Sigma F_y = 0$: $V = W + .707 F_f$ (2)

$H = .707 S$

$V = .707 S$

$F_f = .20 S$

$L = .707 S + (.707)(.20) S$ (3)

$.707 S = W + (.707)(.20) S$ (4)

$(.80)(.707) S = W$ (5)

$L = (1.20)(.707) S$

$S = \frac{L}{(1.20)(.707)}$ (6)

BxA 542

PREPARED BY EBL
CHECKED BY
REVISED BY

ENGINEERING REPORT
Bendix Aerospace Systems Division

DATE 9-5-8 PAGE 3
REPORT No.
MODEL

CASK RELEASE PIN

COMBINING EQ. 6 & EQ. 5,

$$VJ = \frac{(.80 \times .707)}{1} \times \frac{L}{(1.20 \times .707)}$$

$$W = .667\ L$$

THEN, FOR $W = 2.78$ LB.

$$L = \frac{2.78}{.667} = 4.17 \text{ LB.}$$

CONSERVATIVELY ASSUME $L = 5.00$ LB.

THEN TOTAL PULL (P) REQ'D IS

$$P = 3(L)$$

$$\boxed{P \approx 15 \text{ LB.}}$$

CHECKING FOR TENSILE & BENDING STRENGTH.

$$\sigma = \sigma_x + \sigma_b$$

USE S.F. = 1.15 FOR YIELD DESIGN

Assume $M = (2.78)(1.15)$
$= 3.20$
≈ 3.50

$$\sigma_b = \frac{M}{I/c}$$

$$= \frac{(.8)(3.50)(10^4)}{25.4}$$

$$= 110,000 \text{ PSI.}$$

$$\sigma_x = \frac{P}{A_1} = \frac{5\ (1.15)}{(.386 \times 10^{-2})}$$

$$= 1500 \text{ PSI.}$$

$$\sigma = 111,500 \text{ PSI.}$$

@ 600° F $F_{xy} =$

M.S.

BxA 542

CASE RELEASE PIN (6 AL-4V) E = 82% E = (.85)(16) = 13.1 x10⁶

TITANIUM WOULD REDUCE THE PULL-OUT LOAD AND THE STRESS CREATED BY APPROX. $(1-\frac{13.1}{25.7})100 = 48\%$

FOR ANY STEEL, P AND σ WILL TAKE ON VALUES AS INDICATED ABOVE.

RECOMMENDATIONS

CONSIDERING MACHINING AND FORCE REQ'D TO PULL OUT PIN, CHOOSE A MAT'L WHICH WILL HAVE A YIELD STRENGTH ≥ σ @600° F

MAT'L	% F_{sy} @ 600°F	% E @ 600° F
S.S.	84 %	90 %
6 AL-4V	67 %	82 %

BxA 542

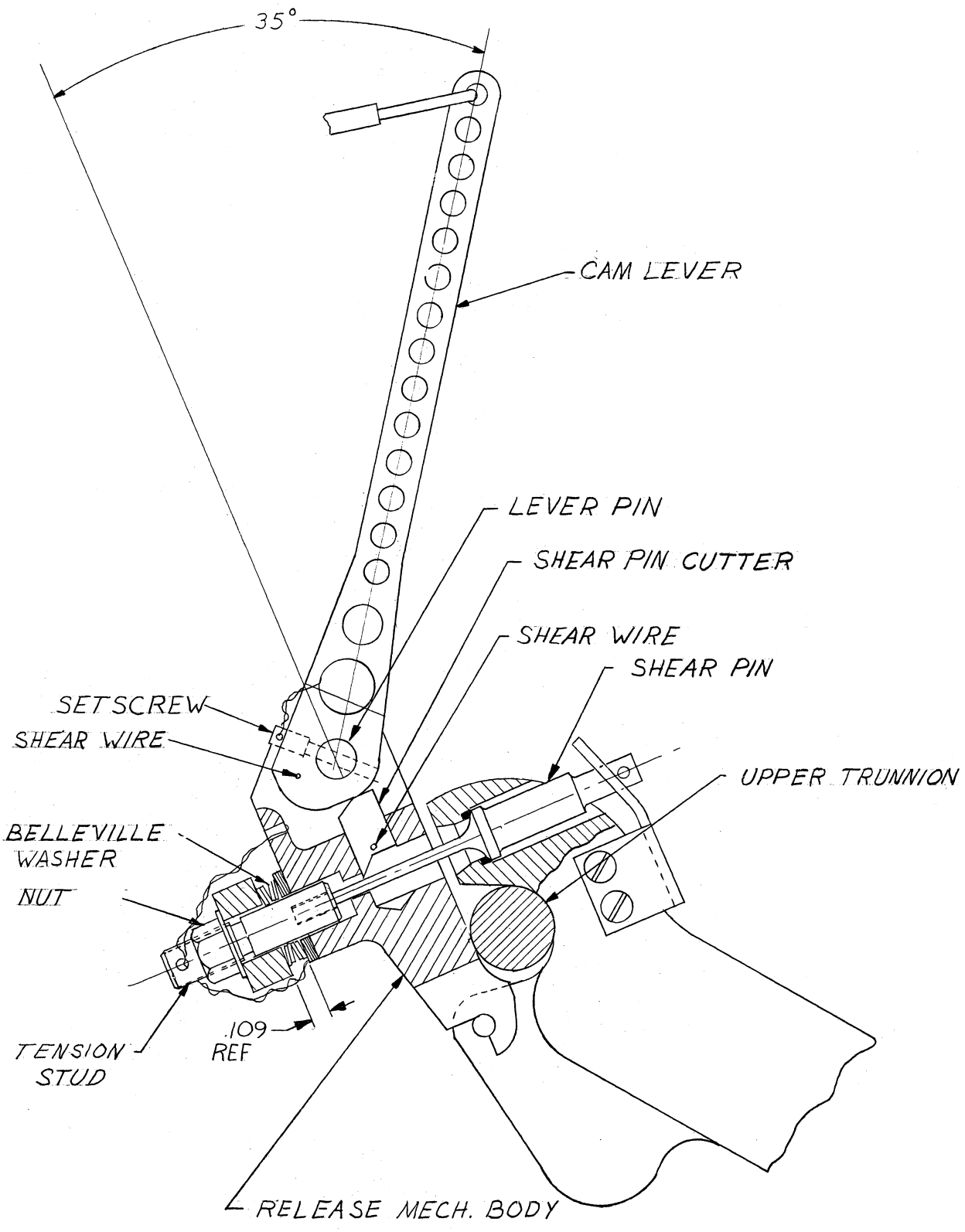

Figure 2.6. Guillotine trunnion release mechanism.

were exceeded the rod would yield and require far greater effort on the part of the astronaut to cut through it. If the ultimate strength were exceeded the rod would prematurely fail.

They decided to use a preload of 250 lb for the tests. On December 14, 1968, the first pull test began with the cutter angle at 10°. This angle required a 39 lb force to cut the rod, the maximum allotted being only 20 lb. Further modifications to the angle to 30° and to 45° resulted in force-requirements of 28 lb and 18 lb, respectively. Changing the lever arm from 2 in. to 4 in. changed the force-requirement to 13.5 lb. Raising the preload to 300 lb resulted in a force-requirement of 11 lb. However, redesigning the astronaut-guard and a straightening of the cam lever also resulted in an 11 lb force-requirement, and this preload of 250 lb was preferable to the former 300 lb preload.

All of these tests were conducted at 600°F. All test pulls were made normal to the cam lever at the beginning of its cutting stroke. However, it was anticipating that discrepancies of up to 40% due to the lunar positions would still result in force requirements of less that 20 lb. A 16 lb force at room temperature would release the cask in case of emergency.

Further tests in December required excessive forces for trunnion release. This discrepancy from Bendix results was explained when it was discovered the tests had been conducted at 180°. Since titaniom loses strength with increasing temperature these differing results would be expected. Again, since aluminum loses nearly 80% of its strength at 700-800°F, it was not considered for this application.

The calculations shown in Exhibit 2.3 are representative of those done for the cutter release mechanism.

Further Release Details

At the request of the astronauts Bendix made the trunnion release, cask dome lock removal, and worm-gear lowering parts of a continuing sequence. A lanyard loop connected all the parts. Those loop parts in contact with the cask were made of stainless steel while the part in contact with the astronaut was a Fiberglas covered cable which enclosed metallic jack-like beads. These ensured him a good grip.

The lanyard was looped neatly inside the ALSEP compartment door. After removing the drawer-like ALSEP components the astronaut would uncoil the lanyard and station himself in front of the cask. Pulling on the lanyard first released the upper right trunnion and detached the guillotine lever assembly. Next, the spline which locked the dome on the cask was pulled and joined the guillotine parts on the lanyard like more clothes on the line. The upper left trunnion released, and further pulling on the lanyard turned the sprocket and lowered the cask. In the first lunar use of the mechanism (Apollo 12) the sequence worked like clockwork. Photographs of this sequence from the actual moon operation of Apollo 12 are included in Appendix I.

2.4 BAND DESIGN

Securing the cask to the support structure was the biggest problem BxA encountered. Ultimately, three titanuim bands, 1.0 in. wide and 0.017 in.

Exhibit 2.3. Guillotine and Shear Wire Calculations. AN #-25

PREPARED BY EBL
CHECKED BY
REVISED BY

ENGINEERING REPORT
Bendix Aerospace Systems Division

DATE 8-4-64 PAGE 1
REPORT No. 25
MODEL

CASE RELEASE MECHANISM #1

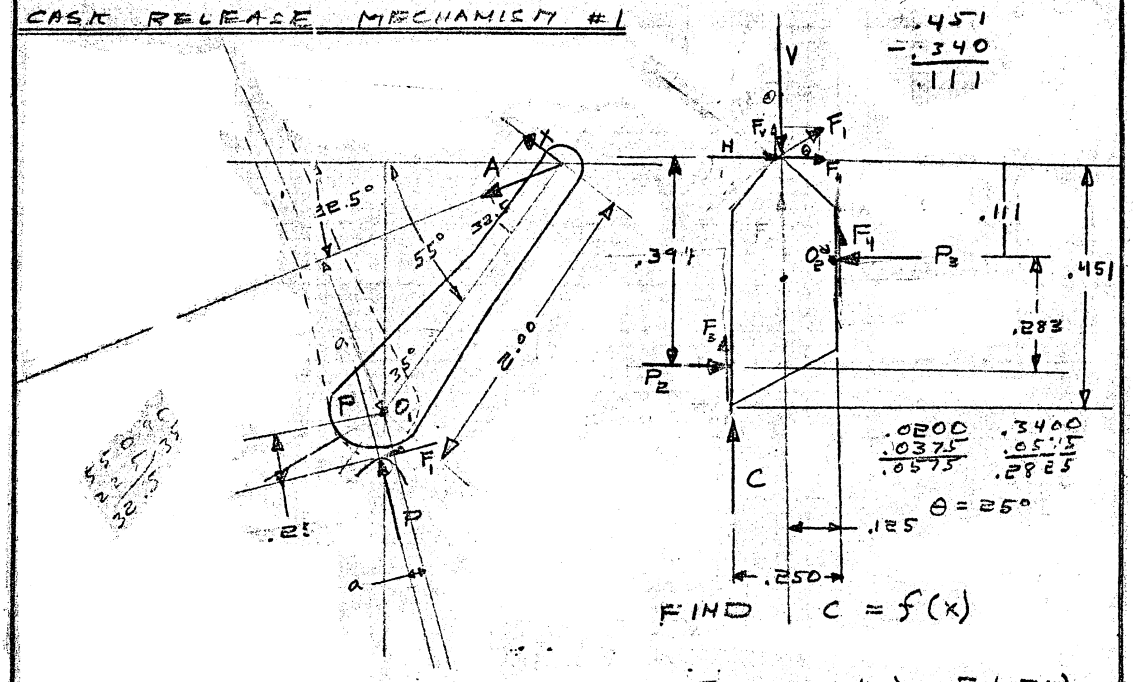

.451
−.340
.111

.0200 .3400
.0375 .0515
.0575 .2825

FIND $C = f(x)$

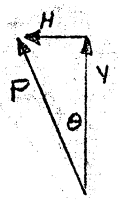

$F_1 = \mu P$

$V = P \cos\theta$

$H = P \sin\theta$

$F_V = F_1 \sin\theta$

$F_H = F_1 \cos\theta$

$\Sigma M_{O_1} = X(2) - F_1(.25) - P(a)$

TO FIND a,

$\frac{X}{P_V} = \frac{1}{20}$ } MECH. ADV.

$P_V = P \cos\theta$

$20X = P\cos\theta$

$\frac{20}{\cos\theta} X = P$

$\frac{20/\cos\theta}{1} = \frac{P}{X}$

$\frac{2\theta\cos\theta}{1} = \frac{2}{a}$

$a = \frac{2}{20/\cos\theta}$

$= .0906$

THEN

(a) $\Sigma M_{O_1} = 0 = X(2) - F_1(.25) - P(.0906)$

$V = P \cos 25° = P(.906)$

$H = P \sin 25° = .423\,P$

$F_V = \mu P \sin 25° = \mu P(.423)$

$F_H = \mu P \cos 25° = \mu P(.906)$

$-\frac{X}{P} = \frac{20/\cos\theta}{1}$

IF SYSTEM WERE 100% EFFICIENT, THE MECH. ADV. WOULD BE 22.1 : 1.0

$\left(\frac{X}{C}\right)_I = \left(\frac{X}{P}\right) = 22.1$

BxA 542

FROM FBD,

(+↻) $\sum M_{O_2} = 0 = F_H(.111) + F_V(.125) + H(.111) - V(.185) + F_2(.250) - P_2(.283) + C(.250)$ (b)

$F_3 = \mu P_2 \qquad F_4 = \mu P_3$

$0 = \mu P(.906)(.111) + \mu P(.423)(.125) + (.423)(.111)P - P(.906)(.125) + \mu P_2(.250) - P_2(.283) + C(.250)$

$0 = P[(\mu)(.1005) + (\mu)(.0567) + .0470 - .113] + P_2[(\mu)(.250) - .283] + C[.250]$

.0567
.1005
.1572
.1130
.0470
.0660

$0 = P[.1534\mu - .066] + P_2[.25\mu - .283] + .25C$ (1)

(+→)

$\sum F_H = 0 = H + F_H - P_3 + P_2$

$0 = .423P + \mu P(.906) - P_3 + P_2$

$0 = P(.906\mu + .423) - P_3 + P_2$ (2)

(+↓)

$\sum F_V = 0 = V - F_V - F_4 - F_3 - C$

$0 = .906P - P\mu(.423) - \mu P_3 - \mu P_2 - C$

$0 = P(.906 - .423\mu) - \mu P_3 - \mu P_2 - C$ (3)

COMBINING EQ'S 2 & 3,

$\frac{1}{\mu} \times$ EQ(3): $0 = P\left(\frac{.906}{\mu} - .423\right) - P_3 - P_2 - \frac{C}{\mu}$

(2): $0 = P(.906\mu + .423) + P_3 + P_2$

(4) $P\left(\frac{.906}{\mu} - .423 + .906\mu + .423\right) - 2P_3 - \frac{C}{\mu} = 0$

$\mu \times$ EQ(4): $P(.906 - .423\mu + .906\mu^2 + .423\mu) - 2P_3\mu - C = 0$

BxA 542

$$P\left(\frac{.906}{\mu} - .423 - .906\mu - .423\right) - P_3 - P_2 - \frac{C}{\mu}$$

$$\pm P_3 - P_2 = 0$$

$$P(.906 - .846\mu - .906\mu^2) \cdots \text{EQ } P_2 - C = 0 \qquad (6)$$

$$P_2 = P\left(\frac{.453}{\mu} - .423 - .453\mu\right) - \frac{C}{2\mu} \qquad (7)$$

INSERTING EQ (6) INTO EQ (1),

$$0 = P(.153\mu - .066) + (.25\mu - .283)\left[P\left(\frac{.453}{\mu} - .423 - .453\mu\right) - \frac{C}{2\mu}\right] + .25C \qquad (8)$$

FROM EQ (4)

$$.0906\,P = 2X - .25(\mu P)$$

$$(.0906 + .25\mu)P = 2X$$

$$P = \frac{2X}{.0906 + .25\mu} \qquad (9)$$

SOLVING FOR P IN EQ. (8),

$$0 = .153\mu P - .066P + (.25)(.453)P - (.25)(.423)\mu P - (.25)(.453)\mu^2 P - \frac{1}{\mu}(.283)(.453)P + (.283)(.423)P + (.283)(.453)\mu P - \frac{.25\mu C}{2\mu} + \frac{(.283)C}{2\mu} + .25C$$

$$0 = P\left[.175\mu + .167 - .113\mu^2 - \frac{.128}{\mu}\right] + C\left[+.125 + \frac{.142}{\mu}\right]$$

(10) SOLUTION A

EMPLOYING EQ'S (9) & (10), ONE CAN ARRIVE AT VARIOUS $\left(\frac{C}{X}\right)_o$ RATIOS FOR TRUE MECHANICAL ADVANTAGE.

−.066	+.153
+.113	−.406
+.180	−.138
+.233	+.291
−.066	−.126
+.167	+.165

BxA 542

SOLUTION B

FOR THE CONDITION OF NO FRICTION AT CAM-CUTTER CONTACT, A NEW $\left(\frac{C}{X}\right)_1$ RATIO WILL BE OBTAINED. $F_N = F_H = 0 = F_1$

SOLUTION C

THE IDEAL $\left(\frac{C}{X}\right)_I$ RATIO IS 22.1/1 (NO FRICTION).

THEN, EFFICIENCY OF CAM-CUTTER SYSTEM FOR A PARTICULAR μ AND FOR TRUE SITUATION IS FOUND BY

SOLUTION D

$$\frac{(C/X)_0}{(C/X)_I} \times 100 = EFF_0$$

SOLUTION E

EFFICIENCY FOR A μ AND FOR NO FRICTION AT CAM-CUTTER INTERFACE,

$$\frac{(C/X)_1}{(C/X)_I} \times 100 = EFF_1$$

SOLUTION F

PERCENT OF LOSS CREATED BY FRICTION AT CAM-CUTTER INTERFACE

$$\left\{1 - \frac{(C/X)_I - (C/X)_1}{(C/X)_I - (C/X)_0}\right\} 100 = \%\ \text{LOSS}$$

SOLUTION G

FOR NO FRICTION AT ANY INTERFACE, $(C/X)_2$ IS OBTAINED. $\mu = 0$. $F_1 = F_3 = F_4 = 0$

SOLUTION H

PERCENT OF LOSS CREATED BY FRICTION AT ALL INTERFACES:

$$\left\{1 - \frac{(C/X)_I - (C/X)_2}{(C/X)_I - (C/X)_0}\right\} 100 = \%\ \text{LOSS}$$

SOLUTION I

PERCENT OF LOSS CREATED BY ELEMENTS OTHER THAN FRICTION.

$100 - \text{SOL. H} = \%$ LOSS

BxA 542

TO FIND $(C/X)_I$, LET $F_1 = 0$. THEN

$F_V = 0$

$F_H = 0$

THEN EQ (a) BECOMES:

$$\Sigma X = .0906\ P$$

$$P = 22.05\ X \quad \text{FOR} \quad (C/X)_I = 20 \tag{12}$$

EQ (b) BECOMES,

$$0 = .111\ H - .125\ V + F_3(.25) - .283\ P_2 + .25C$$

OR

$$0 = -.066\ P + (.25\mu - .283)\ P_2 + .25\ C \tag{13}$$

EQ. (c) BECOMES,

$$0 = .906\ P - \mu P_3 - \mu P_2 - C \tag{14}$$

EQ (2) BECOMES,

$$0 = .423\ P - P_3 + P_2 \tag{15}$$

$\mu \times$ EQ (15): $\quad 0 = .423\mu P - \mu P_3 + \mu P_2 \tag{16}$

COMBINING (14) & (16),

$$0 = .906P - \mu P_3 - \mu P_2 - C - .423\mu P + \mu P_3 - \mu P_2$$

$$0 = P(.906 - .423\mu) - 2\mu P_2 - C$$

$$2\mu P_2 = P(.906 - .423\mu) - C$$

$$P_2 = P\left(\frac{.453}{\mu} - .212\right) - \frac{C}{2\mu} \tag{17}$$

COMBINING EQ'S (17) & (13)

$$0 = -.066\,P + (.25M - .283)\left[P\left(\frac{.453}{M} - .218\right) - \frac{C}{BM}\right] + .25\,C \qquad (18)$$

COMBINING EQ'S (12) & (12), ONE CAN ARRIVE AT $(C/X)_1$ FOR A VALUE OF M.

FOR NO FRICTION, $M = 0$. THEN EQ (1) BECOMES

$$0 = -.066\,P - .283\,P_2 + .25\,C$$

EQ (2) BECOMES,

$$0 = .423\,P - P_2 + P_1$$

EQ (3) BECOMES,

$$0 = .906\,P - C$$

EQ (a) BECOMES

$$BX = P(.0900)$$

$$P = 22.1\,X$$

BUT

$$C = .906\,P$$

$$C = .906\,(22.1)\,X$$

$$(C/X)_2 = 20.0$$

BxA 542

SOLUTION A

FOR $\mu = .2 = \frac{1}{5}$

FROM EQ (9),

$$P = \frac{2x}{.0906 + .25/5} = \frac{2x}{.141} = 14.23\ x$$

FROM EQ (10)

$$.175\,\frac{1}{5} + .167 - .113\,\frac{25}{25} - 5(.128) =$$

$$.035 + .167 - .005 - .640 = -.443$$

$$0 = -.443\ P + C(.125 + 5 \times .142)$$

$$.443\ P = .835\ C$$

$$(.443)(14.23)x = .835\ C$$

$$(C/x)_0 = \frac{.443}{.835}(14.23)$$

$$\boxed{@\mu = .20 \quad (C/x)_0 = 7.57}$$

FOR $\mu = .10 = \frac{1}{10}$

$$P = \frac{2x}{.0906 + .025} = \frac{2x}{.1156} = 17.3\ x$$

$$\overset{.0175}{.175}(.1) + .167 - .113\overset{.001}{(.01)} - 1.28 = -1.096$$

$$0 = -1.096\ P + C(.125 + 1.42)$$

$$1.096\ P = 1.545\ C$$

$$(1.096)(17.3)x = 1.545\ C$$

$$\boxed{@\mu = .10 \quad (C/x)_0 = 12.27}$$

BxA 542

NOW TO COMPUTE THE LANYARD FORCE, ASSUMING WORST CONDITION

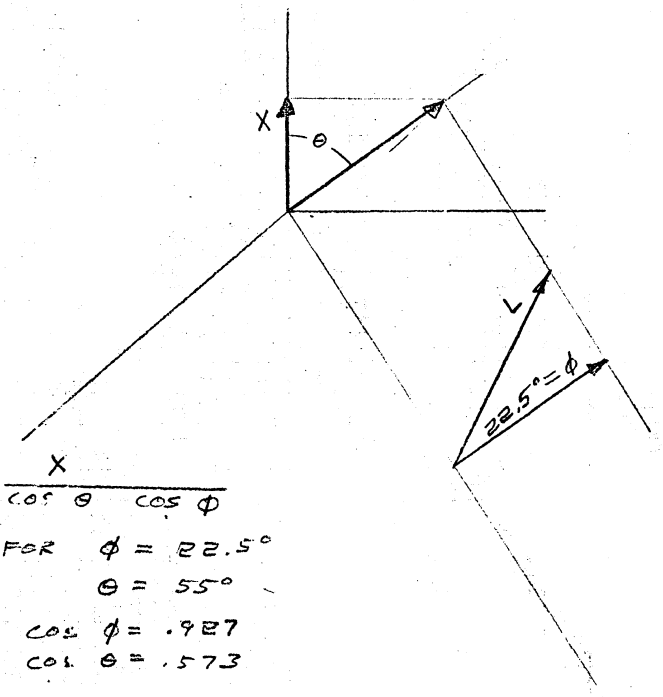

$$L = \frac{X}{\cos\theta \cos\phi}$$

FOR $\phi = 22.5°$

$\theta = 55°$

$\cos\phi = .927$

$\cos\theta = .573$

$$L = \frac{X}{(.927)(.573)}$$

$L = 1.885\ X$ @ $\theta = 55°$ $\phi = 22.5$

FOR $\theta = 45°$ $\phi = 22.5°$

$$L = \frac{X}{(.987)(.707)}$$

$L = 1.53\ X$ @ $\theta = 45°$ $\phi = 22.5°$

BxA 542

SOLUTION B

$\mu = .2 = \frac{1}{5}$

FROM EQ (2)

$$0 = -.066\,P + \left(.25\tfrac{1}{5} - .283\right)\left[P\left(\frac{.453}{1/5} - .212\right) - 2\tfrac{1}{5}C\right] + .25C$$

$$0 = -.066\,P - (.233)(2.053\,P - 2.5\,C) + .25C$$

$$0 = -.066\,P - .478\,P + .582\,C + .25C$$

$$.544\,P = .832\,C$$

$$.544\,(22.65\,X) = .832\,C$$

@ $\mu = .2$	$\left(\frac{C}{X}\right)_1 = 14.45$

FOR $\mu = .1 = \frac{1}{10}$

$$0 = -.066\,P + \left(.025 - .283\right)\left[P\left(4.53 - .212\right) - 5C\right] + .25C$$

$$0 = -.066\,P - 1.115\,P + 1.290\,C + .25C$$

$$+1.181\,P = 1.54\,C$$

$$1.181\,(22.65\,X) = 1.54\,C$$

@ $\mu = .1$	$\left(\frac{C}{X}\right)_1 = 16.90$

BxA 542

FOR $\mu = .05 = \frac{1}{20}$

$$P = \frac{2X}{.0906 + .25(.05)} = \frac{2X}{.0906 + .0125} = 19.4\ X$$

$$.1031$$

$$0 = P\left[.175\left(\frac{1}{20}\right) + .167 - .113\left(\frac{1}{20}\right)^2 - \frac{.128}{1/20}\right] + C\left[.125 + \frac{.142}{1/20}\right]$$

$$0 = P[.0088 + .167 - .0003 - 2.56] + C[.125 + 2.84]$$

$$0 = P[-2.3845] + C[2.965]$$

$$P = \frac{2.965}{2.385}C = 1.24\ C$$

$$1.24\ C = 19.4\ X$$

$$\left(\frac{C}{X}\right)_o = 15.65$$

BxA 542

PREPARED BY _____
CHECKED BY _____
REVISED BY _____

ENGINEERING REPORT

Bendix Aerospace Systems Division

DATE _____ PAGE 11
REPORT No. _____
MODEL _____

CUTTER FORCE/NORMAL FORCE
VS.
COEF. OF FRICTION

L = LENGTH OF LEVER
C = CUTTER FORCE
X = NORMAL FORCE ON LEVER
M = COEF. OF FRICTION
θ = ANGLE OF PULL FROM HORIZONTAL
L = LANYARD TENSION

$$L/X = \frac{}{.927 \cos(25)}$$

$$L/C = \left(\frac{C}{X}\right)_0 \div \left(\frac{L}{X}\right)$$

% REDUCTION IN L DUE TO CHANGE IN θ $= \frac{2.00}{\theta + 25}(100)$ 1

% REDUCTION IN L DUE TO CHANGE IN WIRE DIA $= \left(\frac{d_0^2}{d_0^2 + d_1^2}\right) 100$

$= \frac{.562}{.562 + (d_1 \times 10)^2}(100)$

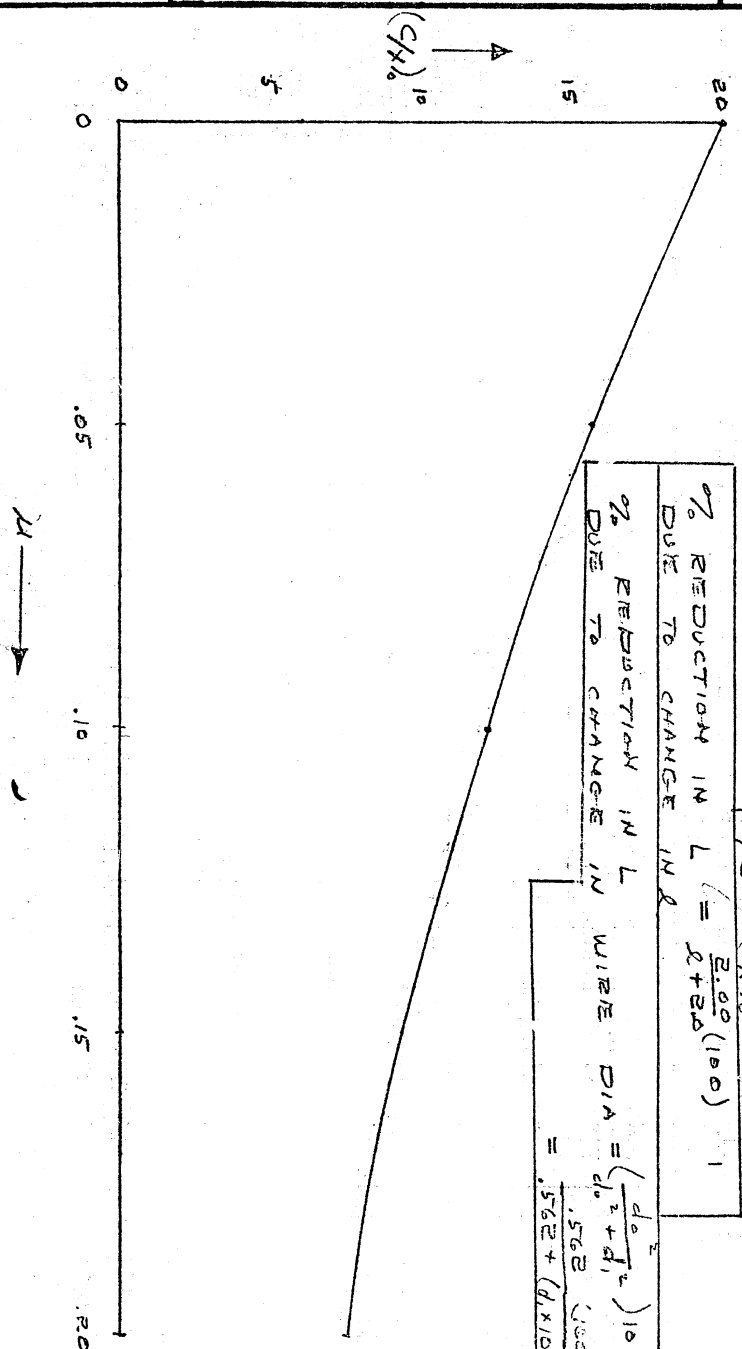

BxA 542

SOLUTION D -- EFFICIENCY OF CAM-CUTTER SYSTEM

FOR $\mu = 0$

$$EFF_0 = \frac{(C/X)_0}{(C/X)_I} \times 100 = \frac{20}{22.1} \times 100 = \underline{90.4\%}$$

FOR $\mu = .05$

$$EFF_0 = \frac{15.65}{22.1} \times 100 = \underline{70.8\%}$$

FOR $\mu = .10$

$$EFF_0 = \frac{12.57}{22.1} \times 100 = \underline{56.8\%}$$

FOR $\mu = .20$

$$EFF_0 = \frac{7.6}{22.1} \times 100 = \underline{34.4\%}$$

SOLUTION E EFFICIENCY FOR NO FRICTION AT CAM-CUTTER INTERFACE FOR $\mu = .1$

FOR $\mu = .1$

$$EFF_1 = \frac{16.9}{22.1} \cdot 100 = \underline{76.5\%}$$

SOLUTION F % LOSS CREATED BY CAM-CUTTER INTERFACE AT $\mu = .1$

$$1 - \frac{22.1 - 16.9}{22.1 - 12.6} = 1 - \frac{5.2}{9.5} = \underline{45.3\%}$$

SOLUTION H % LOSS CREATED BY SYSTEM FRICTION AT $\mu = .10$

$$1 - \frac{22.1 - 20.0}{22.1 - 12.6} = 1 - \frac{2.1}{9.5} = \underline{77.9\%}$$

BxA 542

SEE REP NO AN. # 26

PREPARED BY EBL
CHECKED BY
REVISED BY

ENGINEERING REPORT
Bendix Aerospace Systems Division

DATE 7-18-8 PAGE 1
REPORT No. 2C
MODEL

SHEAR-PIN ANALYSIS FOR CASE (MECHANISM #1)

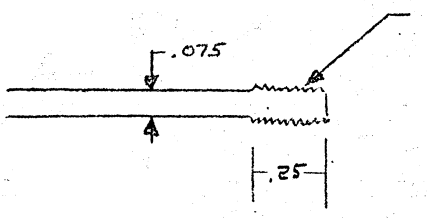

MAT'L - Ti 6AL-4V
F_{su} = 80 KSI
F_{tu} = 130 KSI
F_{xy} = 120 KSI

MIN. SHEAR AREA / IN. = .1524

$A_s = .25\,(.1524) = .0381$

F_{su} @ 600° = .74 F_{su} @ R.T.
F_{xy} @ 600° = .67 F_{xy} @ R.T.
F_{tu} @ 600 = .74 F_{tu} @ R.T.

THREADS:

$S_u = (.74)\frac{1}{1.5}(80)(10^3)(38.1)(10^{-3})$
$= 1503$ LB. @ 600°

$d = .075$
$A_x = 44.1 \times 10^{-4}$
$= .00441$ IN²

FOR NO YIELD WIRE: $d = .075$

$T_y = (.67)\frac{1}{1.15}(120)(10^3)(4.41)(10^{-3})$ (70)
$= 1308$ LB.

FOR NO BREAK, $d = .075$

$T_u = .74\,\frac{1}{1.50}(130)(10^3)(4.41)(10^{-3})$ (64)

FOR NO YIELD AND PRELOAD OF 250 LB.,

$250 = (70)10^3(A)$
$A = 3.58 \times 10^{-3} = .00358$
$\frac{\pi}{4}d^2 = .00358$
$d^2 = .00456$
$d = .0676 = .068$

BxA 542

PREPARED BY EKL
CHECKED BY
REVISED BY

ENGINEERING REPORT

Bendix Aerospace Systems Division

DATE 9-17-68 PAGE 32
REPORT No. 26
MODEL

SHEAR - PIN ANALYSIS FOR CASE

FORCE REQ'D TO SHEAR .068 PIN AT 600° F.

REDUCTION OF FORCE:

$$F_c = \frac{.00352}{.00441} F = .812 F$$

BxA 542

thick, retained the cask. Two bands were arranged circumferentially, 13.25 in, apart, and the other axially as shown in Figure 2.7. BxA considered this arrangement by no means ideal, however it was the best considering the following restraints on their design, made by GE:

(1) The design must provide adequate radiative cooling for the cask. (This is the only mode of cooling in the hard vacuum of outer space.)

(2) The design must allow the cask to separate from the LM should the mission fail and the LM reenter the earth's atmosphere. (The reasons for this restraint are discussed in the Introduction on page 2.)

In addition, the design must retain the cask in all positions, at all temperatures encountered, and during the dome removal operation.

When first faced with the problem of securing the cask BxA asked GE to provide either grooves, holes, or protrusions on the cask. (See Chapter 6, page 133.) Had this been possible, securing the cask would have obviously much easier. Consequently, the band arrangement was the only design considered. First of all, the bands left a large amount of the cask surface uncovered for radiative cooling. Secondly, the thin bands would indeed disintegrate upon reentry through the earth's atmosphere and thus allow the cask to separate from the LM.

Since friction loading between the cask and the bands was the mode of securing the cask, the following problems were apparent:

(1) How will temperature fluctuations of the cask during the

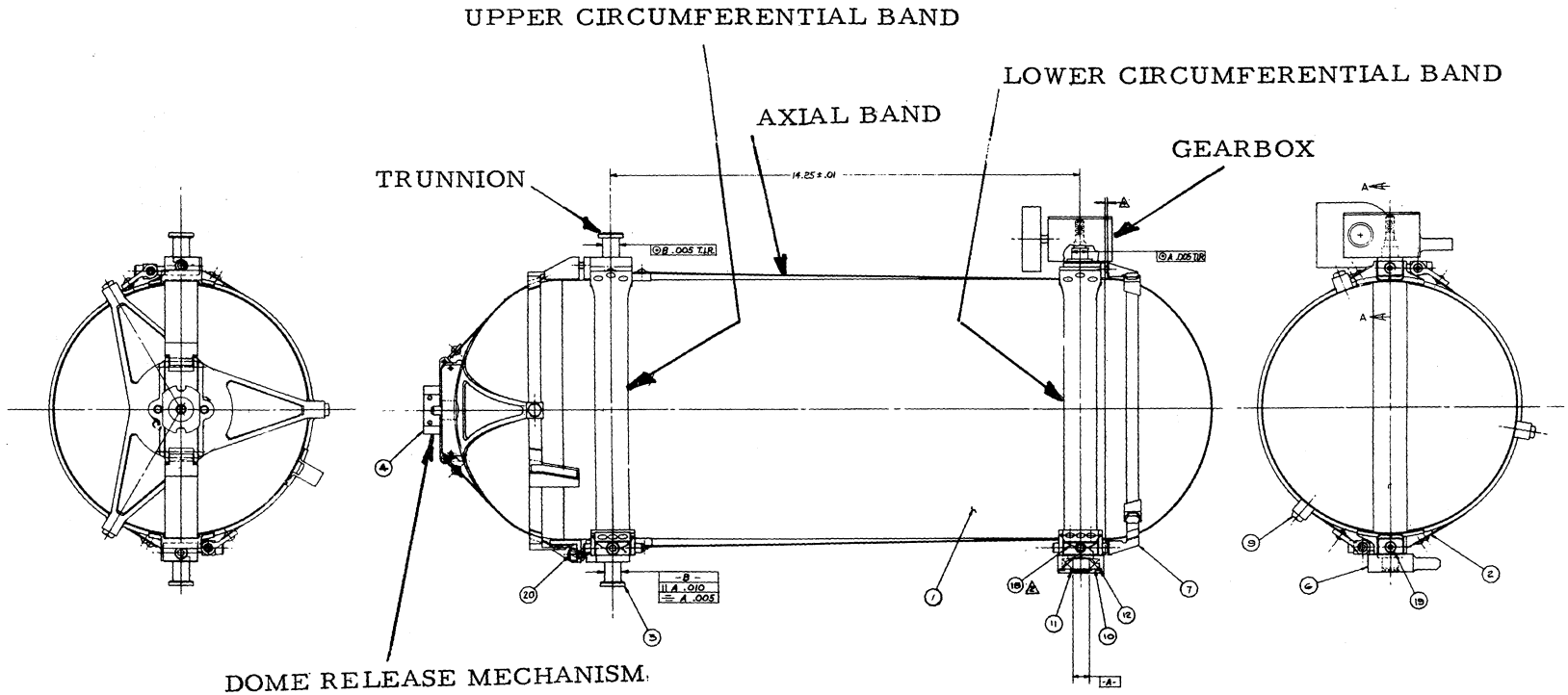

Figure 2.7. Cask/band assembly.

flight affect the frictional load?

(2) What material should the bands be made of?

(3) How tight should the bands be (how much pretension is needed) to maintain an adequate friction load?

These three problems were solved by BxA's Stress Analysis department and a discussion of the subsequent analysis is presented in the next chapter. However, this section is mainly concerned with the band design.

Above all, the amount of pretension in the circumferential bands was most important—it must ensure that the graphite cask is not overstressed at room temperature, when the adjustment is made, and it must ensure that when the cask has reached its final working temperature there is still sufficient residual tension in the bands to secure the cask against the dome unlocking torque. In addition, the pretension in the circumferential bands must prevent axial motion of the cask when the dome is removed.

To accomplish this each circumferential band was made in two halves. One end of a half band was riveted to a trunnion block while the other end was attached to the opposite trunnion block by a bolt in a swivel and yoke arrangement (See Figure 2.7). With this arrangement each band could be adjusted to obtain coaxial alignment of the trunnion blocks. In addition the correct amount of pretension was attained by tightening the bolts. A torque of 8 in.-lb produced the required pretension (from the stress analysis) in the bands. This figure was obtained from band tensioning tests where strain gages, mounted on the bands, monitored the pretension in the bands. Furthermore this procedure was carried out prior to launch to maintain the pretension

determined from the tests.

The axial band was also made in two halves. One end of each half was riveted to the upper trunnion blocks, while the other ends were attached to a yoke arrangement located at the bottom of the cask (See photo 4 in Appendix I). Pretensioning was accomplished as described above for the circumferential bands. With this arrangement axial loads on the cask were supported by the axial band and the upper circumferential band, while loading in the "y" and "z" directions were supported by both the upper and lower circumferential bands.

The cask-band/trunnion assembly was supported at the upper and lower U members at the trunnion blocks.

3. STRESS ANALYSIS

The peak stresses and temperatures which occur throughout the titanium support structure are summarized in Figure 3.1. These stresses were calculated using three-dimensional strength of materials formulas assuming 60 g loading (maximum) and a 45-lb cask. However, the most difficult task of the stress analysis was to determine the stress environment between the cask and the band-trunnion mechanism which directly supports the cask. As indicated in Section 2.4, the stress analysis was complicated by the various temperature fluctuations and loading conditions encountered by the cask and support structure during the flight. In essence, a detailed analysis was required to determine an appropriate material for the bands and an adequate clamping load which would retain the cask in all phases of the flight.

During the early design stages of the support structure the circumferential bands had a channel-type cross section which fit into grooves in the graphite cask. However, the evolution of the smooth surface cask (any grooves, slots, etc., in the cask would jeopardize its safe return to earth should the mission be aborted in space) indicated a different band design also. A simple flat band with negligible bending stress was the solution. In fact, this type design had significant advantages over the previous design. The most significant advantage was its lower thermal (pretension) stress. Other advantages were less weight, lower cost, and fewer tolerance problems. However, the most significant disadvantage was the difficulty in accurately pretensioning the bands.

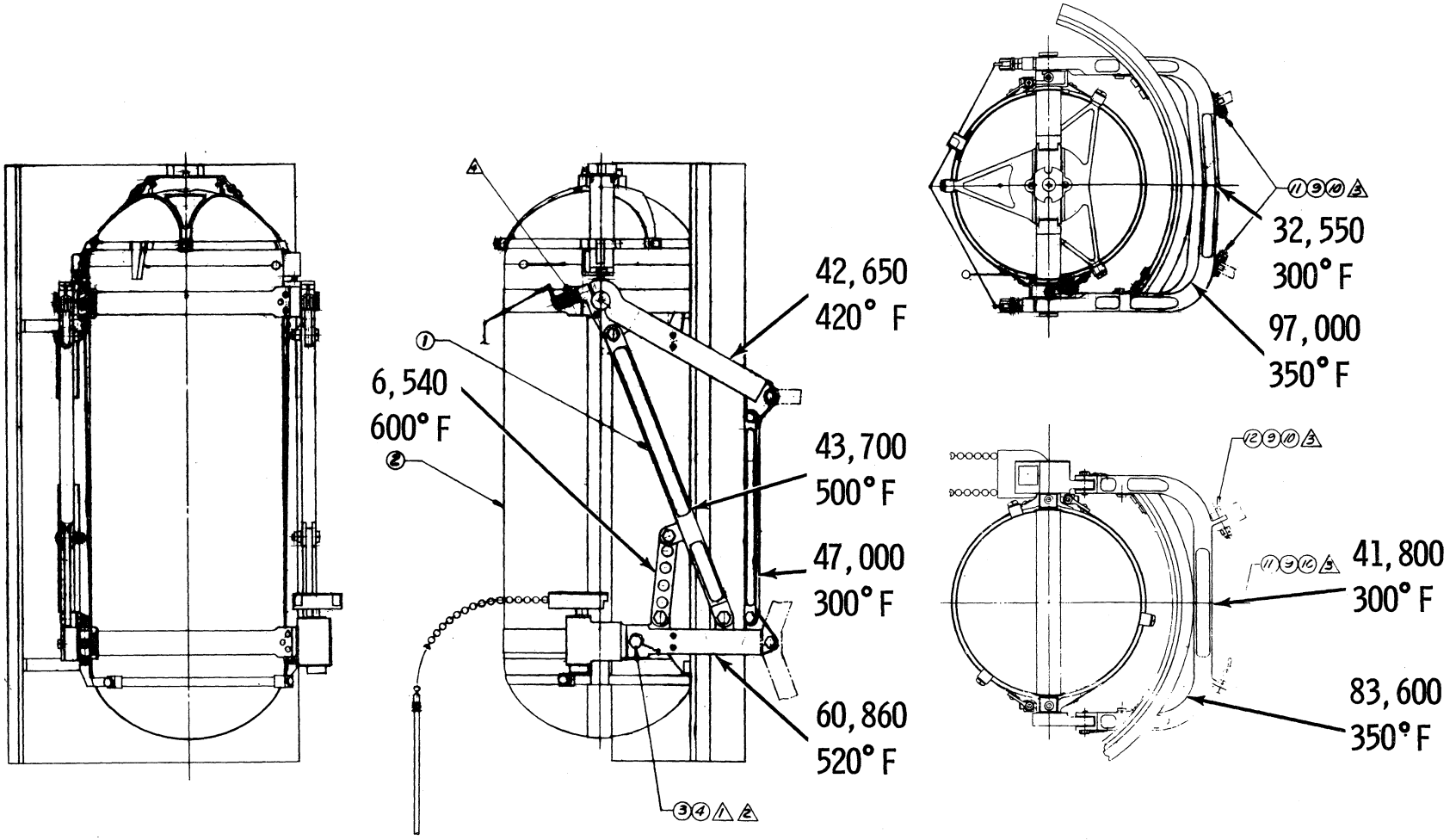

Figure 3.1. Peak temperature and stresses.

There were three sources of stress in the bands. They are pretension stress, stress caused by "g" loading, and stress due to misalignment or tolerance problems. The stresses due to pretensioning and maximum "g" loading were determined analytically while the stresses caused by misalignment were taken into account with the design "margin of safety" requirement.

3.1 MATERIAL SELECTION

The clamping load required to retain the cask is a function of the coefficent of friction (μ). Since friction forces are generally greater in a vacuum than in the atmosphere, a coefficient of friction of 0.2 or greater was presumed a conservative estimate of the cask-band surface combination. Therefore, a line load requirement of 3 lb/in. was chosen as design goal for the band line load on the lunar surface. This number was determined from Figure 3.2, provided by NASA. The line load on the cask is equal to the direct tensile load (P) in the circumferential band divided by the cask radius (R). The equation used to compute the direct tensile load is shown in Figure 3.3. As the equation indicates, the line load is directly proportional to temperature variations. Therefore, the task was to select a material which minimized the band load due to temperature fluctuations.

In selecting a material for the bands the coefficient of thermal expansion (α), stiffness (Young's Modulus), and the strength/density ratio were material properties of primary importance. These properties were considered at the high temperatures of the cask and their importance was as follows:

(1) Ideally the bands should have a coefficient of thermal expansion

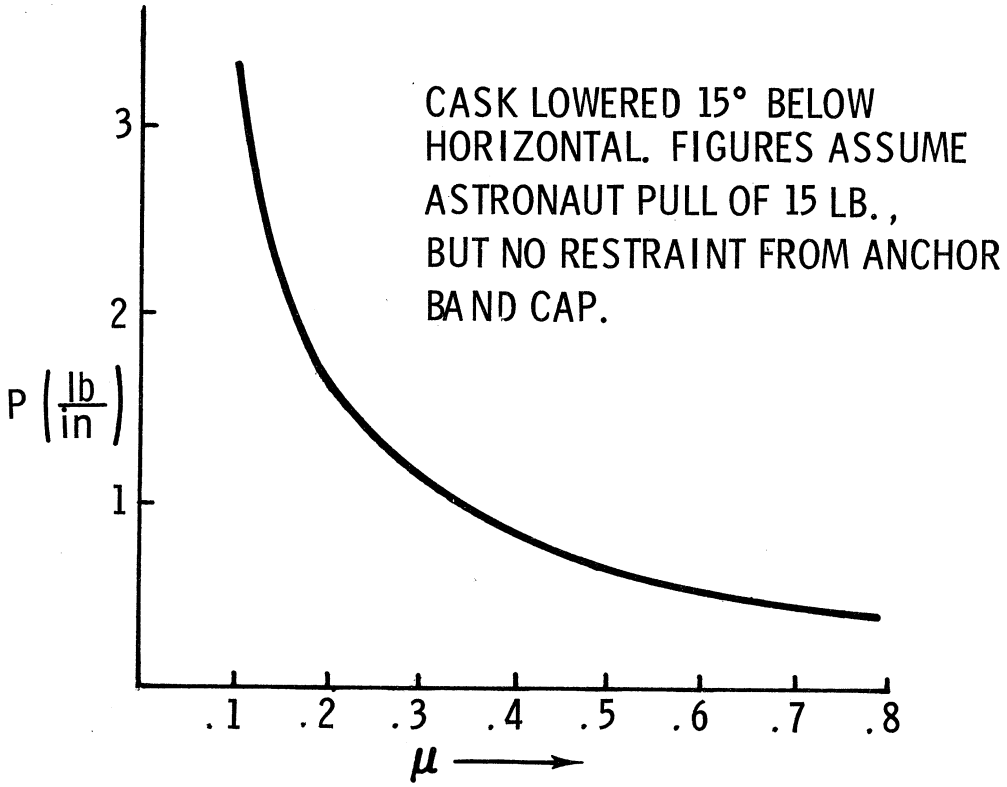

Figure 3.2. Required clamping load versus friction coefficient.

$$P = \frac{(\alpha_G - \alpha_M)\,\Delta T}{\left(\frac{1}{A_M E_M} + \frac{1}{A_G E_G}\right)}$$

- T ~ TEMPERATURE
- α ~ COEFFICIENT OF THERMAL EXPANSION
- A ~ CROSS SECTIONAL AREA
- E ~ MODULUS OF ELASTICITY
- G ~ GRAPHITE
- M ~ METAL

DESIRE TO MINIMIZE:

- $(\alpha_G - \alpha_M)$
- ΔT
- A E

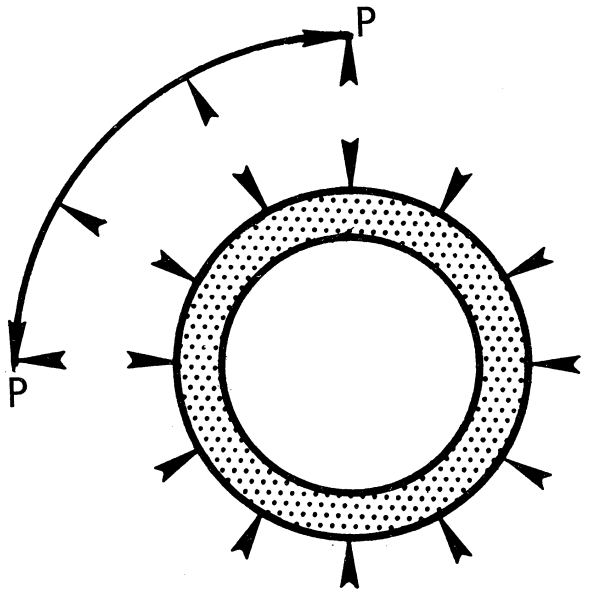

Figure 3.3. Band load equation.

identical to that of the graphite cask.

(2) Thermal expansion stresses are also minimized if the bands comply to the surface of the cask. This is obtained by minimizing Young's Modulus of elasticity (E). [Note: generally stiffness is considered to be a function of area times the Young's Modulus (AE), however since A is not a material property E is of greater importance in selecting a material.]

(3) Thermal stresses are not directly affected by strength/density ratios, but the weight of the band structure will be inversely proportional to this factor. Therefore high values of the strength/density ratio are desired.

In addition, the material must have a high melting point because of the high temperatures of the cask. The materials considered are shown in Figure 3.4. Of these, BxA chose titanium as the best compromise of the above criterion.

3.2 COMPUTATION OF BAND STRESSES

Using the band load equation of Figure 3.3, values of E and α for titanium from Figure 3.4, and the line criterion of 3 lb/in. on the lunar surface; the line load requirement at room temperature (70°F) was computed as 147 lb/in. The band was assumed to be 1.0 in. wide by 0.017 in. thick, and the cask thickness was 0.35 in. Furthermore, the band stress at room temperature and on the lunar surface were calculated as follows:

$$\sigma_B = P_L \cdot R/A$$

MATERIAL	$EX10^{-6}$	$\alpha X10^{6}$	DUCTILITY	F_{tu} KSI
GRAPHITE	1.5	1.775	0	5.22
TANTALUM	27	3.6	95 %	60
TUNGSTEN	59	2.5	0	220
TZM	46	2.7	55 %	125
S GLASS	10.5	1.6	0	665
TITANIUM 6A14V	16	5.3	10 %	160
STAINLESS STEEL 17-7PH (H1050)	29	6.3	9 %	200

Figure 3.4. Band materials considered.

where σ_B is the band stress in psi; P_L is the line load in lb/in.; R is the radius of the cask in in.; and A is the cross sectional area of the band in $in.^2$

Therefore,

$$\sigma_B(\text{at room temp.}) = 147 \cdot 4/0.017 = 34{,}600 \text{ psi}$$

$$\sigma_B(\text{at lunar surface}) = 3 \cdot 4/0.017 = 705 \text{ psi}$$

However, most significant was the band stress which occurs at the maximum "g" loading. The calculation of the load due to 60 g (maximum loading) is shown in Figure 3.5. At the maximum "g" loading the temperature was 550°F. Consequently, the temperature effects tend to decrease the line load and band stress because the bands expand more rapidly than the cask. Figure 3.6 summarizes the line load on the cask and the band stress at room temperature, maximum "g" loading, and lunar conditions.

3.3 FORMING THE BANDS

In bending the normally flat bands a residual bending stress occurred in the bands. Since the circumferential bands must retain a compressive line load in order to retain the cask, yielding cannot be permitted. Therefore, the residual stress was removed by a stress relief anneal. However the axial bands were formed requiring a curved section, around the lower dome, and a flat section along the side of the cylindrical cask. Consequently a stress concentration existed at the intersection of the flat portion with the curved portion of the band. As illustrated in Figure 3.7, this bending stress was

AXIAL BAND

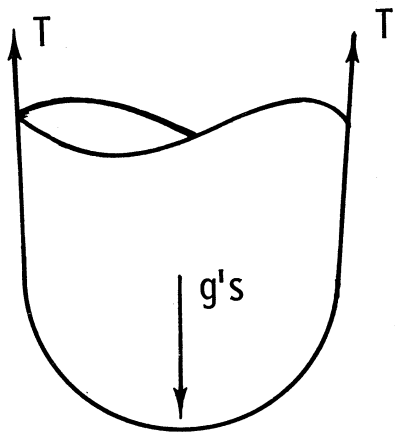

$2T = 45\ (60)$

$T = 1350$

TOP BAND

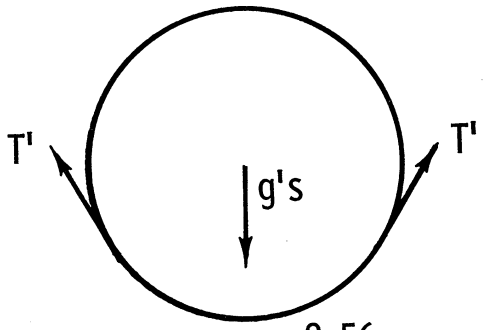

$$2T' \cos 30^\circ = \frac{8.56}{14.25}\ (45)\ (60)$$

$T' = 935$

Figure 3.5. "g" loading.

TOP BAND:

	LINE LOAD ON CASK lb/in.	STRESS IN BAND PSI
70° F, ROOM TEMPERATURE	147	34,600
550° F, MAX VIBRATION	52	12,200
800° F, LUNAR OPERATIONAL	3	705

Figure 3.6. Pretension requirements.

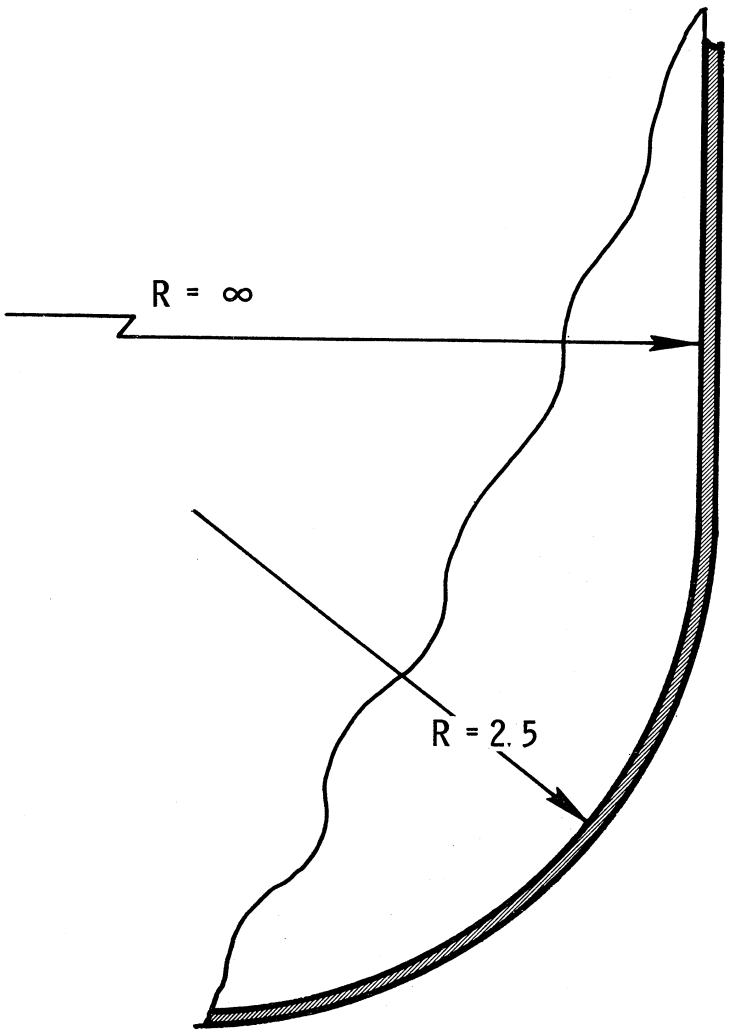

$$\epsilon = \frac{t}{2R} = \frac{.017}{5}$$

$$\sigma = E\epsilon = 16 \times 10^6 \frac{.017}{5}$$

$$= 54,500 \text{ PSI}$$

Figure 3.7. Stress due to forming the bands.

equal to 54,500 psi. This meant that any tolerance buildup between the band perimeter and the cask perimeter and any stretch of the band due to the "g" loading would cause the 54,500 psi stress to occur at the intersection of the curved and flat portions. Therefore, a prestressing procedure was used in forming the axial bands. This procedure consisted of winding the flat band around a small diameter mandrel and allowing it to spring back to an intermediate radius between 2.5 in. and an infinite radius shown in Figure 3.7. This produced a residual compressive stress in the outside fiber of 21,600 psi. An additional 8500 psi compressive stress was induced by bending the prestressed band back to the flat configuration. Since the curved portion of the band has a tensile stress of 46,000 psi on its outer surface, the total stress of the prestressed band is 46,000 - 21,600 = 24,400 psi tensile. Consequently, the prestressing process effectively divides the maximum bending stress into two smaller components as illustrated in Figure 3.8.

3.4 MARGIN OF SAFETY

A summary of the various band stresses and yield strengths of titanium are shown in Figure 3.9. The total stress in the top circumferential band was higher than that of the bottom circumferential band because the cask center of gravity (CG) was closer to the top and the cask was thicker here also. Comparing the top band stress total of 79,385 psi with the strength of annealed titanium at 550°F, the margin of safety is equal to 0.028 based on yielding. That is,

$$MS = 1.0 - \frac{\sigma_B}{F_{ty}}$$

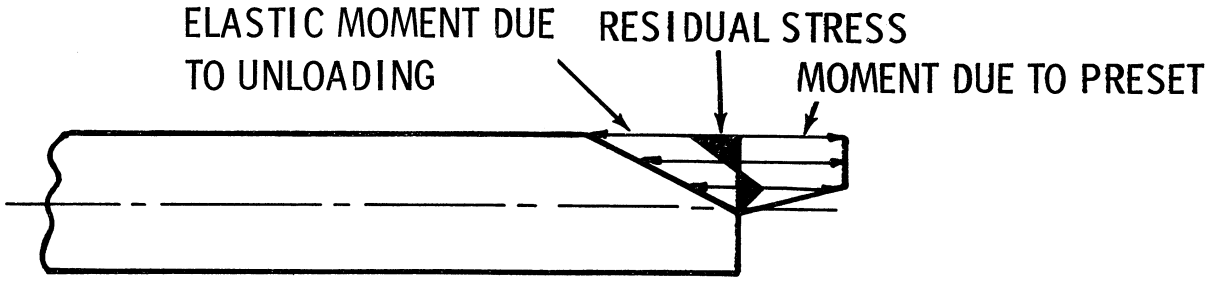

FOR SPRINGBACK RADIUS = 16 in., RESIDUAL STRESS = 21,600 PSI.

ON FLAT SURFACE, TOTAL = 21,600 + 8,500 = 30,100 PSI { COMP OUT / TENSION IN

ON CURVED SURFACE, TOTAL = 46,000 - 21,600 = 24,400 PSI { TENS OUT / COMP IN

54,500 PSI

Figure 3.8. Effect of prestressing the bands.

STRESS SOURCE	PSI AXIAL BAND	PSI TOP BAND	BOTTOM BAND
1. PRETENSION	12,290	12,290	10,000
2. "g" LOADING	79,500	55,000	43,000
3. BENDING	30,100	21,145	21,145
TOTAL	121,890	79,385	77,095

BAND STRESS TOTALS

MIL HdbK 5 Ti 6 Al 4V	F_{ty} KSI ANNEALED	F_{ty} (B) KSI STA
RT	120	148 KSI
550° F	.68 (120) = 81 6	.70(148) = 103.7
800° F	.62 (120) = 74.5	.61(148) = 90.4

YIELD STRENGTH OF TITANIUM

Figure 3.9. Summary of band stresses and yield strengths of titanium.

where, MS is the margin of safety; σ_B is the band stress; and F_{ty} is the yield strength of titanium.

The stresses in the axial band could not be added in the same way since the assumption of elastic behavior did not apply. That is, yielding occurred in the axial band thereby relieving a portion of the bending and pretension stresses. Comparing the stress developed by the "g" loading to the ultimate tensile strength of the titanium at 550°F resulted in a margin of safety of 0.14 based on fracture. Consequently the band design based on material selection and stress requirements was satisfactory with an adequate margin of safety. (BxA specified a margin of safety greater than zero was adequate.)

4. DYNAMIC ANALYSIS AND TESTING

The purpose of the dynamic analysis and testing program was to determine the vibrational characteristics of the cask assembly. The first step of the dynamic analysis was to determine an analytical model for the system. The development of the model was carried out by Dr. H. P. Lee and K. H. Wadleigh. Their results were reported in March of 1968. Following this, extensive testing was performed at the BxA research laboratories during April on a prototype assembly. Vibrations tests were also conducted at GE and GEAC. A comparison between the analytical data and the test data showed a fairly close correlation. Overall, the results of the dynamics program were successful. That is, there were no structural failures and the system was indeed stable.

4.1 ANALYTICAL DEVELOPMENT

The ultimate purpose of the dynamic analysis was to indicate to GE the probable vibration environment which the BxA support system would transmit (via the BxA/GE interface points) to the cask. Due to the high cost of building the cask, GE wanted a thorough dynamic analysis of the assembly before they would consent to using a prototype cask for the actual vibrations testing program. Moreoever, BxA wanted assurance that their assembly would not suffer structural failures when subjected to qualification level vibration loads on the test stand.

Two-Dimensional Model

During the early stages of the design the approach to an analytical model of the system began with the development of an adequate two-dimensional representation. Although limited to a study of three degrees of motion, this model did provide essential information as to the vibration characteristics of the structure. The information derived was the natural frequencies, the mode shapes, and transmissibilities of the system.

The physical model of the cask assembly used in the dynamic analysis is shown in Figure 4.1, it includes the bands, gear box unit, and the mounting structure. For the two-dimensional analysis a simplified model was used as shown in Figure 4.2. In order to develop a mathematical expression for the model the following assumptions and constraints were made:

(1) The fuel cask was rigid and axially symmetric.

(2) The mounting supports at the LM were rigid.

(3) The mounting structure was simplified to a three-member truss as shown in Figure 4.2. The two supporting points of the mounting structure to the cask shell at 1 and 2 have translational motions in x and z axes, and rotation ϕ about the origin.

(4) The truss members were treated as massless springs which contribute only to the stiffness.

(5) Hinged joints were assumed between any two truss members.

(6) A damping constant of 5% of the value for critical viscous

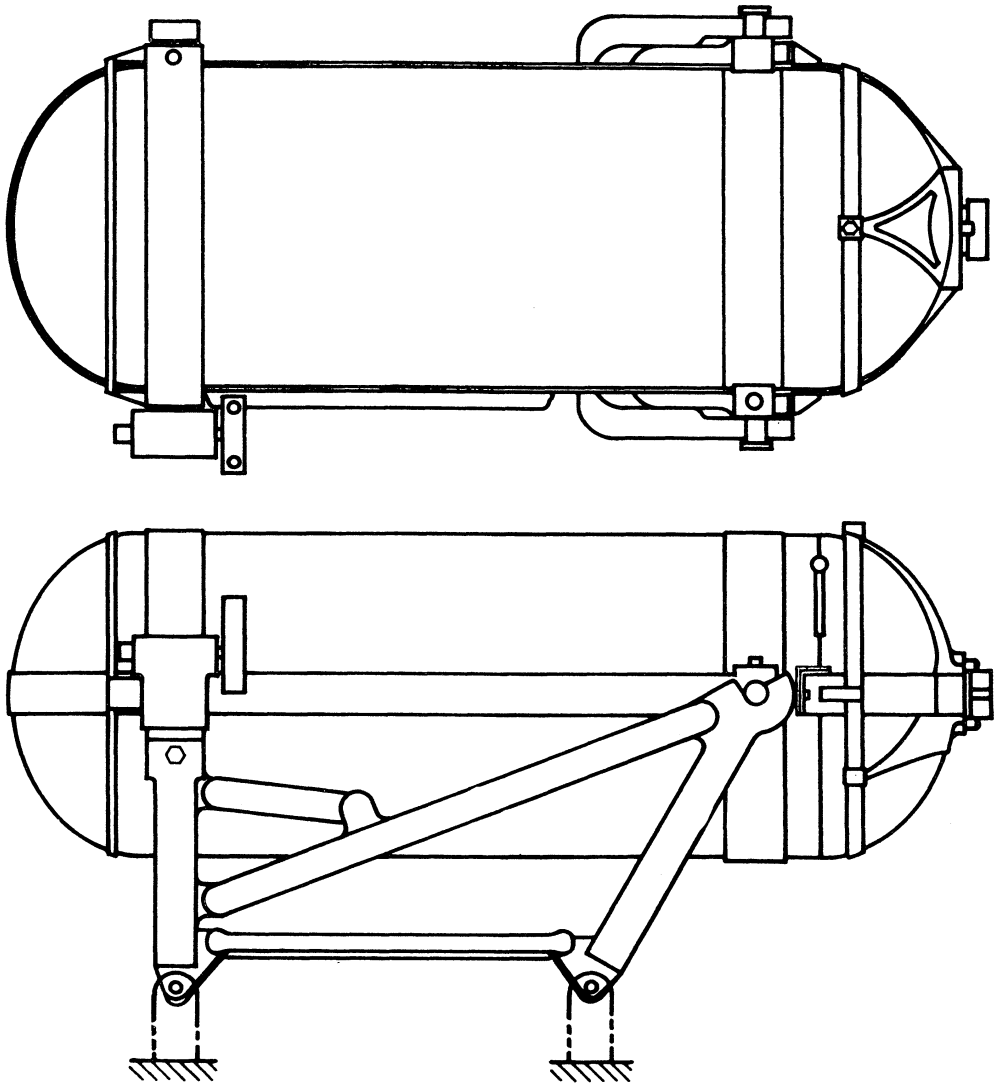

Figure 4.1. Physical mode of cask assembly and the mounting structure.

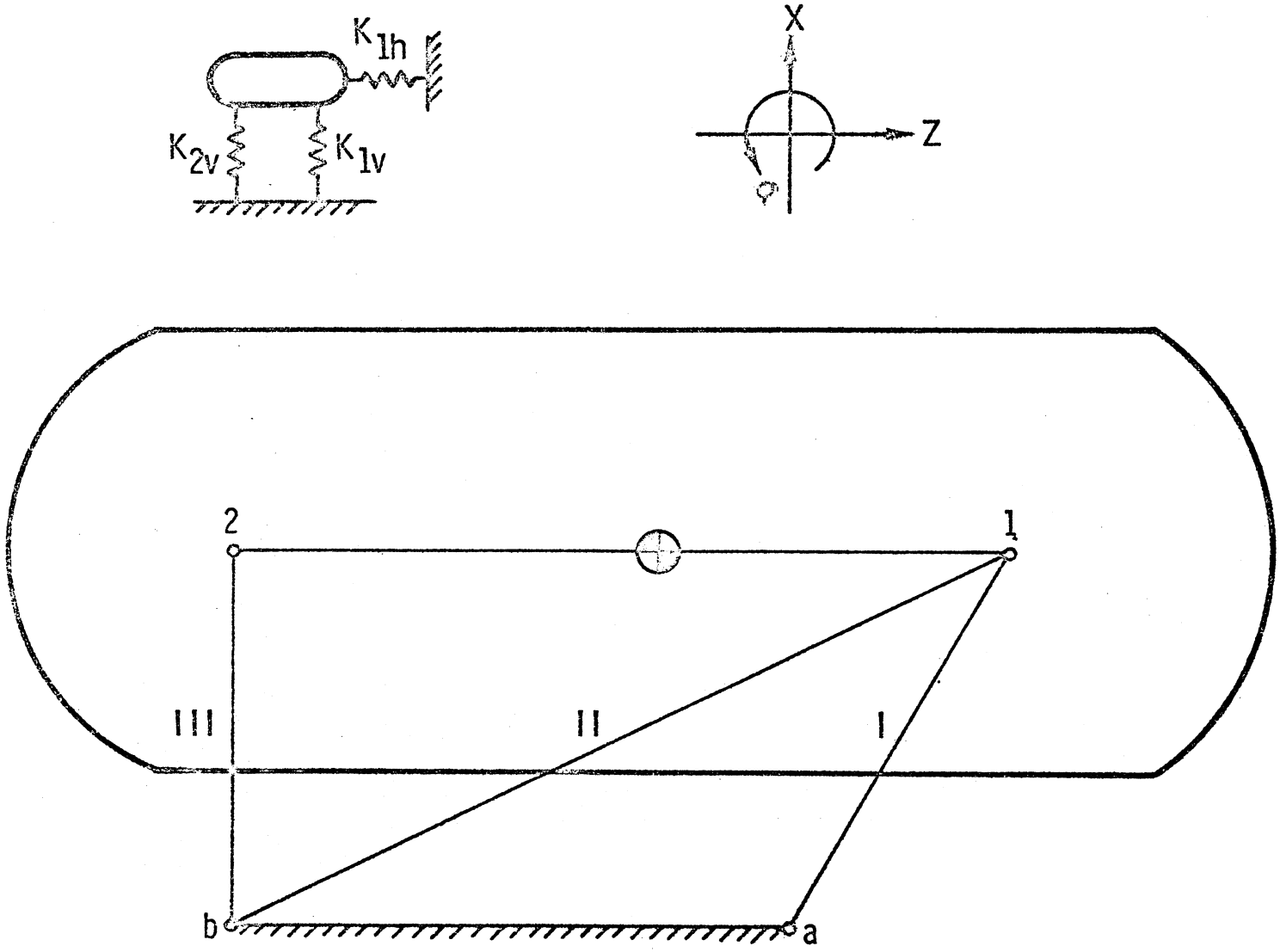

Figure 4.2. Two-dimensional model and the coordinate system.

damping* was used in the numerical calculations.

(7) The responses at the two supporting points 1 and 2 were assumed to have identical motions in the z-direction, i.e., $w_1 = w_2$; but the motions in the x-direction at 1 and 2 are different, being denoted by u_1 and u_2, respectively. Consequently, the vibrational system had three degrees-of-freedom.

The known weights of constituent components and the mass movements of inertia of the cask assembly were lumped at the center of gravity (CG) of the cask unit. Finally, the analytical procedure involved forming the three controlling matrices of the system. They were the mass matrix [M], the stiffness matrix [K], and the forcing matrix [Q]. The matrices were then transformed from the cask CG to the GE/BxA interface (points 1 and 2 on Figure 4.2) where the results were sought. The computer output indicated that there were three natural frequencies at 246, 837, and 1002 cps. And the resulting transmissibility versus frequency curves are shown in Figures 4.3 to 4.8. However, the primary points of interest are the responses to sinusoidal excitations and random excitations. NASA provided two input levels for the sinusoidal and random excitations. This input data (shown in Figures 4.9 and 4.10) was based on the worst vibrations condition, which occurred during the launch and boost phase of the flight. The system response to the given input levels was then calculated using the following formulas:

*The hysteresis damping of the system was assumed to be viscous in order to simplify the analysis.

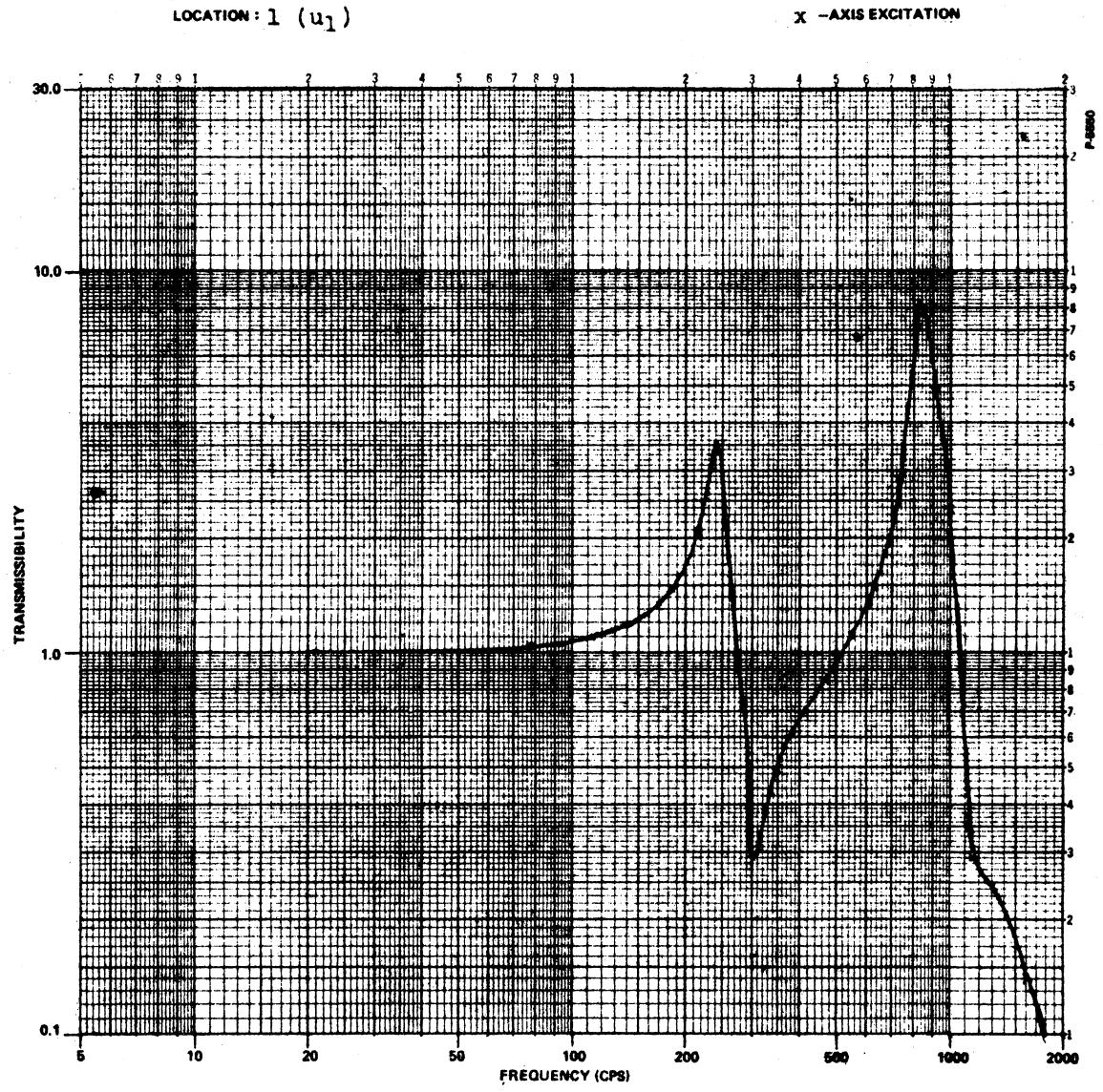

Figure 4.3. Transmissibility data; x-axis excitation; location 1.

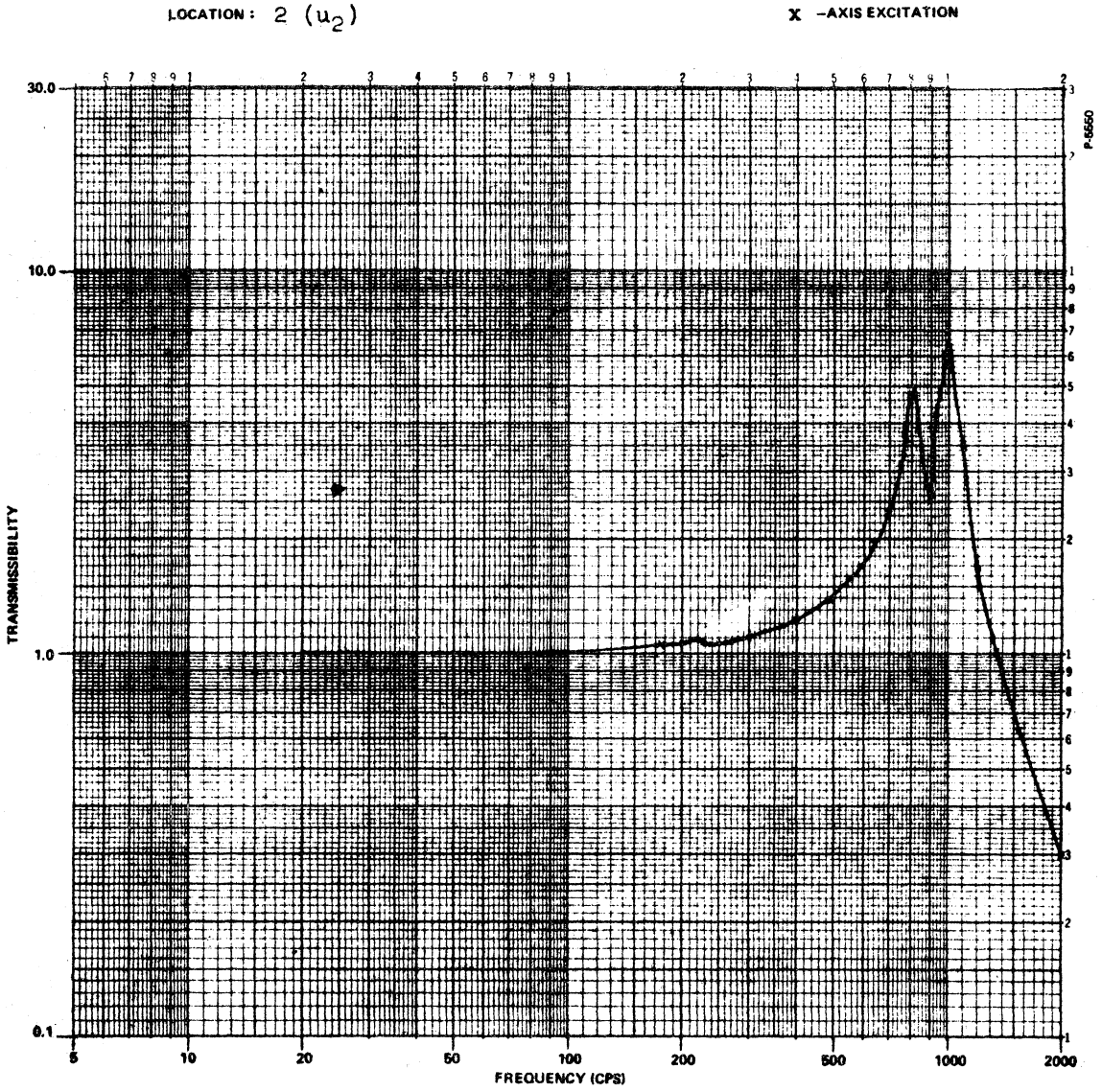

Figure 4.4. Transmissibility data; x-axis excitation; location 2.

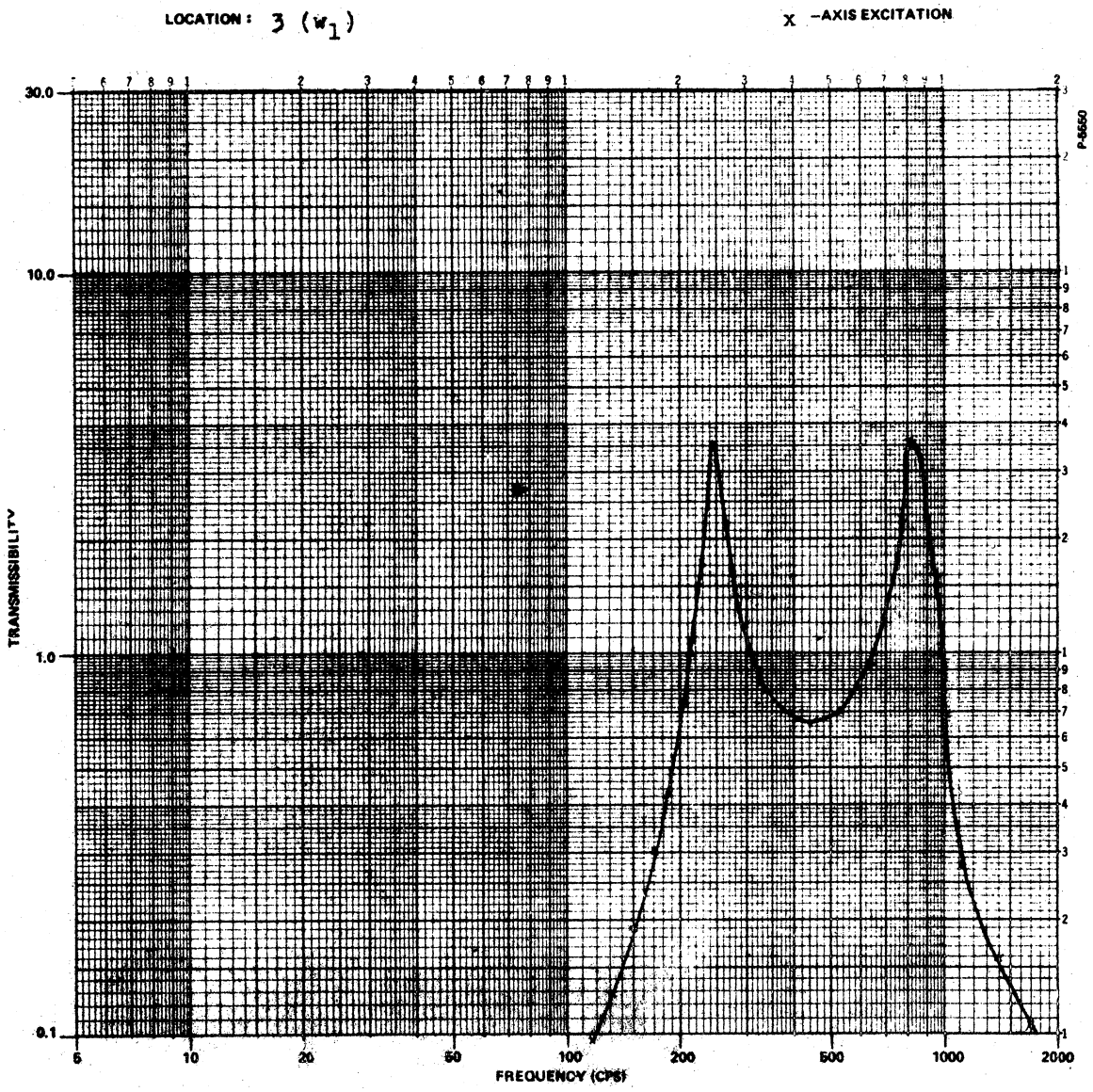

Figure 4.5. Transmissibility data; x-axis excitation; location 3.

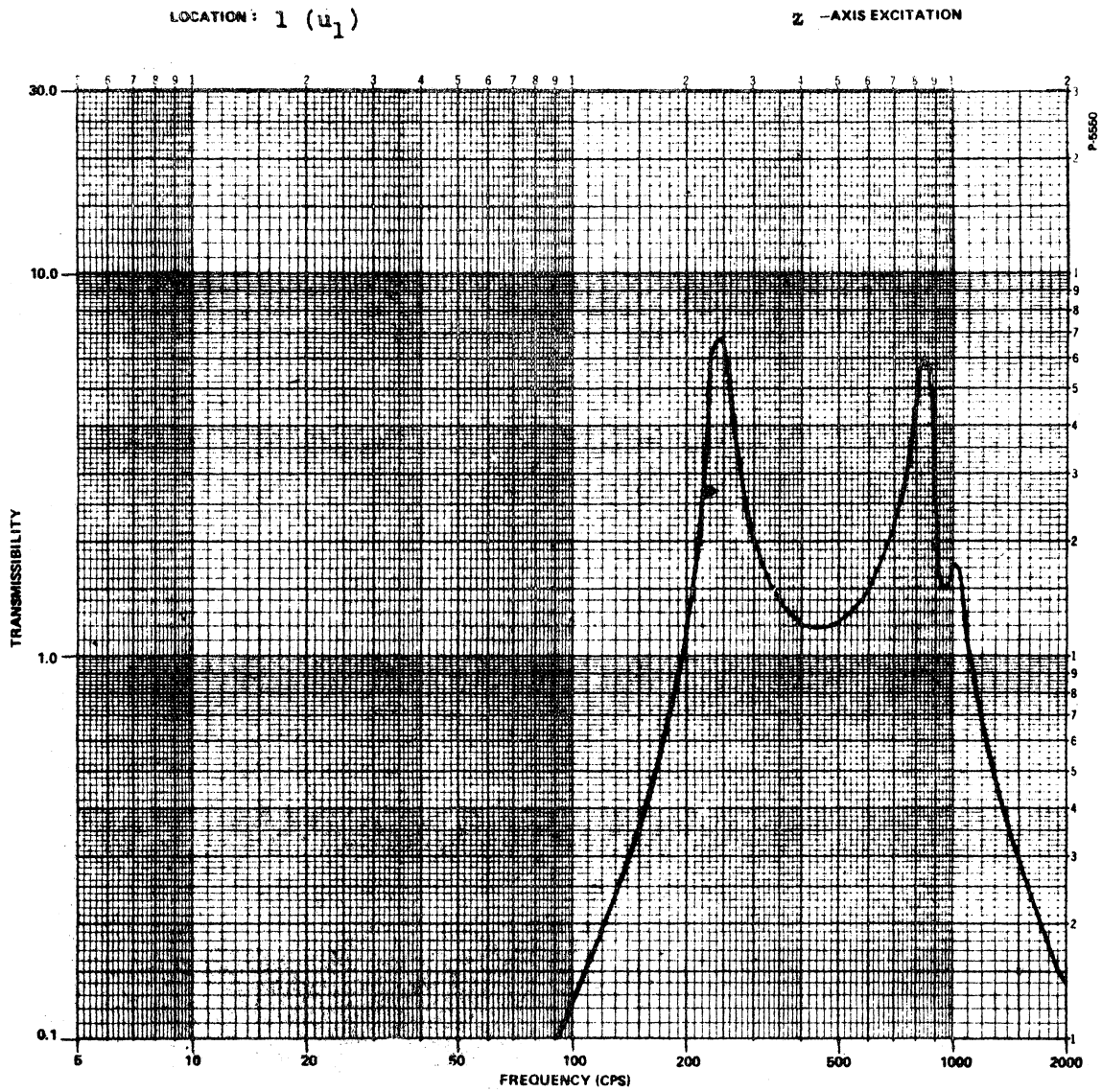

Figure 4.6. Transmissibility data; z-axis excitation; location 1.

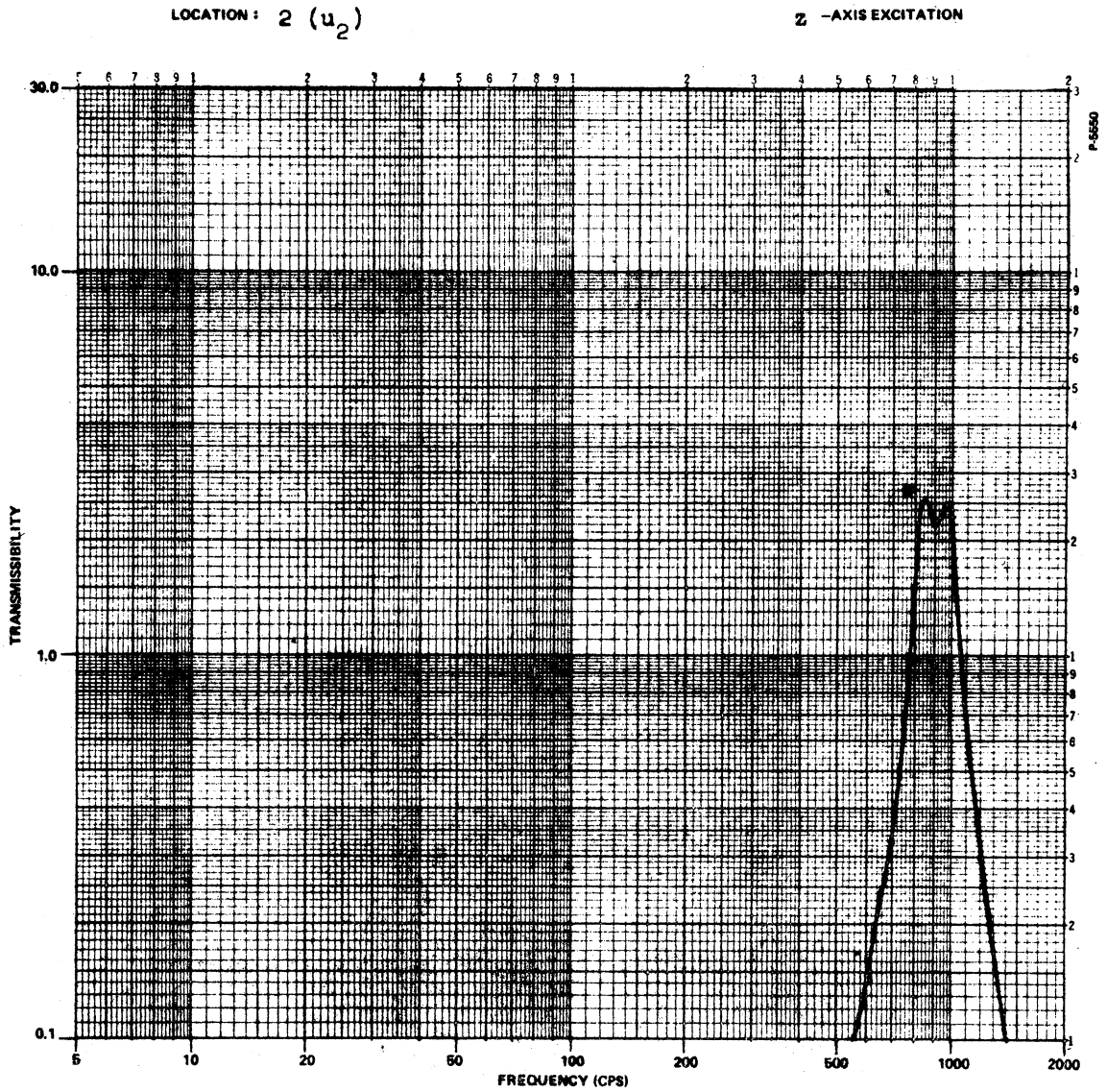

Figure 4.7. Transmissibility data; z-axis excitation; location 2.

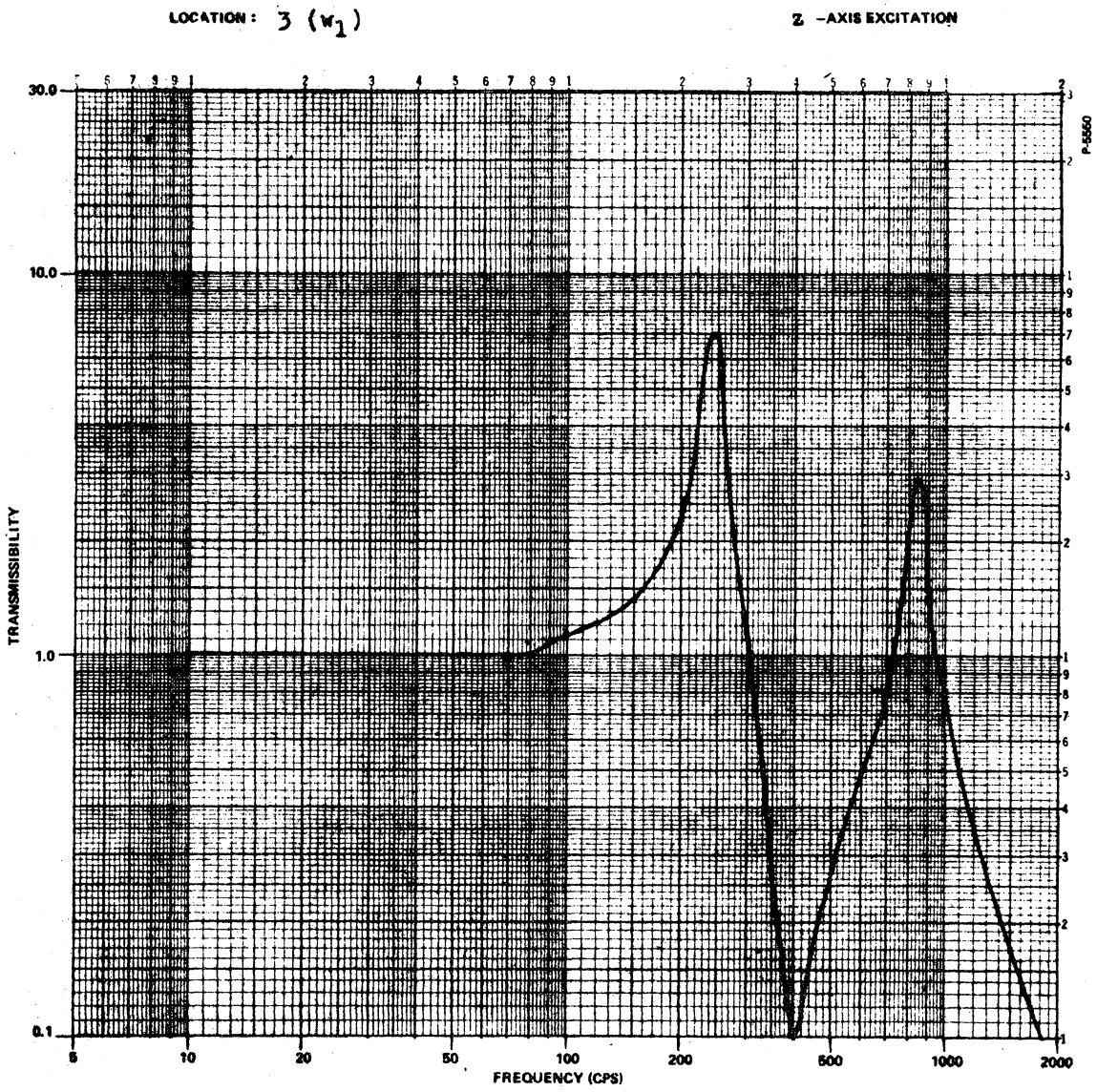

Figure 4.8. Transmissibility data; z-axis excitation; location 3.

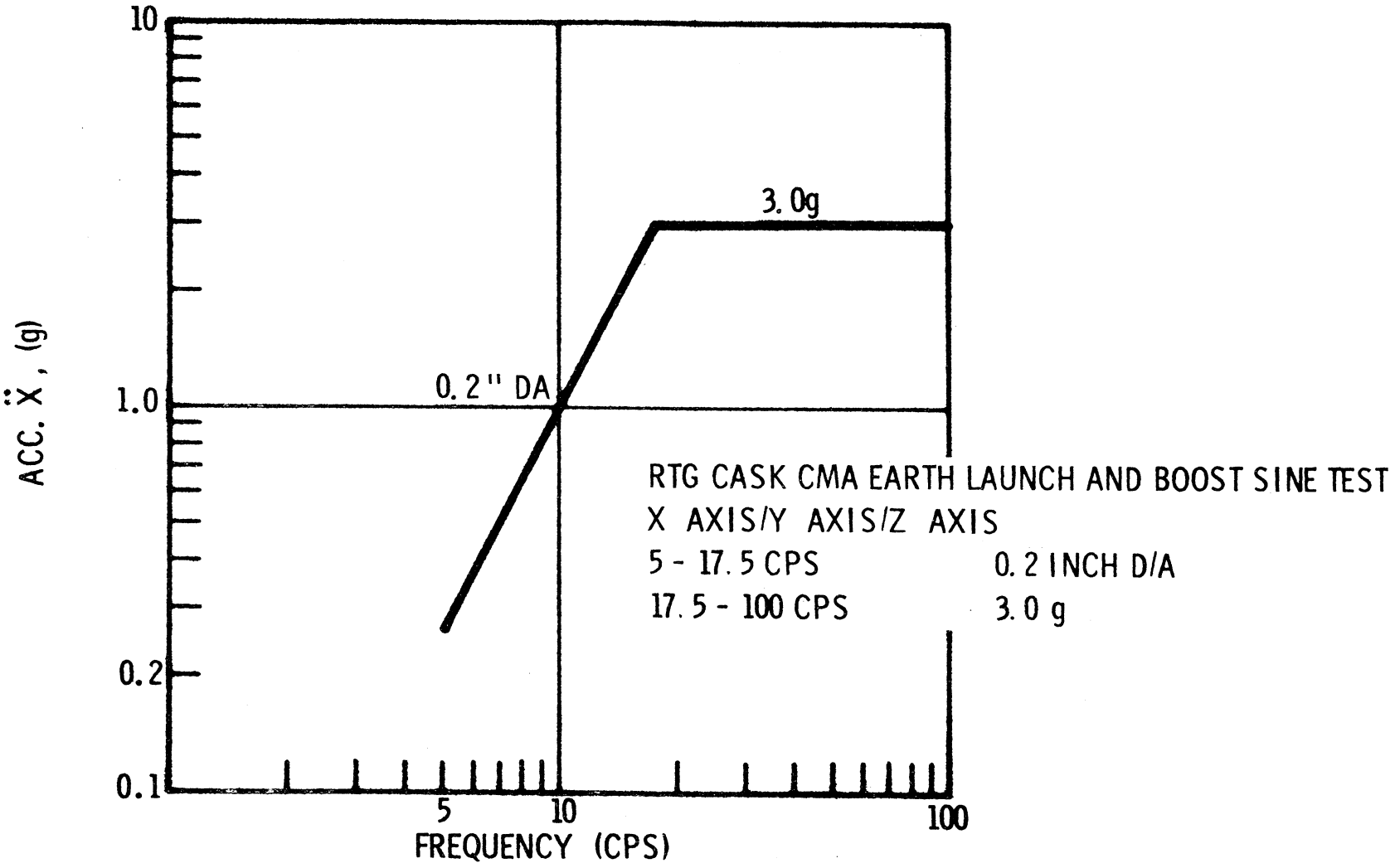

Figure 4.9. Input random vibration level.

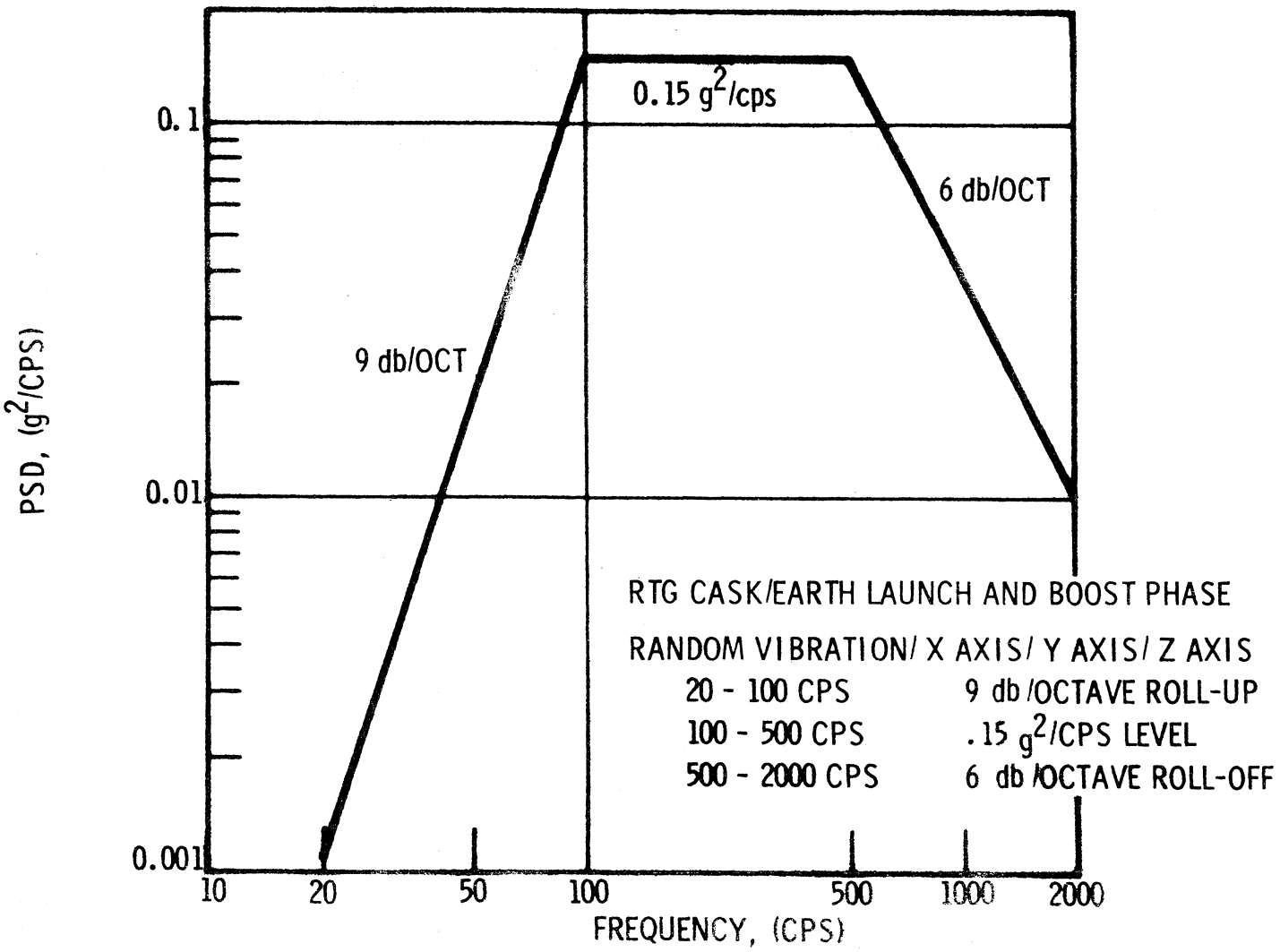

Figure 4.10. Input random.

1. Response to the sinusoidal excitation

$$\ddot{X}_r(f) = T(f)\,\ddot{X}_o(f)$$

2. Response to the random excitation

$$PSD_r(f) = T^2(f)\,PSD_o(f)$$

where, T(f) is the transmissibility as a function of frequency (CPS) in a given direction (Figures 4.3 to 4.8); $\ddot{X}$ is the acceleration (in g's); PSD is the power spectral density (g^2/CPS); the subscript "o" denotes input, while "r" denotes response.

Since the range of the sinusoidal inputs was from 5 to 100 cps, as indicated by Figure 4.10, and the resulting values of transmissibilities in this range were less than or equal to 1, then the values of $\ddot{X}_r$ were less than or equal to $\ddot{X}_o$. Hence, sinusoidal excitations were not detrimental to the stability of the system. However, the PSD versus frequency curves are shown in Figures 4.11 to 4.16, here, the RMS responses are the equivalent "g" loadings. The results of this preliminary analysis indicated that the cask assembly would withstand the imposing vibration environment it should encounter during the flight. However, a more extensive analysis was needed before testing could proceed.

Three-Dimension Model

With the accumulation of more information on the design of the cask assembly a three-dimensional model was developed. This model was a much better

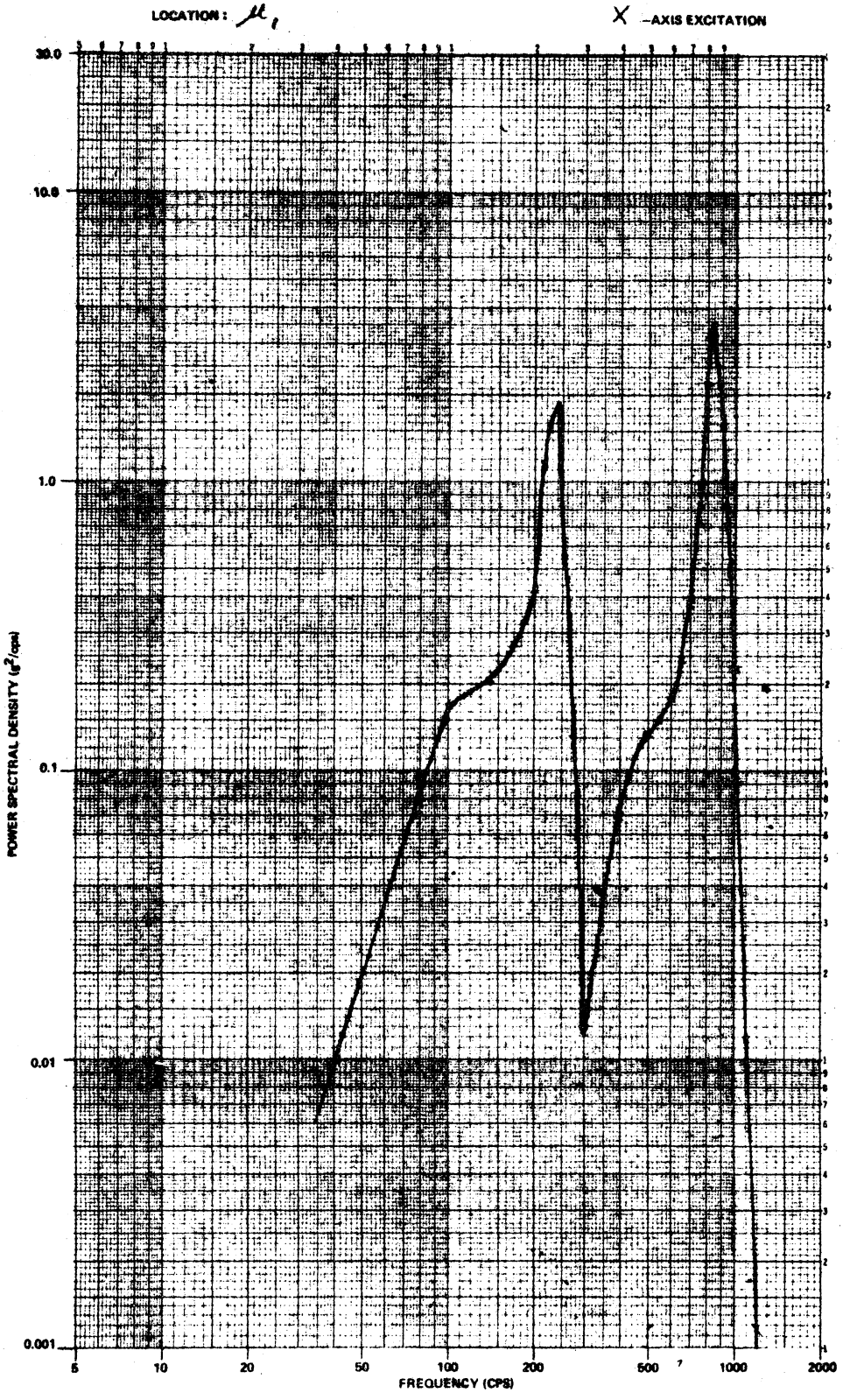

Figure 4.11. Random vibration spectrum; x-axis excitation; location 1.

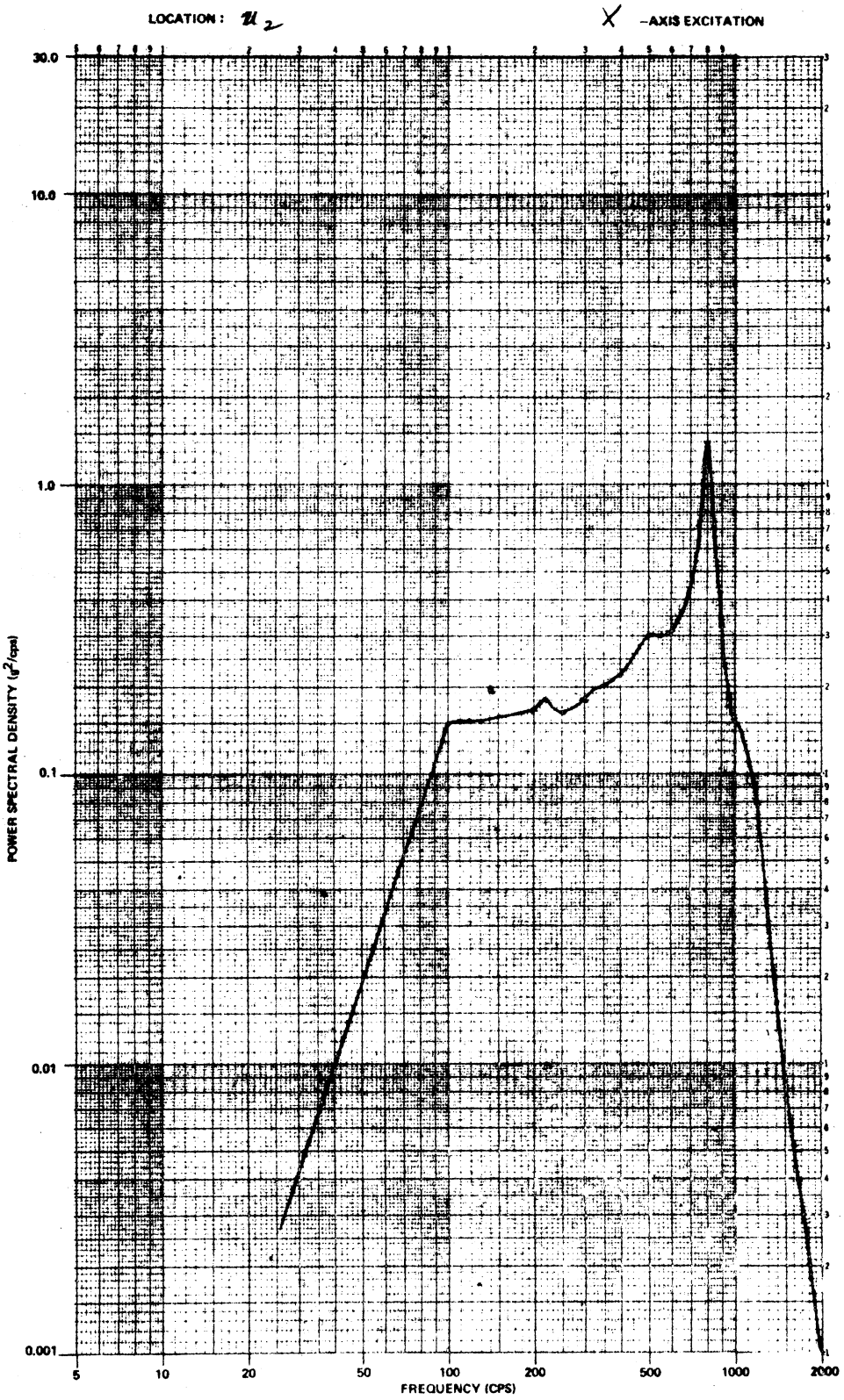

Figure 4.12. Random vibration spectrum; x-axis excitation; location 2.

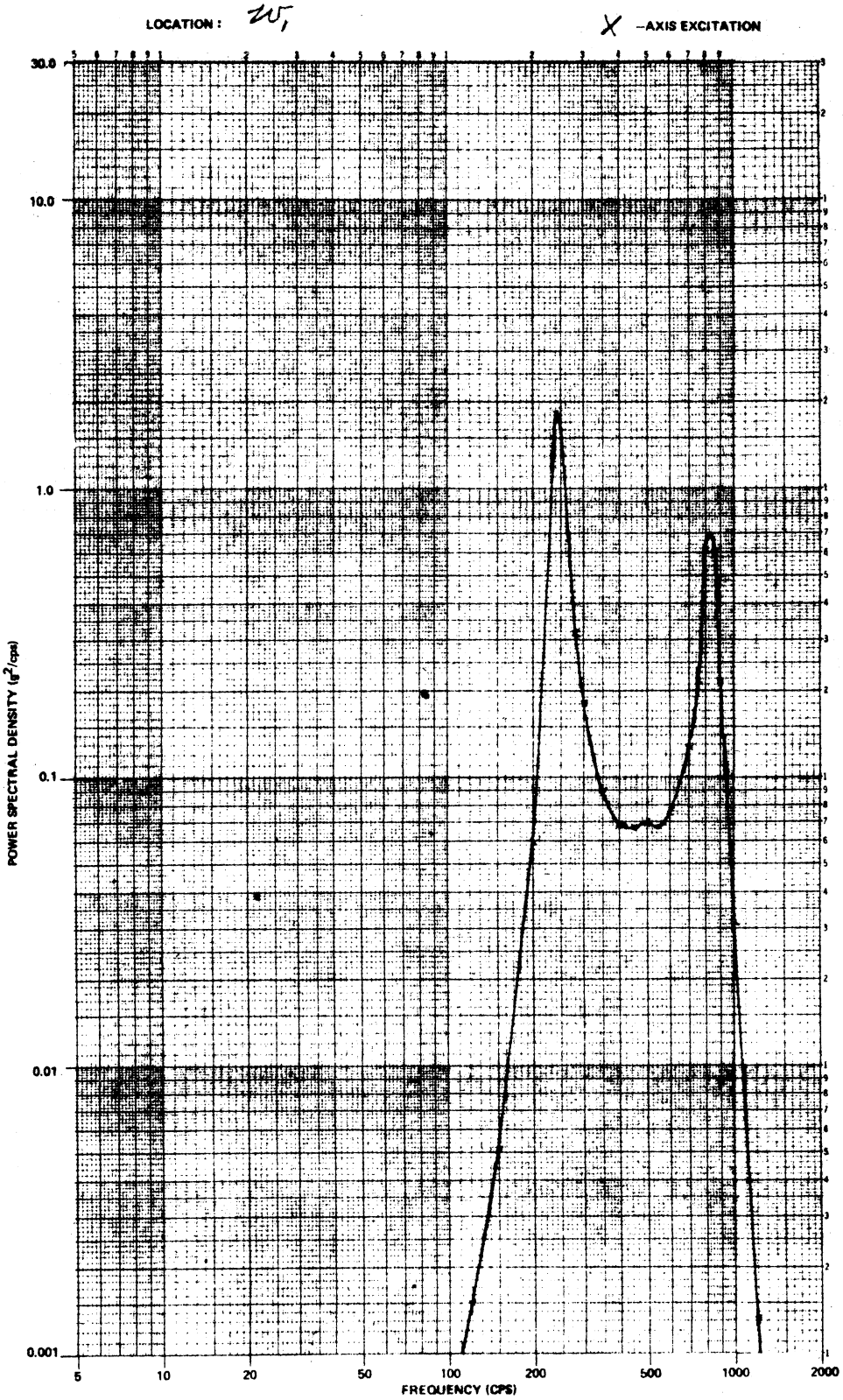

Figure 4.13. Random vibration spectrum; x-axis excitation; location 3.

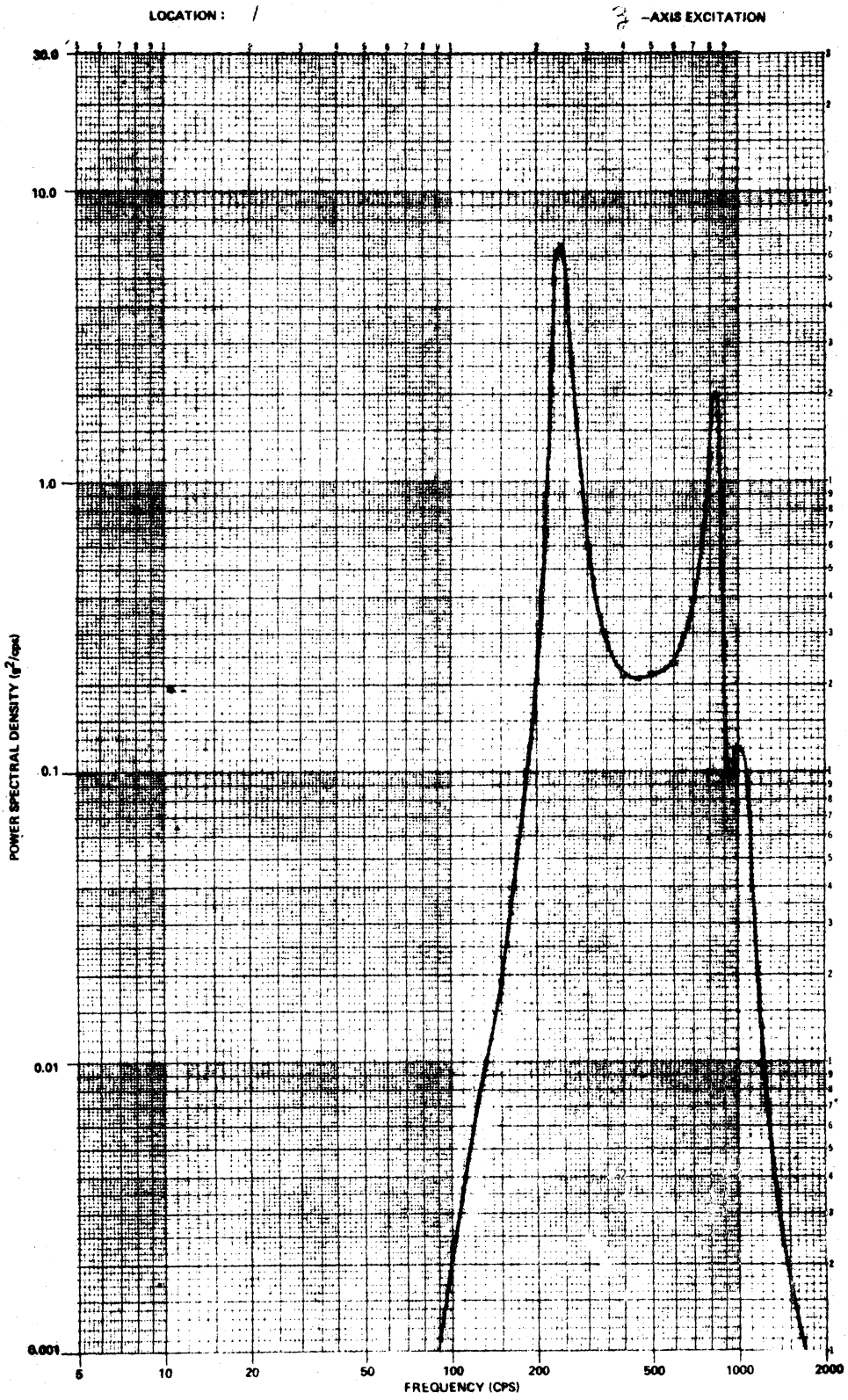

Figure 4.14. Random vibration spectrum; z-axis excitation; location 1.

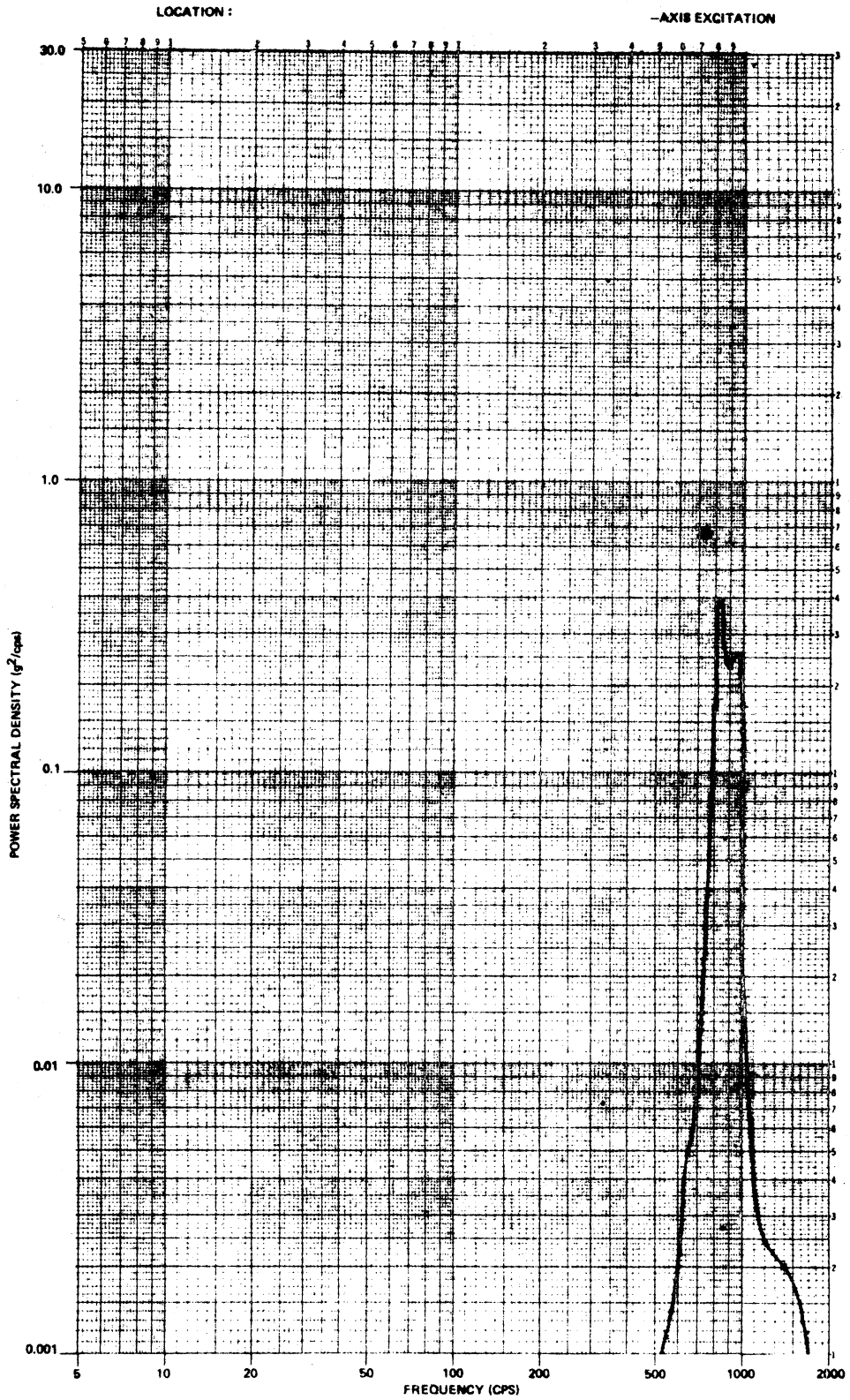

Figure 4.15. Random vibration spectrum; z-axis excitation; location 2.

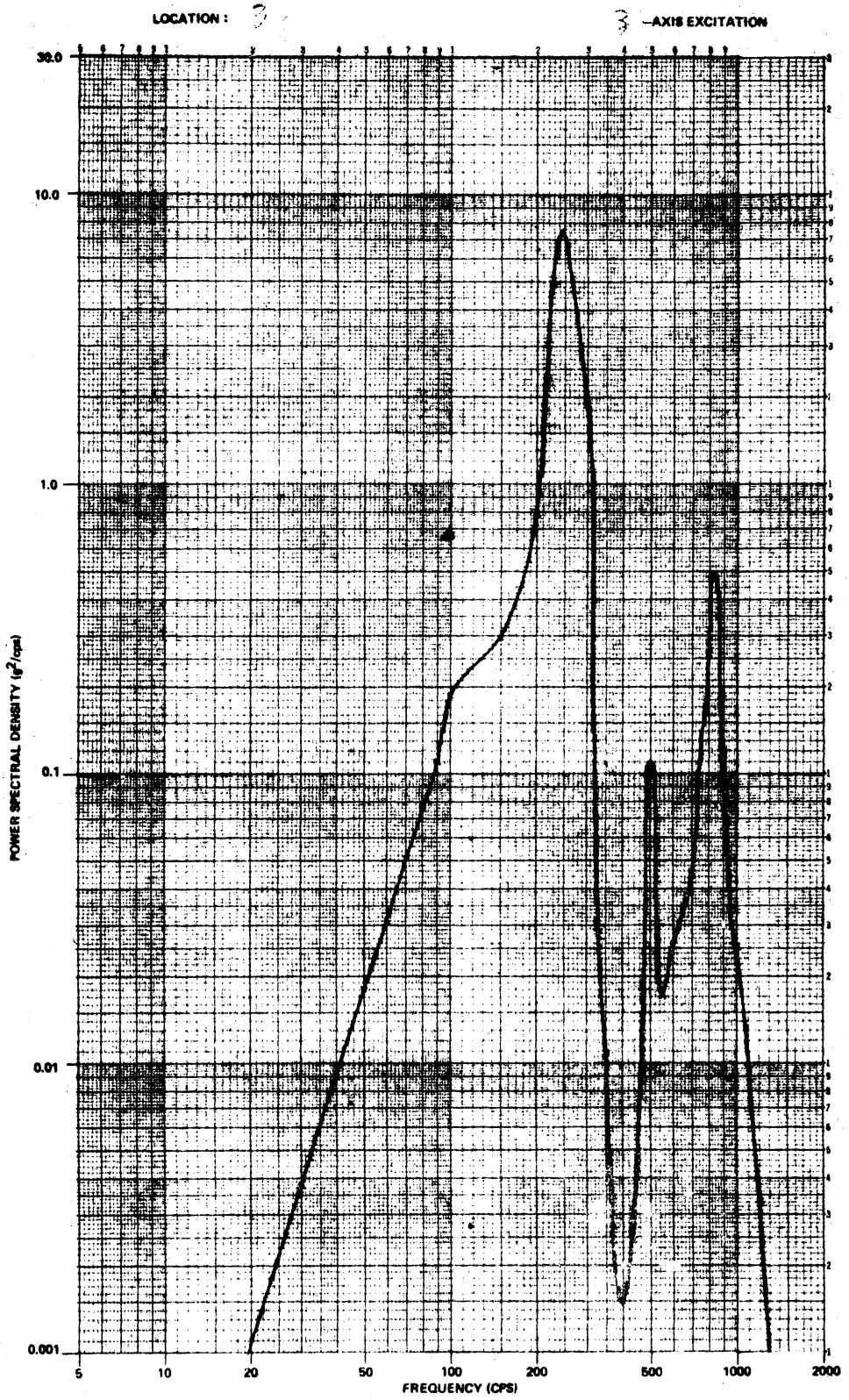

Figure 4.16. Random vibration spectrum; z-axis excitation; location 3.

attempt to predict the behavior of the system. In this analysis six degrees-of-freedom were considered and provision was given to the unsymmetrical weight distribution at the four supporting points in addition to the cask weight at its own CG.

Again as in the two-dimensional analysis, the actual physical model of the system is shown in Figure 4.1. However, a slightly simplified model shown in Figure 4.17 was used for the dynamic analysis. (Table 4.1 shows the data given and the location of the loads used in this analysis.) In addition, the following assumptions and restraints were made in developing the mathematical formulation:

(1) The fuel cask was rigid and axially symmetric.

(2) The mounting structure assembly supports with the LM were rigid.

(3) The truss members in the mounting structure were treated as massless springs which would contribute only to the stiffness, although half of the total weight of the mounting structure was approximately (not equally) distributed at the four supporting points between the cask and the trunnions.

(4) The system damping was assumed to be viscous.

(5) Six modes of loading, namely the axial load, torsion, two lateral loads, and two bendings in two orthogonal directions at each end of the beam element were considered. Moreover, the six general loading modes for the U-members were derived and incorporated in the analysis.

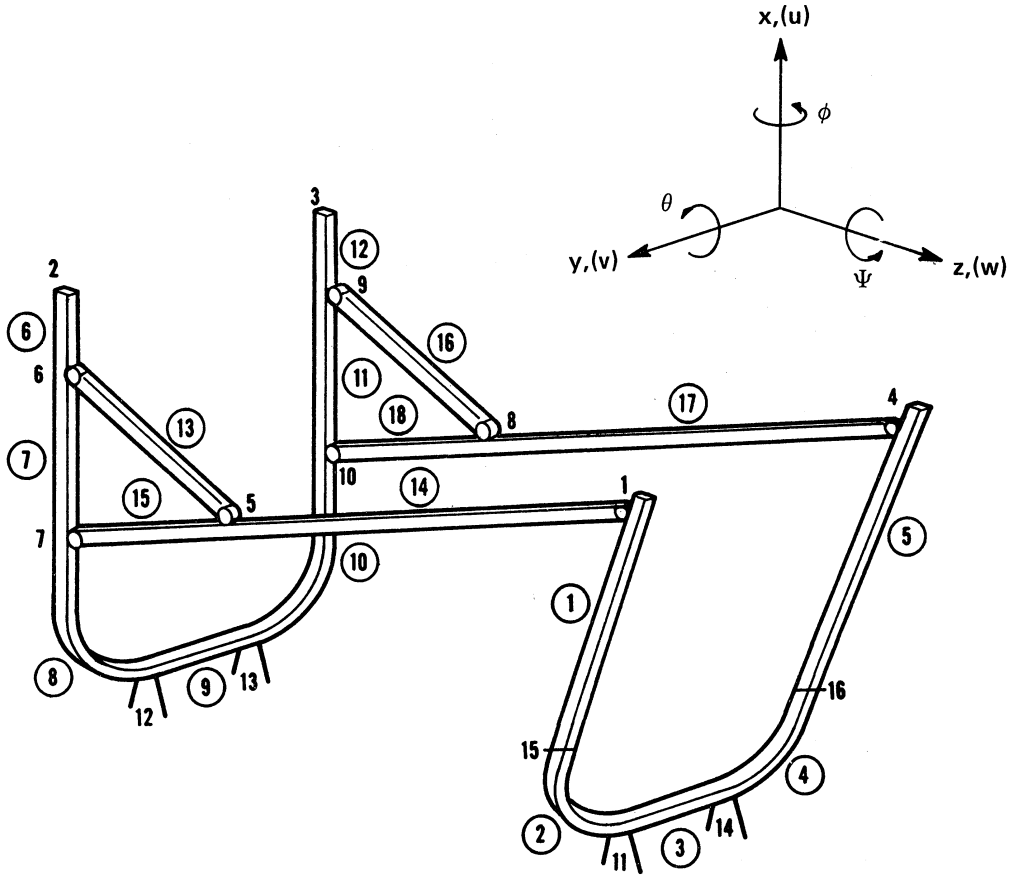

1 2 3 4 – INTERFACE SUPPORTING POINTS OF THE FUEL CASK AND THE BENDIX MOUNTING STRUCTURE

11 12 13 14 – INTERFACE JOINTS OF THE BENDIX AND GRUMMAN STRUTS

Note: Uncircled numerals denote nodal designation and circled numerals denote sectional designation.

Figure 4.17. Three-dimensional model.

TABLE 4.1

GIVEN AND LUMPED WEIGHTS FOR THE THREE-DIMENSIONAL MODEL

Given Data:

W_C (Cask assembly including shell and fuel element) = 39.7 lb

W_B (Bands) = 4 lb

W_G (Gear Box Unit) = 1.2 lb

$W_{uc} = W_{\text{upper cradle}} = 2.6$ lb

$W_{lc} = W_{\text{lower cradle}} = 2.6$ lb

$W_{dm} = W_{\text{diagonal member}} = 0.447$ lb

$W_{bm} = W_{\text{bracing member}} = 0.078$ lb

$W_b = W_{\text{bolts}} = 0.5$ lb

$I_{xx} = I_{yy} = 1792$ lb-in.^{2}

$I_{zz} = 338.2$ lb-in.^{2}

Lumped Weights in Calculation:

$$W_{B1} = W_{B4} = \frac{1}{2} \times \frac{2.25}{3.87} \times W_B = 1.162 \text{ lb}$$

$$W_{B2} = W_{B3} = \frac{1}{2} \times \frac{1.62}{3.87} \times W_B = 0.838 \text{ lb}$$

$$W_{s1} = W_{s4} = \frac{1}{2} \times \left(\frac{1}{3} W_{uc} + W_{dm}\right) + \frac{1}{8} \times W_b = 0.7195 \text{ lb}$$

$$W_{s2} = W_{s3} = \frac{1}{2} \times \frac{1}{3} W_{lc} + W_{bm} + \frac{1}{8} \times W_b = 0.571 \text{ lb}$$

$$W_1 = W_4 = W_{B1} + W_{s1} = 1.8815 \text{ lb}$$

$$W_2 = W_{B2} + W_{s2} + W_G = 2.609 \text{ lb}$$

$$W_3 = W_{B3} + W_{s3} = 1.409 \text{ lb}$$

(6) To correlate the absolute coordinate (x,y,z) to the relative coordinates (u,v,w) and the inputs (X_o, Y_o, Z_o), the following relationships were used in the derivation:

$$x_j = u_j + x_o$$

$$y_j = v_j + y_o$$

$$z_j = w_j + z_o$$

where the subscript j denotes the locations of the supporting points, i.e., j = 1, 2, 3, 4.

(7) A solid body motion of the cask assembly was assumed. Consequently, the following kinematic relationships were used for the cask configuration of concern:

$$u_4 = u_1 - u_2 + u_3$$

$$v_1 = v_4$$

$$v_2 = v_3$$

$$w_1 = w_2$$

$$w_3 = w_4$$

$$w_1 = w_4 - \frac{2c}{a+b} v_1 + \frac{2c}{a+b} v_2$$

Therefore, the six degrees-of-freedom in the relative coordinates at the desired supporting points 1, 2, 3, and 4 are sufficient to be described by u_1, u_2, u_3, v_1, v_2, w_1 which explicitly relate to three of the four

supporting points.

Similar although more complex than the two-dimensional analysis, the governing matrices were determined for the three-dimensional case. However due to the mass distribution assumed for this model, the energy-Lagrange model was used in forming the mass and forcing matrices. Because the systems damping ratio was unknown two sets of data with different damping constant were obtained from the numerical calculations. Also, at the time of this analysis the joining mode between the cask and the trunnions was uncertain due to the presence of bands encircling the cask. Consequently, two distinct boundary conditions were possible, they were, fixed or hinged joints at points 1, 2, 3, and 4 of Figure 4.17. Therefore, four sets of results were obtained as follows:

Case 1 Fixed-end supports with 5% of the critical viscous damping.*

Case 2 Fixed-end supports with 10% of the critical viscous damping.

Case 3 Hinged-end supports with 5% of the critical viscous damping.

Case 4 Hinged-end supports with 10% of the critical viscous damping.

The computer results yielded six sets of natural frequencies summarized below, included are the natural frequencies calculated from the two-dimensional analysis for the purpose of comparison.

*As in the two-dimensional analysis, the hysteresis damping was assumed to be viscous for simplification.

Natural Frequencies: in CPS

Case 1 and Case 2	Case 3 and Case 4	2-D Case
70 (w)	43 (v)	---
86 (v)	68 (w)	---
127 (v)	108 (v)	246 (w)
309 (u)	278 (u)	837 (u)
562 (u)	516 (u)	---
703 (u)	659 (u)	1002 (u)

Calculations of the responses ($\ddot{X}_r$,PSD_r) to sinusoidal excitations and random excitations were obtained using the formulas discussed for the two-dimensional model on page 83. The same input excitations were used ($\ddot{X}_o$,PSD_o), shown in Figures 4.9 and 4.10. As a result, this analysis produced 72 graphs representing T vs. f, $\ddot{X}_r$ vs. f, PSD_r vs. f, for all three directions (x,y,z), and for all four cases.

Of particular importance were the responses due to sinusoidal excitations and random excitations the results of which are summarized in Tables 4.2 and 4.3. From these tables it was apparent the maximum "g" loading due to sinusoidal or random vibrations was 34 g.

Since the stress analysis of the cask support structure was based on 60 g loading, a safety factor of 1.8 was established based on "g" loading due to the vibrational environment of the launch and boost phase of the flight. (Note: NASA specified that the 14 g acceleration loads would not be combined with the vibration loads during launch and boost.) Satisfied with the results of the dynamic analysis, GE sent BxA a prototype cask for the actual vibrations testing conducted at the BxA Research Laboratories.

TABLE 4.2

RESPONSES DUE TO SINUSOIDAL EXCITATIONS

LOCATION*	EXCITATION	RESPONSE (g)			
		CASE 1	CASE 2	CASE 3	CASE 4
1 (u_1)	x	9.0	5.9	9.7	6.1
	y	3.4	1.8	1.9	0.9
	z	17.5	8.9	17.5	8.8
2 (u_2)	x	3.4	3.0	3.0	3.0
	y	3.0	1.8	2.0	0.9
	z	**	**	**	**
3 (u_3)	x	3.1	3.0	3.1	3.0
	y	3.0	1.7	1.9	0.9
	z	**	**	**	**
4 (v_1)	x	**	**	**	**
	y	34.0	18.5	33.5	16.7
	z	**	**	**	**
5 (v_2)	x	**	**	**	**
	y	27.0	11.5	29.5	12.8
	z	**	**	**	**
6 (w_1)	x	10.0	5.6	10.0	5.9
	y	3.1	1.9	1.9	1.0
	z	21.9	10.8	20.0	10.8

*"Location" denotes where an accelerometer may be placed and measures the respondent acceleration in a given axis due to a given excitation.

**Response is much less than 1.

TABLE 4.3

THE ROOT-MEAN-SQUARE RESPONSES DUE TO THE RANDOM EXCITATION

LOCATION*	EXCITATION	Root-Mean-Square Response (g)			
		CASE 1	CASE 2	CASE 3	CASE 4
1 (u_1)	x	21.6	15.2	20.05	14.16
	y	4.2	3.1	2.29	1.67
	z	15.8	11.3	15.37	10.96
2 (u_2)	x	34.0	23.8	34.20	23.71
	y	3.78	2.41	2.04	1.55
	z	1.56	1.06	1.89	1.28
3 (u_3)	x	29.1	21.5	29.46	21.44
	y	4.66	3.31	2.57	1.82
	z	1.35	0.95	1.56	1.15
4 (v_1)	x	0.23	0.16	0.25	0.17
	y	12.4	8.49	3.27	2.36
	z	0.16	0.11	0.15	0.11
5 (v_2)	x	0.75	0.45	0.56	0.35
	y	9.18	6.66	2.92	2.16
	z	0.16	0.12	0.19	0.13
6 (w_1)	x	10.1	7.17	9.87	7.00
	y	2.1	1.38	0.93	0.63
	z	8.43	6.0	8.37	5.92

*"Location" denotes where an accelerometer may be placed and measures the respondent acceleration in a given axis due to a given excitation.

4.2 VIBRATIONS TESTING

Procedure

The object of the vibrations testing was to ascertain the reliability of the cask assembly when subjected to qualification level sinusoidal and random vibration levels at elevated temperatures. Tests were conducted on a prototype cask/support structure assembly at the launch and boost, and lunar descent temperatures established during the thermal/vacuum testing.

The input vibration test series were initiated and controlled at the cask support structure/LM strut interface. Figure 4.18 shows the test set-up including the accelerometer locations. Their purpose was to record the vibrations environment at the interface of the BxA support structure and GE cask. The following tests were conducted in each orthogonal axis as defined in Figure 4.18:

(a) Transmissibility survey (1 g sinusoidal sweep) from 5 to 2000 cps at launch and boost flight phase temperature (280°F)

(b) Transmissibility survey (1 g sinusoidal sweep) from 5 to 2000 cps at lunar descent flight phase temperature (600°F)

(c) Launch and boost phase sinusoidal vibration

(d) Launch and boost phase random vibration

The input specifications for the vibrations testing are given in Appendix II. However the input specifications for tests (c) and (d) are graphically shown in Figures 4.9 and 4.10.

1 Response Accelerometer in direction of vibration
4 Response Accelerometer in direction of vibration
5 Triaxial Response Accelerometer
6 Triaxial Response Accelerometer

NOTE: Location 2 and 3 will be used if the accelerometer blocks at locations 5 and 6 come off during vibration.

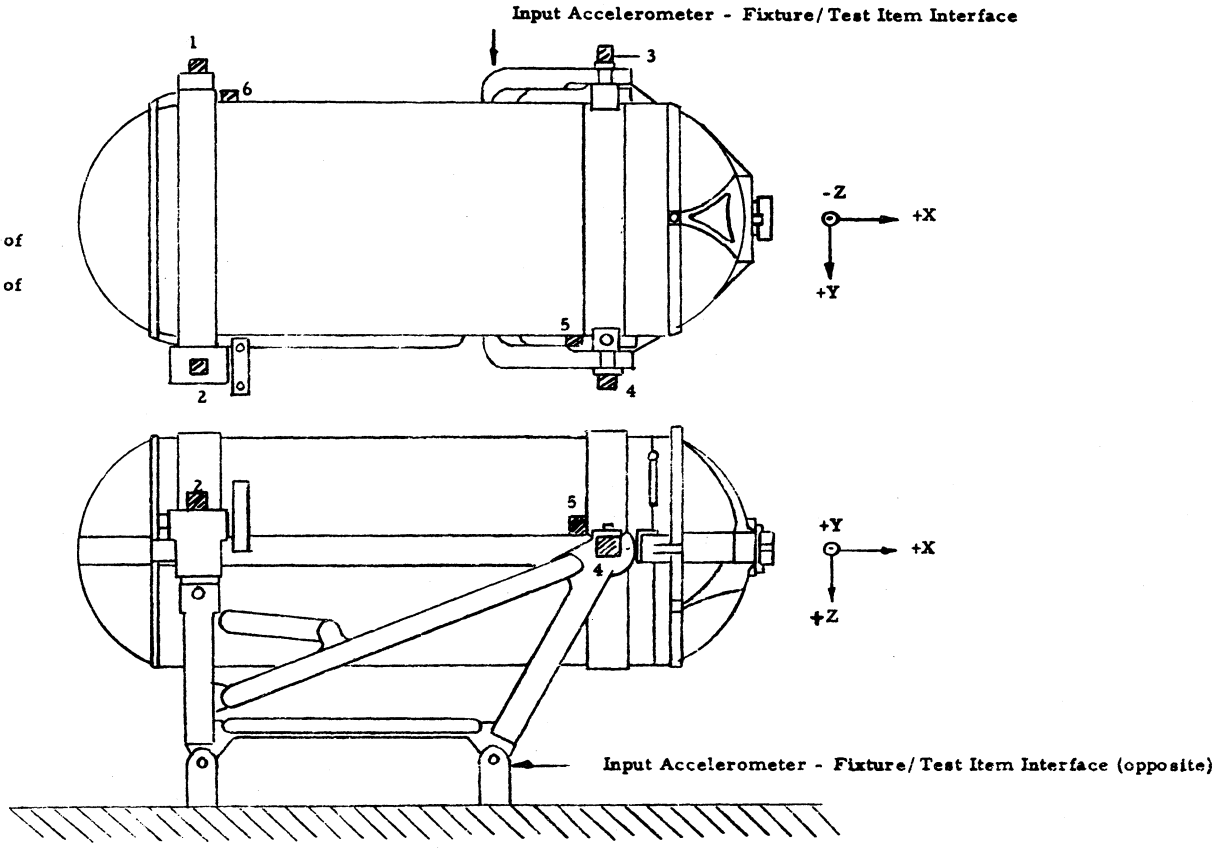

Figure 4.18. Accelerometer locations.

Results

The most important result of the vibrations testing was that there were no structural failures in the cask assembly. Also, an evaluation of the test results provided a set of cask vibration specifications for launch and boost, and descent stages of the Apollo flight, which were of particular interest to GE. Figures 4.19 to 4.23 represent a sample of the output obtained from the tests mentioned above. Figure 4.24 shows the cask sinusoidal vibration specification as determined from the equation: $\ddot{X}_r = T(f) \cdot \ddot{X}_o$. Moreover, the data obtained from the five accelerometer locations indicated no substantial differences from one location to another.

Because the qualification input levels for the lunar descent phase of the flight were considerably less than those for launch and boost (see Appendix II), the lunar descent sine and random tests were not conducted on the prototype cask assembly. However the temperature difference between the two phases of flight prompted BxA to run a 1 g sinusoidal survey from 5 - 2000 cps at the lunar descent temperature as indicated under test (b). With this data and the formula given in the preceding paragraph BxA was able to calculate the sinusoidal response at lunar descent conditions.

As with the sinusoidal data, the lunar descent random response data had to be calculated also. The formula is output equals input times the square of the transmissibility at a given frequency. However the lunar descent random vibrations levels were insignificant compared to the launch and boost levels and therefore did not warrant much attention.

Although the launch and boost and lunar descent phases of the flight

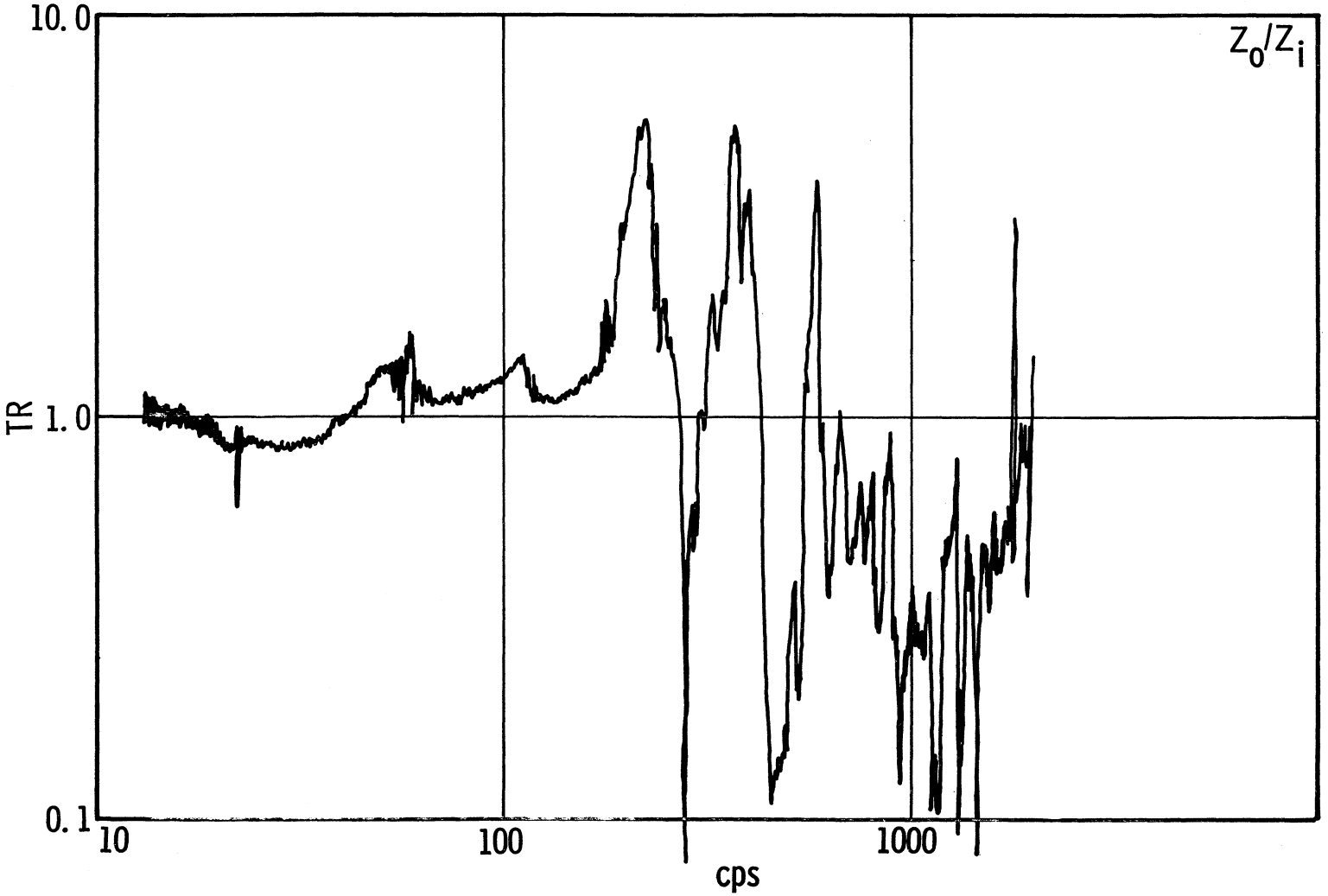

Figure 4.19. 1 g survey; launch and boost; z_o/z_i.

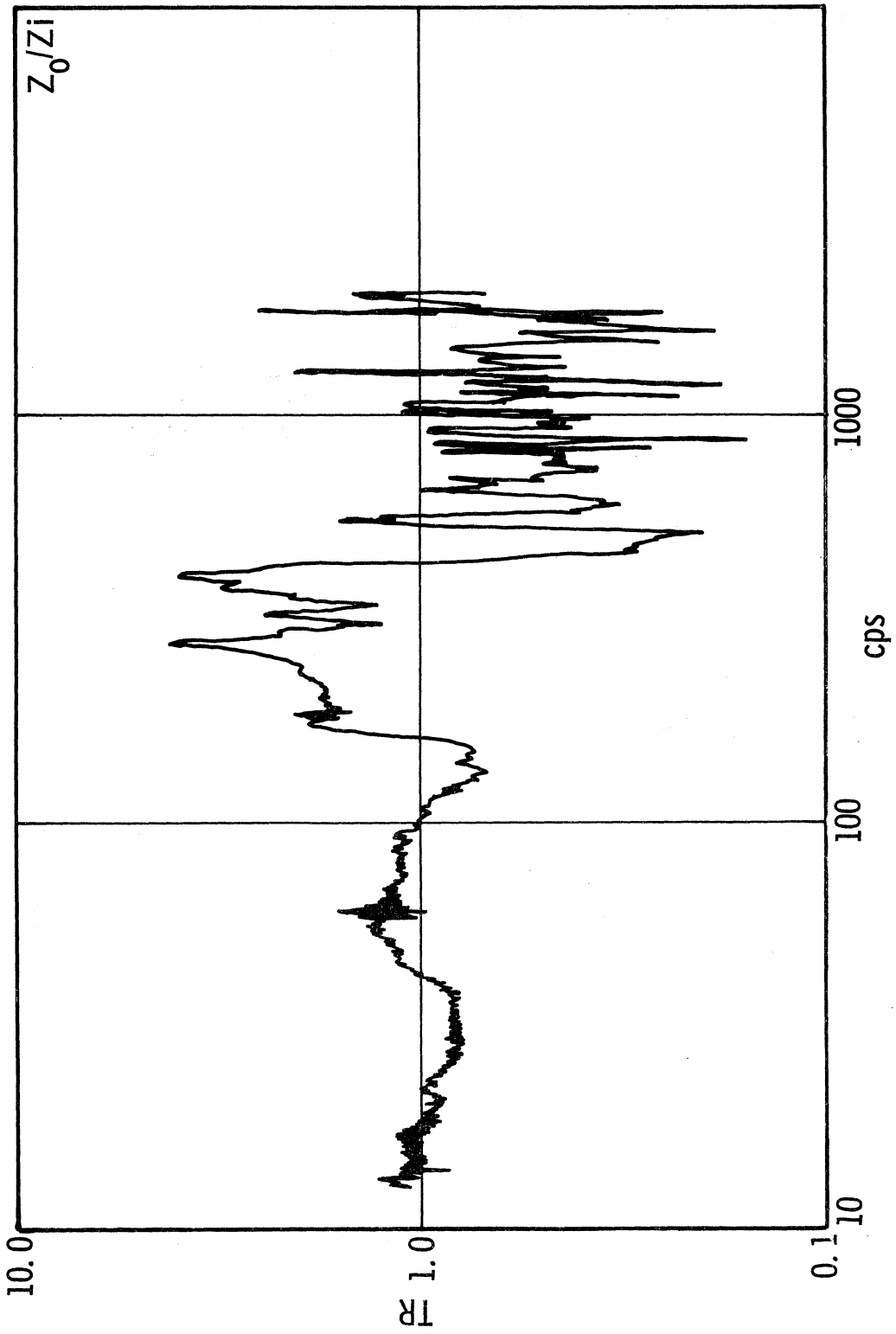

Figure 4.20. 1 g survey; lunar descent; z_o/z_i.

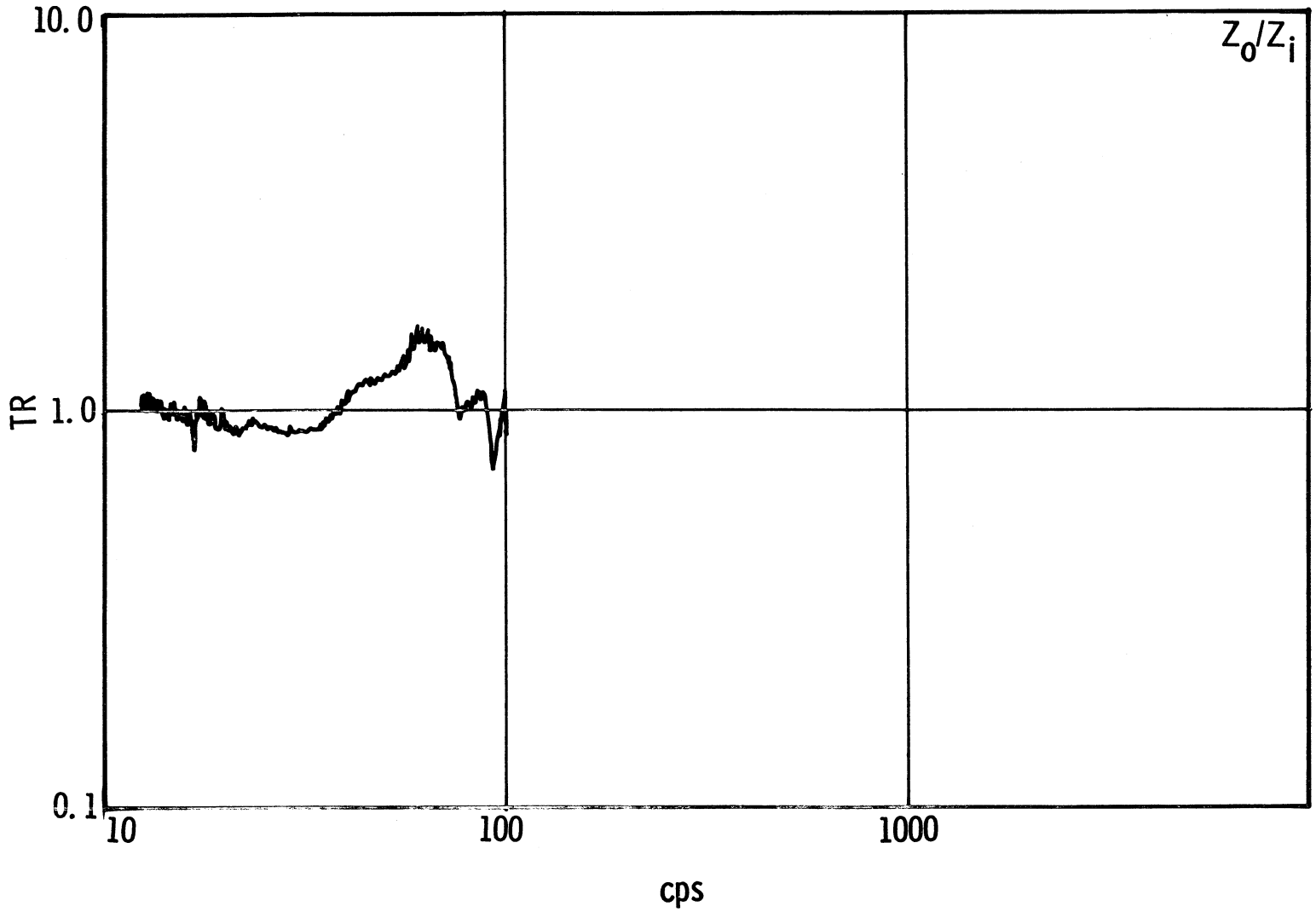

Figure 4.21. Sinusoidal vibration; launch and boost; z_o/z_i.

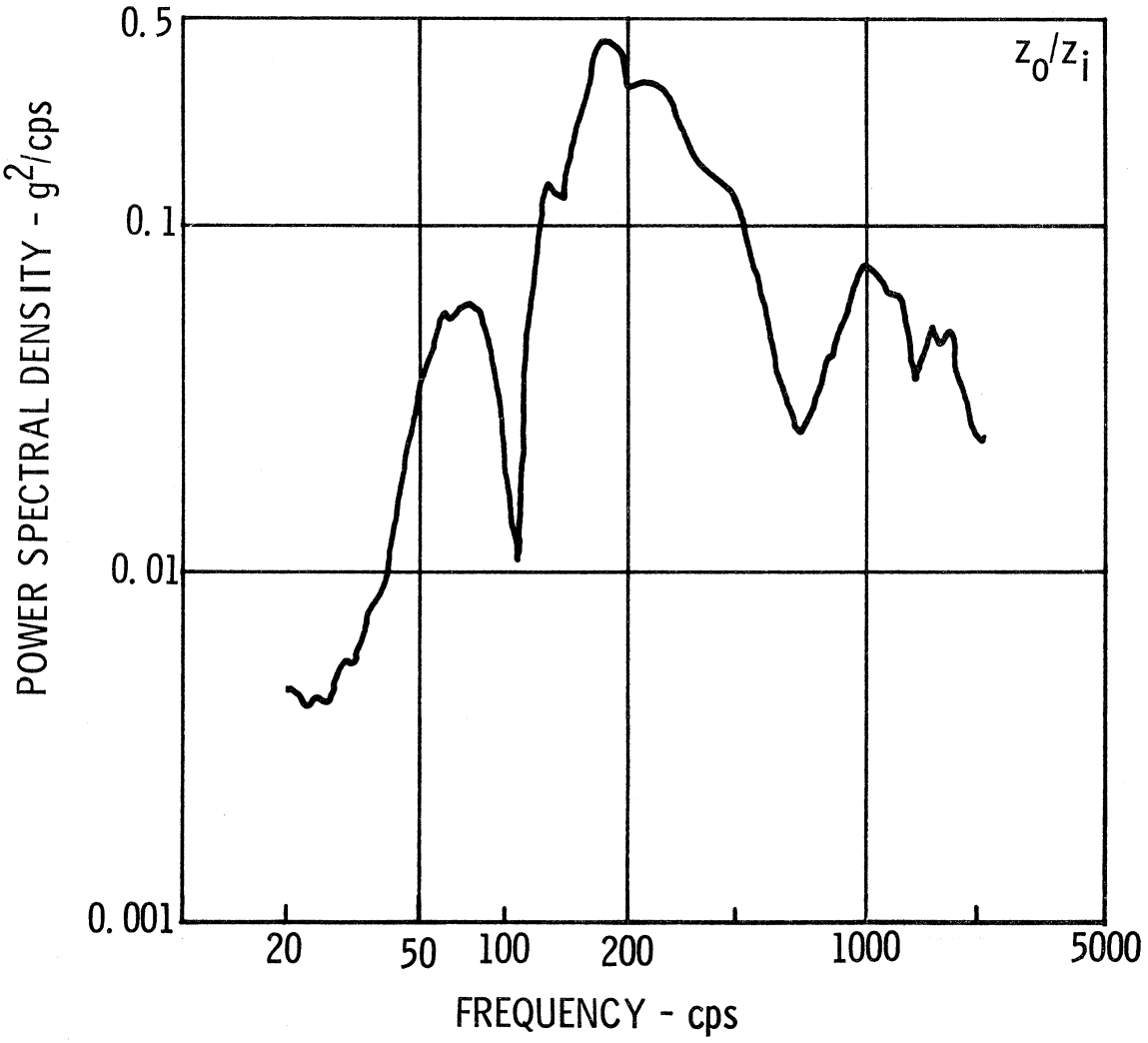

Figure 4.22. Random vibration spectrum; launch and boost; z_o/z_i.

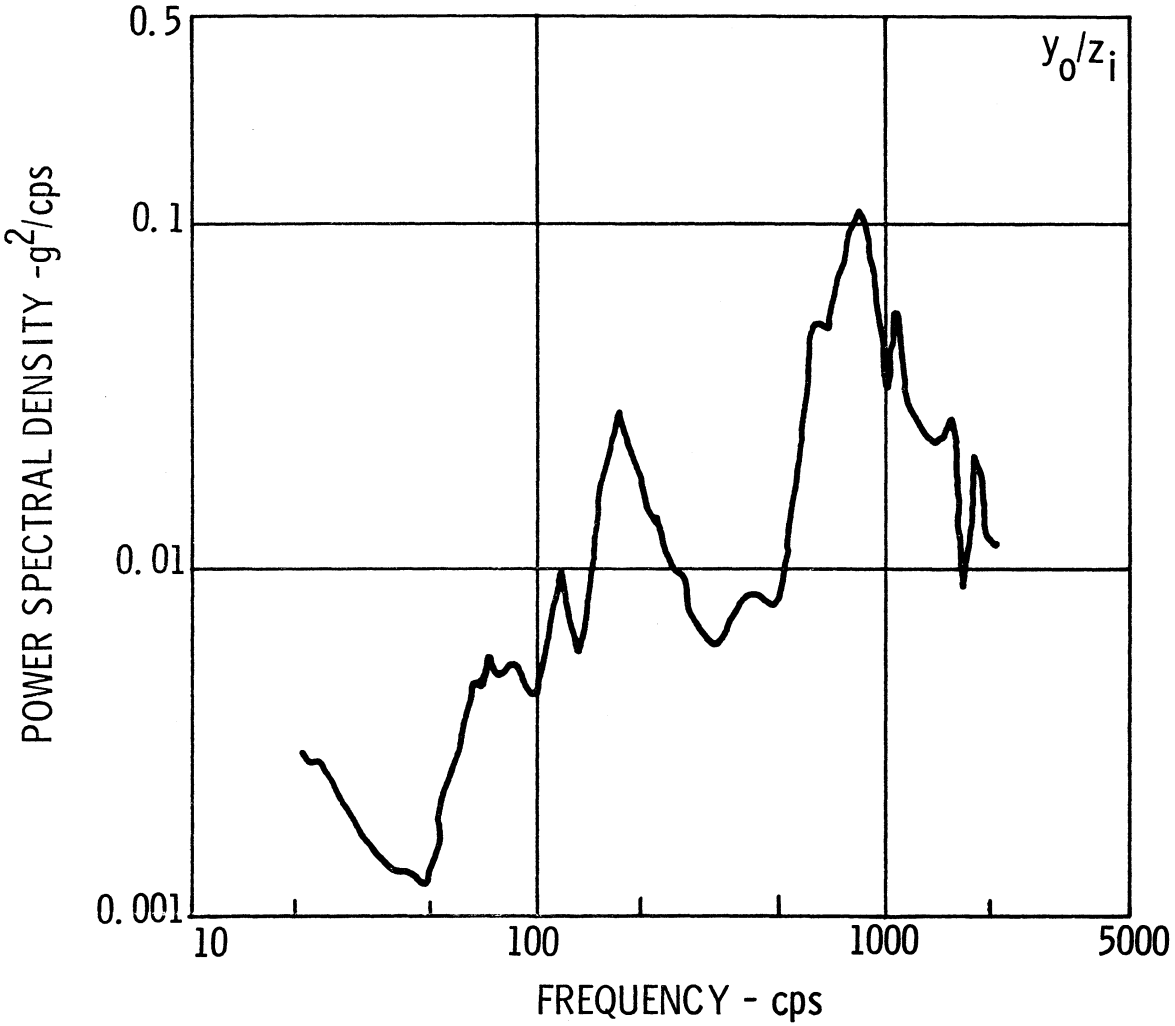

Figure 4.23. Random vibration spectrum; launch and boost; y_o/z_i.

x - axis :	5-23 cps	0.5 in. d.a.
	23-100 cps	13 g - peak
y - axis :	5-30 cps	0.5 in. d.a.
	30-100 cps	23 g - peak
z - axis :	5-18 cps	0.3 in. d.a.
	18-100 cps	5.0 g - peak

Figure 4.24. Fuel cask sinusoidal launch and boost input specification.

occurred at different temperatures (280°F and 600°F, respectively) this was not a significant effect. A comparison of the 1 g transmissibilities at the two temperatures showed that the transmissibilities increased slightly in the x and y directions as the temperature increased, however the opposite trend was noticed in the z direction.

4.3 ANALYSIS VS. TEST

The correlation between analysis (Case 4; hinged-end supports and 10% viscous damping; gave the best correlation) and test results were fairly good for transmissibility (1 g), but the calculated random and full level sinusoidal responses did not correlate with experimental results very well. The major factor attributed to the discrepancies was the presence of nonlinear damping. That is, generally the degree of damping within a structure is dependent upon the level of dynamic loading.

Figures 4.25, 4.26, and 4.27 graphically depict the comparison between analysis and test results for the full level sinusoidal excitation. In the x direction, the first mode transmissibility increased from 3.3 to 3.8. In the y direction, the transmissibility increased from 4.0 to 5.9 and the natural frequency shifted from 31 to 40 cps. There were no significant changes in the z direction for frequencies below 100 cps (the full level sinusoidal tests do not exceed 100 cps).

The combination of structural members which make up the cask support structure have an inherent damping mechanism which is not capable of absorbing energy beyond a certain limit. Therefore, when the energy put into the

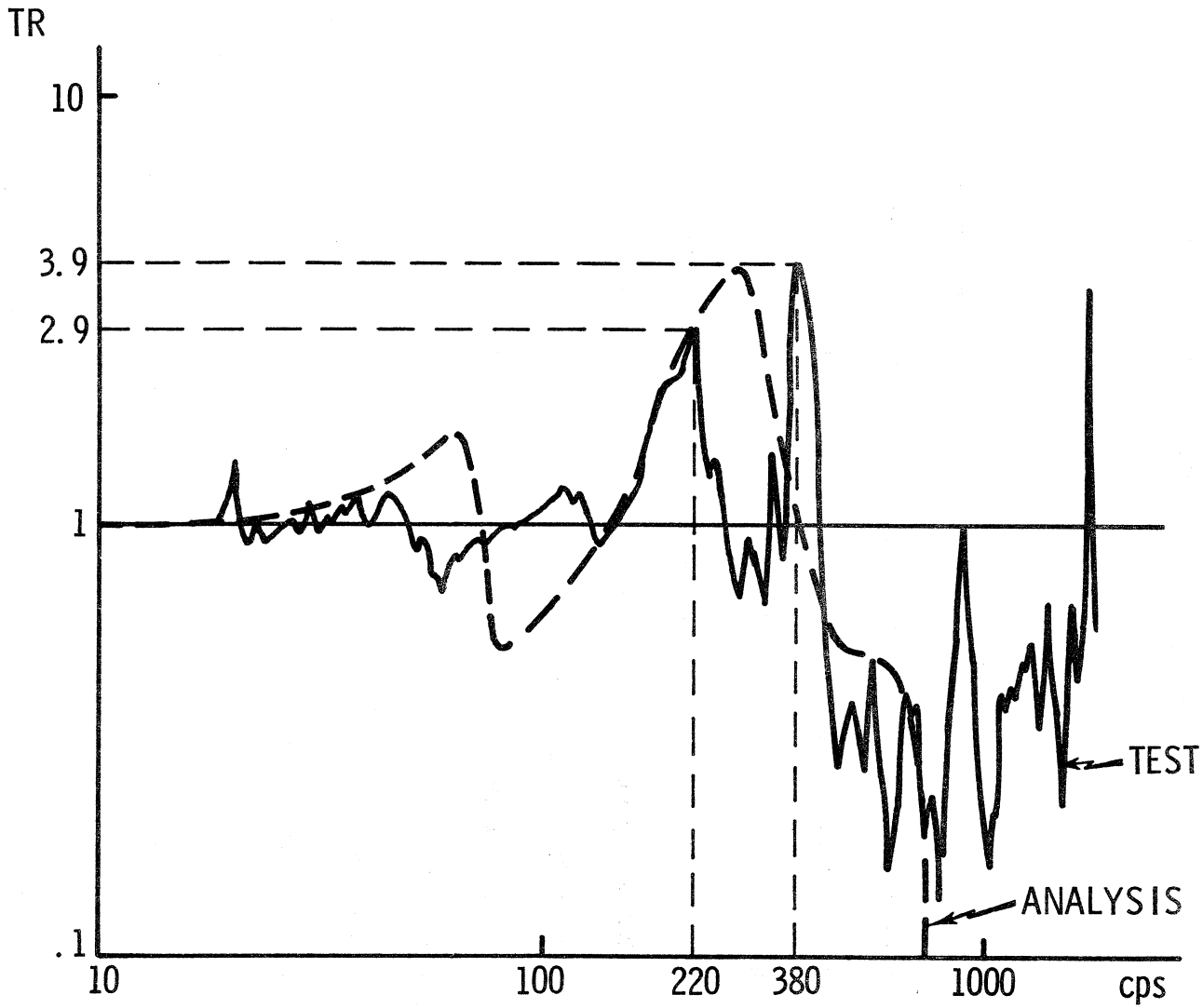

Figure 4.25. Analysis vs. test data; sinusoidal vibration; x_o/x_i.

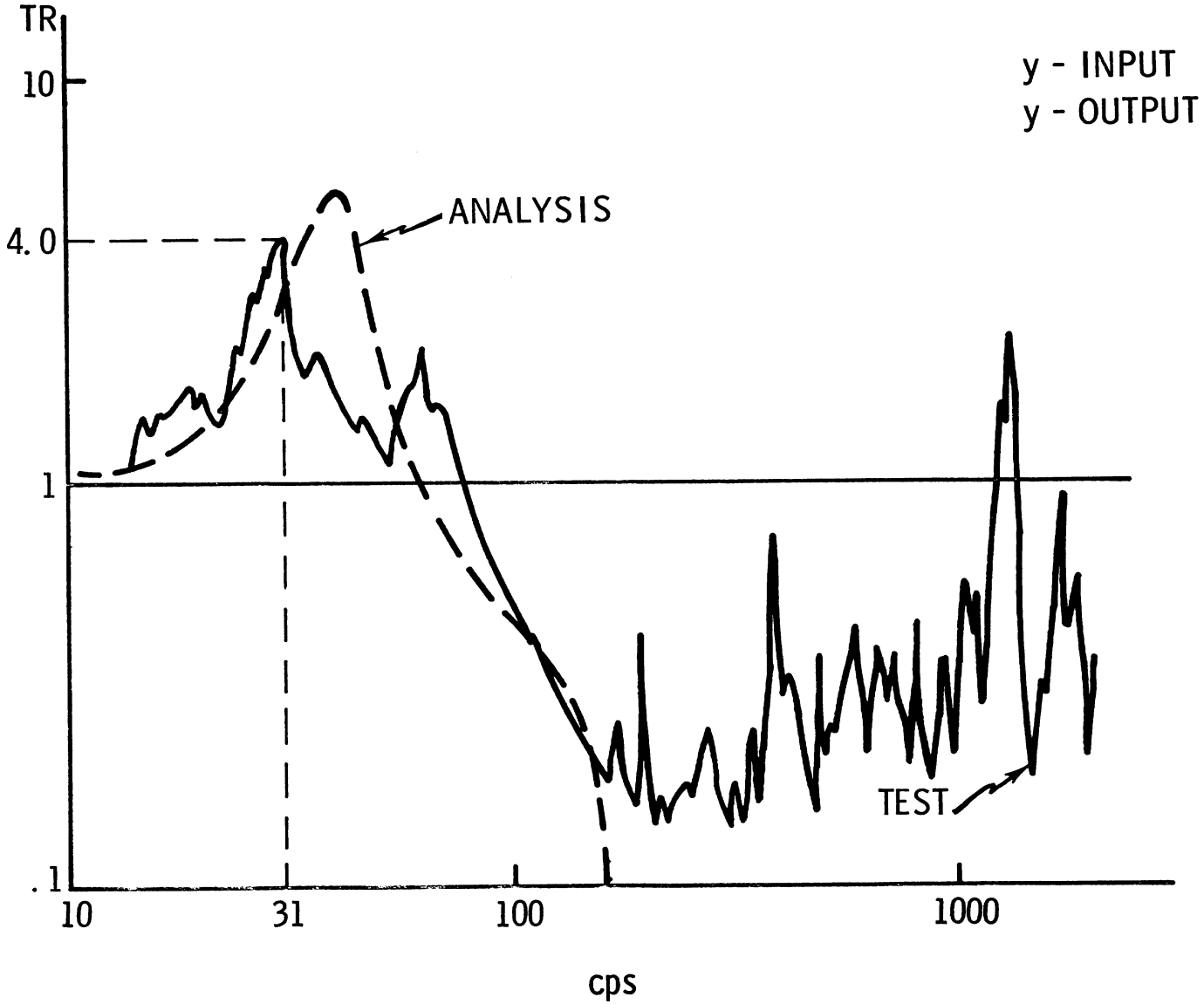

Figure 4.26. Analysis vs. test data; sinusoidal vibration; y_o/y_i.

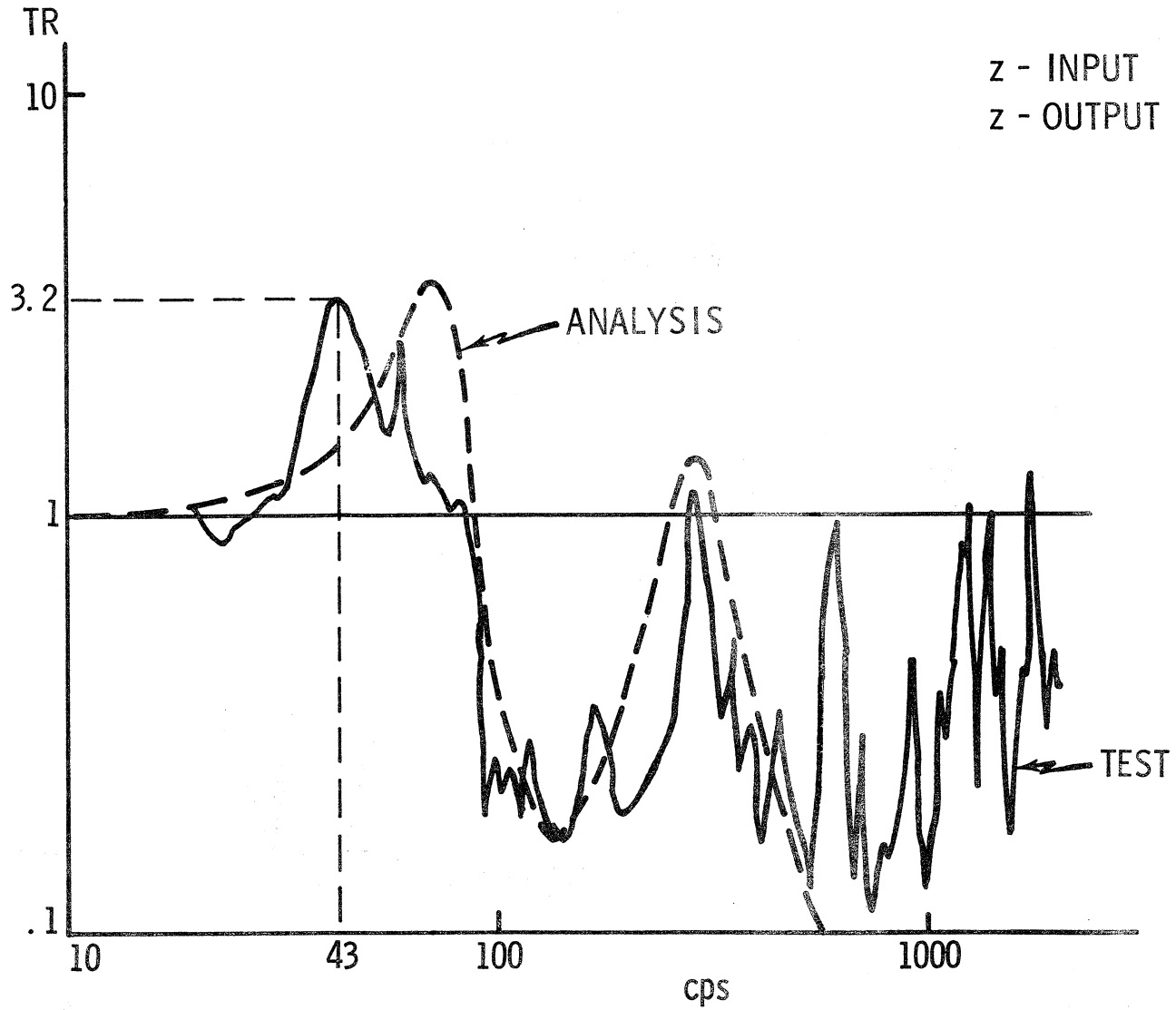

Figure 4.27. Analysis vs. test data; sinusoidal vibration; z_o/z_i.

system increases beyond the limit then the resulting transmissibility increases. This seems to account for the behavior noted above.

4.4 CONCLUSIONS

As a result of the dynamic analysis and testing the following conclusions were made by BxA:

(1) The transmissibilities obtained from the 1 g sweep surveys were in fair agreement with predicted values determined by analysis. However, due to nonlinear damping effects, the response to full level sinusoidal and random vibrations were somewhat different from predicted values.

(2) The difference in transmissibility between points on the cask and on the trunnion was negligible (location 4 on the trunnion and 5 on the cask).

(3) Comparing 1 g sweep transmissibility data at 600°F and 280°F shows that the temperature difference between launch and boost conditions and lunar descent conditions does affect the system dynamic characteristics, but not significantly.

Note: The dynamic analysis and testing program was carried out at BxA before the final change in trunnion release mechanism and relocation of the gear box unit. However, vibrations tests with the final assembly were carried out at GE. The results were likewise successful. Due to the costs of testing BxA did not repeat their tests.

5. THERMAL ANALYSIS

5.1 COMPUTER SIMULATION

A detailed thermal analysis and integration of the graphite fuel cask with the LM Descent Stage vehicle was conducted for several reasons. The first being to insure the safe isolation of the fuel source from human beings on the launching pad, during the space mission, and in case of an accidental reentry of the fuel cask into the earth's atmosphere. Secondly, to determine the radiative and conductive heat leaks into the LM for different vehicle flight phases. Thirdly, to determine temperature levels and gradients on the cask, support structure, LM, and SLA.

To initiate the thermal analysis, BxA created a thermal model of the ALSEP/cask/LM configuration using the interface and design specifications supplied by the companies below:

Bendix Specifications

1. Prototype support structure configuration (Figure 5.1)
2. Prototype thermal shield design (Figure 5.1)
   A. Circumferential angle of shield with cask is 135°
   B. Total hemispherical emittance $\leq$ .10
3. Maximum cask surface temperature of 800°F
4. Circumferential temperature gradient around the cask of 150°F.

G.E. Specifications

1. 19 D cask design configuration (Figure 5.2)
2. Graphite coatings for a total emittance $\geq$ 0.80 per 19 D cask design configuration

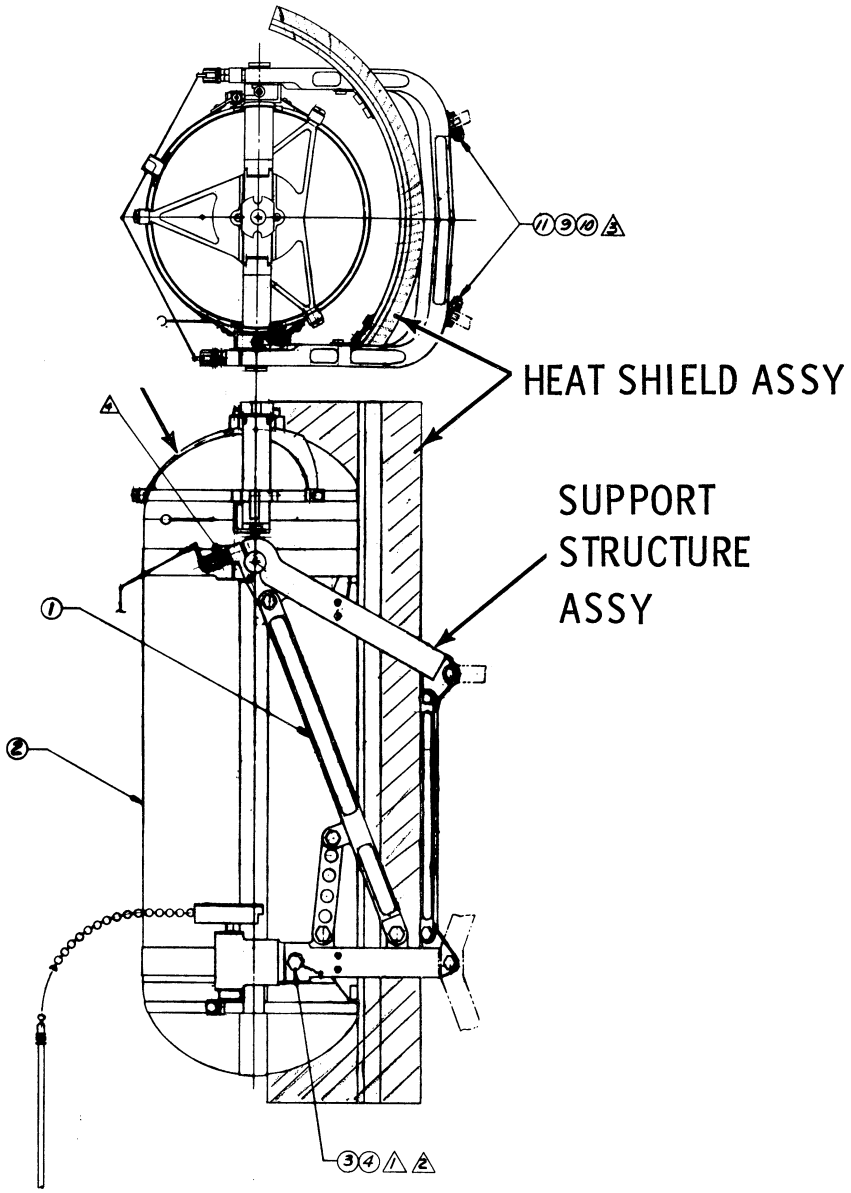

Figure 5.1. Prototype assembly.

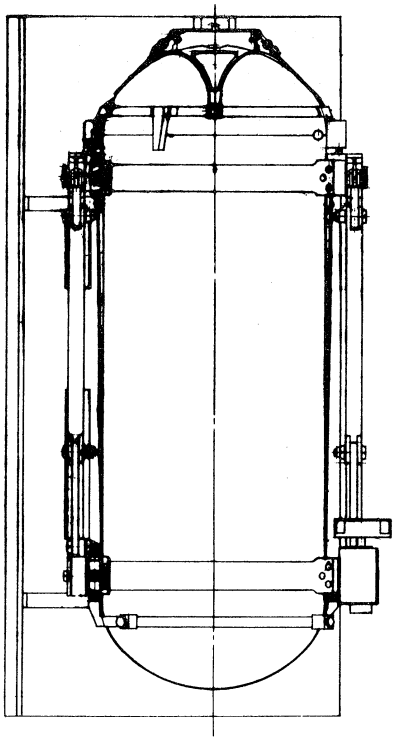

Figure 5.2. 19 D cask design configuration.

3. 1530 watts maximum power output from fuel element.

GAEC Specifications

1. 100 Btu/hr maximum heat leak into LM due to direct cask radiation and conduction
2. Maximum allowable temperature on LM of 270°F

These data from the three organizations were used to establish the overall assumptions and input criteria required for the BxA digital computer models of the cask interface. BxA created the mathematical models using nodal heat transfer equations applied to steady-state conditions. The computer programs used for the thermal analysis are outlined below:

1. 15 node, 3-dimensional thermal model for ALSEP/cask/LM configuration
2. 25 node, 3-dimensional thermal model of ALSEP/LM vehicle interface to evaluate GAEC temperatures on the thermal door and landing gear.
3. 22 node, 3-dimensional thermal model of BxA/GAEC support structure interface for conduction heat leak evaluation.
4. 20 node, 3-dimensional thermal model of ALSEP/cask interface to evaluate axial and circumferential gradients for on pad cooling temperatures and thermal stresses.
5. 35 node, 2-dimensional model of SIVB Instrumentation Unit (IU) manifold to determine flow distribution and pressure gradients.

5.2 HEAT SHIELD

Figure 5-3 indicates the preliminary results of the BxA thermal analysis for various operational phases. After vehicle lift off, and the subsequent

loss of the convective portion of the cooling, the GLFC surface temperature increases to the range of 700°-800°F. In order to reduce the heat leak to the LM, a heat shield was devised to fit between the cask and the LM vehicle. Once out in space in a total vacuum, the mode of heat transfer becomes primarily radiative. Therefore, the heat shield was designed to act as a reflector, re-radiating the heat energy back to the capsule and out to space. The results of the preliminary analytical model indicated that the thermal shield front surface temperature would be around 450°-500°F. This meant that only gold was feasilbe for a reflective surface. However, as the backup plate for the reflective surface was titanium, the gold layer had to be .0025 inches thick. This is because at elevated temperatures, titanium absorbs gold, and to last the length of the mission, a substantial layer had to be deposited. Behind the titanium backing were twenty layers of an aluminized polymer, to further enhance the radiative insulation. This assembly proved to be satisfactory in later tests, as it allowed only 50 Btu/hr heat leak to the LM, well below the specified 100 Btu/hr.

5.3 FORCED COOLING ON THE PAD

On the launching pad with free convective heat transfer, the cask surface temperature was determined to be around 600°F. The spontaneous ignition temperature (SIT) of the command module and service module propellant, monomethyl hydrazine (MMH) is on the order of 380°F, while the other vehicle propellants have higher SIT's. Because of the possibility of propellant leakage the cask assembly presented a potential ignition hazard and therefore had to

	Surface Description	Ambient Temperatures, °F	Translunar Temperatures, °F			Lunar Surface Temperatures, °F	
		On Pad $h_c = 1.0$	SLA On, Sun Orientated	SLA Off, Sun Orientated	SLA Off, Sun Orientated	Sun-Orientated	Space-Orientated
1	Cask Barrel Surface	588-622	689-740	689-726	661-713	707-743	684-733
2	Cask Ends	348	428	417	413	429	433-445
3	Fuel Capsule	1346	1372	1370	1363	1376	1370
4	Thermal Shield - Front	156	474	441	427	467	458
5	Thermal Shield - Rear	92	233	53	22	125	105
6	LM	95, $\epsilon = 36$	183	106	-206	153	0.6
7	SLA/Space	92	250	-459	-459	(Lur) 85 (Sp) -459	(Lur) 85 (Sp) -459

*Results based on -19D cask design using HITCO material properties

Figure 5.3. Preliminary results of BxA thermal analysis.

be actively cooled below the 380°F SIT.

To guide the selection and evaluation of the various possible cask cooling systems, the following ground rules were established.

1. The design approach should preserve current BxA/GE/GAEC flight interfaces in order to minimize the impact on existing design.
2. The implementation of the design should utilize the existing cooling facility capabilities from both the ground and airborne systems.
3. Only on-pad cooling of the cask would be required.
4. The GE 19D graphite fuel cask design would be used for all thermal analysis and design.
5. Only single fuel leakage failure would be accommodated.

Three basic cooling concepts were judged worthy of study, as several air/purge systems were in the vicinity of the cask, and a water supply system could be made available. These three concepts are listed below along with a brief summary of their advantages, disadvantages, and requirements.

Concept I—Forced Convection, Air/Purge System

Advantages:

(1) Air supply is readily available from SIVB IU purge duct.

(2) The purge source located below the nozzle yields the simplest approach, with a minimal impact on flight hardware.

(3) Implementation is fast and inexpensive.

Requirements:

(1) Air flow rate of 20 to 50 lb/min.

(2) Air supply pressure of 0.25 - 0.5 psig.

Concept II—Open and Closed Water Cooling Systems.

Disadvantages:

(1) SIVB IV water/methanol system not recommended for supply source by NASA.

(2) Mechanical disconnection of supply and removal of cooling system at lift off.

(3) Monitor of water level.

Requirements:

(1) Open system, flow rate of 4-5 lb/hr, closed system, flow rate of 60 lb/hr for up to 60 hr.

(2) Venting to avoid inside vapor problems.

Concept III—Finned Graphite Fuel Cask.

Advantages:

(1) Passive system with free convective cooling.

Requirements:

(1) 110 fins, 9 in. long, 0.1 in. thick, and 1.5 in. high.

(2) Removal of fins after vehicle launch

Disadvantages:

(1) Total revision of the BxA/GE/GAEC interface including new cask support structure, etc.

(2) Additional ALSEP weight of 5 lb.

Concept III was immediately eliminated as it required total revision of the existing designs, and further study began on Concepts I and II. Some of the early conceptual cask cooling systems are shown in Figure 5.4. As

indicated in Figure 5.4 from the standpoint of required mass flow and pressure differential, the fully enclosed systems presented the most efficient means of cooling. However, since the thermal dissipation from the cask is by pure radiation after the early portion of the launch sequence, it would have been necessary to mechanically remove any enclosed cooling system after the air system was shut down. Therefore, the early phases of the study also included an investigation of the possible mechanisms of cooling shroud removal and/or destruction systems.

Because of the added complications and interference problems of the shrouded cooling systems, only the full axial shroud was actually fabricated for testing and the majority of testing was carried out with the various open flow configurations as pictured in Figure 5.5. The test set up is shown in Figure 5.6 using a detached plugged nozzle.

After the initial series of tests, it was discovered that the actual cask cooling was more efficient than had been predicted by the pre-test analysis. This meant that the test plan had to be modified to provide data in the marginal temperature range and also to provide testing for the discarded remote nozzle locations. (The remote nozzle locations were previously thought to provide inadequate cooling with the available flow conditions.)

The fact that the actual cask cooling was more effective than had been predicted was not a result of erroneous pretest analysis. After reduction of the test data it was found that the measured values of the convective heat transfer coefficients were well above both the experimental and theoretical values which existed in the open literature.

COMPARISON OF AIR/GN_2 PURGE SYSTEMS AND WATER SHROUD SYSTEMS
FOR ON PAD CASK COOLING CONFIGURATION

	AIR/GN_2 PURGE SYSTEMS				WATER SHROUD SYSTEMS	
	AXIAL FLOW			ENCLOSED FLOW	CLOSED	OPEN (BOILING)
	NOZZLE ATTACHED OPEN	NOZZLE ATTACHED SHROUDED	NOZZLE DETACHED			
	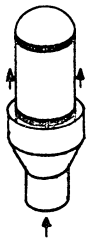	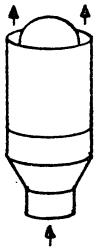	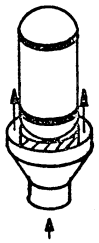	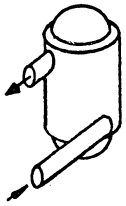	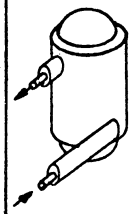	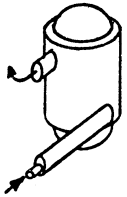
ANALYTICAL CALCULATION						
REQUIRED MASS FLOW RATE, #/MIN.	HIGH 35-50	MODERATE 20-40	HIGH 50	LOW 5-10	HIGH 60-80 (#/HR)	LOW 4-5 (#/HR)
REQUIRED PRESSURE DIFFERENTIAL, PSIG	1.0	0.4-0.8	1.0	0.1-0.3	3.0	5.0
DESIGN CONFIDENCE LEVEL	FAIR	GOOD	FAIR	GOOD	GOOD	GOOD
WEIGHT PENALTY	LOW	MODERATE	LOW	MODERATE	HIGH	HIGH
ON PAD CASK TEMPERATURE GRADIENTS	MODERATE	LOW	MODERATE	LOW	LOW	MODERATE
POST LAUNCH INTERFACE INTERFERENCES	LOW	HIGH	NONE	HIGH	HIGH	HIGH
MECHANICAL/THERMAL RELEASE SYSTEM REQUIRED	NO	YES	NO	YES	YES	YES

Figure 5.4. Early cooling concepts.

Various detached nozzle configurations were tested in several axial positions below the cask. In addition, it was found that the thermal shield on the inboard side of the cask would function as a flow deflector so that the nozzles could also be placed outboard and at an angle with respect to the cask axis. Finally, a fully shrouded axial flow configuration was tested for purposes of comparison with the pretest analysis.

The correlation formulas for the open flow cooling system were found to be

$$\Delta T = 62\left[\frac{x + 1.9\,\frac{\sqrt{m}}{\Delta p^{1/4}}}{(\sqrt{m}\,\Delta p^{1/4})}\right]^{0.71}$$

for a plugged nozzle, and

$$\Delta T = 48\left[\frac{x + 1.9\,\frac{\sqrt{m}}{\Delta p^{1/4}}}{\cos\Theta\,\sqrt{m\,\Delta p^{1/4}}}\right]^{0.71}$$

where ΔT = temperature differential, °F

x = surface distance from nozzle to cask, feet

m = mass flow, lb/sec

Δp = pressure differential, psf

Θ = angle between nozzle axis and cask axis.

Although a thermal analysis was not used (or necessary) in the correlation of the experimental data, several analyses were carried out to verify that the experimentally derived convective heat transfer coefficients were compatible with the measured cask temperatures. The basic model for the

	ATTACHED NOZZLE	ATTACHED PLUGGED NOZZLE	OPEN AXIAL FLOW	DETACHED PLUGGED NOZZLE	DETACHED NOZZLE AXIAL FLOW	DETACHED NOZZLE 45° ANGLE	SHROUDED AXIAL FLOW
	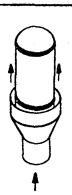	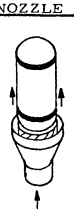	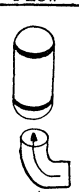	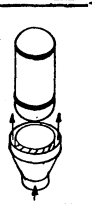	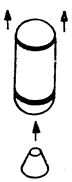	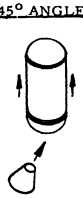	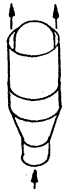
Configuration Number	1	2	3	4	5	6	7
Run Number	1 to 12	13 to 18 30 to 35	19 to 21	22 to 27	28 to 29	36 to 40	41 to 43
Range of Flow Conditions — Mass Flow #/min	4-50	10-50	24-53	18-35	22-35	18-43	5-20
Range of Flow Conditions — Pressures psi	.06-.83	.03-.42	.01-.05	.10-.33	.06-.13	.04-.56	.02-.19
Range of Flow Conditions — Nozzle Area in^2	2.80-8.40	3.56-9.16	19.6	3.56-7.8	8.95	3.14-19.6	5.17

Typical Flow Conditions to Maintain a Maximum Cask Wall Temperature of 200°F (using 70°F cooling air)

Flow Rate, #/min	15	25	50	35	30	30	8
Pressure Differential, psi	0.04	0.06	0.05	0.09	0.15	0.25	0.06
Maximum Velocity 3 feet above cask, fps	7	10	18	10	8	9	3

Figure 5.5. Test nozzle configurations.

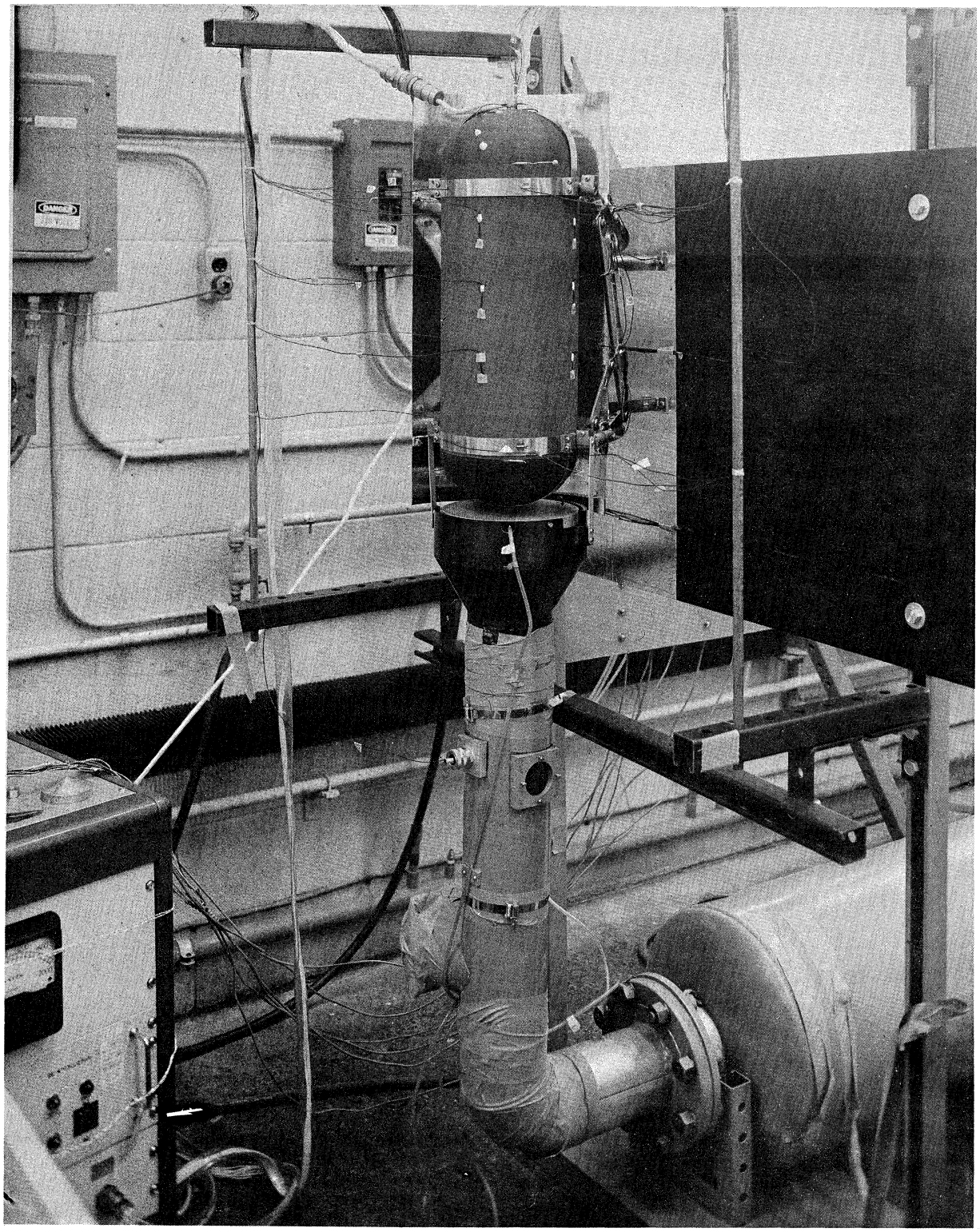

Figure 5.6. Forced convection test set up - plugged nozzle.

thermal analysis used a finite difference approach where the physical configuration was subdivided into discrete finite elements—each of which was assumed to be isothermal. The mass of each element was assumed to be concentrated at its geometric center or node. These nodes had individual heat sources and were linked together in a resistance network like an electrical circuit. In this analogy the temperature is the analog of the voltage and the heat flow is the analog of the current.

A 26-node model was used in the analysis and in Figure 5.7 the predicted and measured temperatures are given for the nodes—along with the convective heat transfer coefficients. This data indicated that the convective heat transfer coefficients were in the proper range for the measured temperatures.

The results of this series of tests indicated that the cooling problem was less critical than had been originally anticipated. There was a considerable design latitude in the various cask cooling configurations which could hold the cask surface temperature below 300°F with the suggested amount of cooling flow (20-25 lb/min). This information allowed the prototype cooling system to be designed on the basis of minimal weight and interference problems, and with only secondary considerations given to the actual efficiency of the cooling system.

From an interference standpoint, a more remote placement of the nozzle was desirable. Therefore, a second series of tests were run with the nozzle at distances of 15, 24, and 36 in. below the cask and included several off axis positions as well as the axially aligned case. At those distances a conical nozzle (Figure 5.8) was more effective in cooling and lighter than a

plugged nozzle (Figure 5.6). Thus, only a few plugged nozzle tests were carried out to tie in these test results with the previous test results. The majority of testing was carried out with a conical nozzle having a 2.25 in. throat diameter. Also a 2.75 in. diameter nozzle was used to take care of the higher mass flow rates of the test.

Just prior to this test, information was received which indicated that there was a possibility that the instrumentation unit (IU) cooling flow rate might be substantially reduced during the prelaunch period when technicians would be working inside the SLA. With this reduction, the cooling nozzle would recieve 15-20 lb/min. However, from the relative sequencing of the prelaunch cask loading and hydrogen fuel tank loading, it appeared that the temperature of this reduced flow would always be near ambient rather than the 130°F temperature that was later used to maintain instrumentation temperature in the IU section. But to remain on the safe side, reduced mass flow tests were carried out using both 75°F and 130°F supply air (test result examples Figures 5.9 and 5.10).

As the cooling nozzle was a part of the IU cooling system, the sizing of the nozzle played an important part in the overall IU system performance. That is, since there were no controls between the IU cooling duct and the cask cooling nozzle, the relative amount of cooling flow leaving the IU orifices and the cask cooling nozzle was proportional to the ratio of the effective exhaust areas. As was determined above, a variety of nozzles satisfied the basic cask cooling requirements. Further, because of the relatively small amount of flow taken from the IU system by the cooling nozzle, a

FILM COEFFICIENT, h ~ BTU/HR, FT^2 ^oF

TEMPERATURES ~ ^oF, PREDICTED &MEASURED

Location	Free Conv.		Test Run #4		Test Run #5		Test Run #6	
	h	Pred/Meas	h	Pred/Meas	h	Pred/Meas	h	Pred/Meas
Barrel (SLA)	1.0	527/529	24.0	133/137	34.0	115/119	45.0	105/113
Barrel (Shield)	1.0	556/556	25.0	132/130	34.0	116/108	48.0	103/104
Band (upper)	1.0	430/463	5.8	127/140	9.2	108/114	13.1	96/112
Band (lower)	1.0	432/457	26.9	97/94	38.5	87/89	46.0	82/90
Dome (upper)	1.5	364/377	6.8	121/129	11.0	103/110	15.4	93/106
Dome (lower)	1.0	437/	3.9	169/	4.8	155/	6.1	142/
Shield (front)	1.5	117/105	25.0	70/70	34.0	70/70	39.3	70/70
Shield (rear)	1.0	75/	1.0	70/	1.0	70/	1.0	70/
Barrel In. (SLA)	0.3	560/571	0.3	183/195	0.4	166/175	0.4	155/168
Barrel In. (Sh)	0.3	586/589	0.3	182/196	0.4	166/176	0.4	154/175
Fuel		1419/-		1313/-		1311/-		1310/-
Capsule	0.4	1017/1001	1.0	899/873	0.9	896/862	0.9	895/842
End Plate	0.7	570/581	1.0	328/312	1.0	317/258	1.0	311/269
Internal Air		634/-		225/-		221/-		218/-
LM	1.0	77/85	1.0	70/70	1.0	70/70	1.0	70/70
SLA	Sink	70/70	Sink	70/70	Sink	70/70	Sink	70/70

Figure 5.7. Cask temperature correlations.

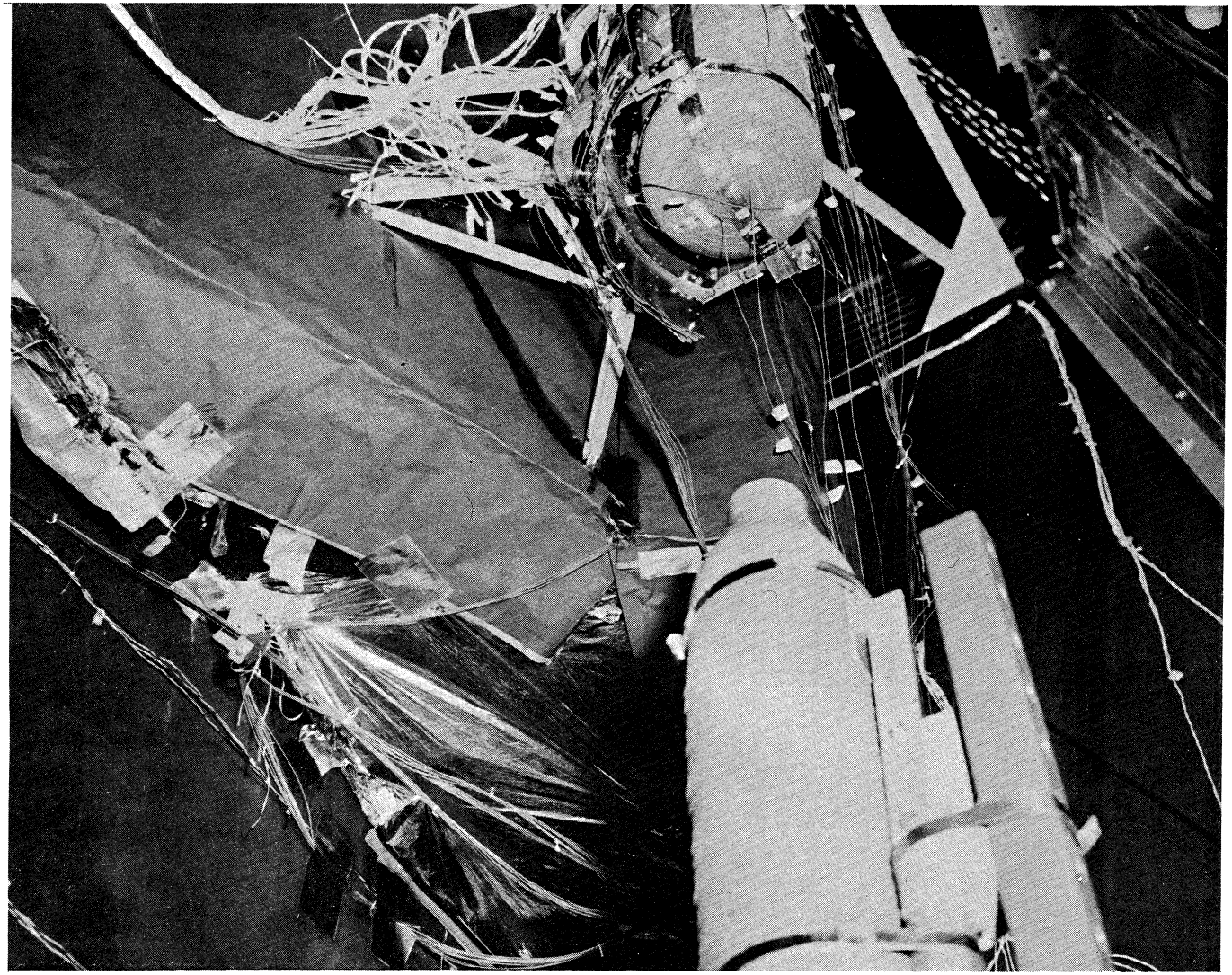

Figure 5.8. Forced convection test set up - conical nozzle.

Run no. 1
2.25 in dia. Conical Nozzle
24 in. separation

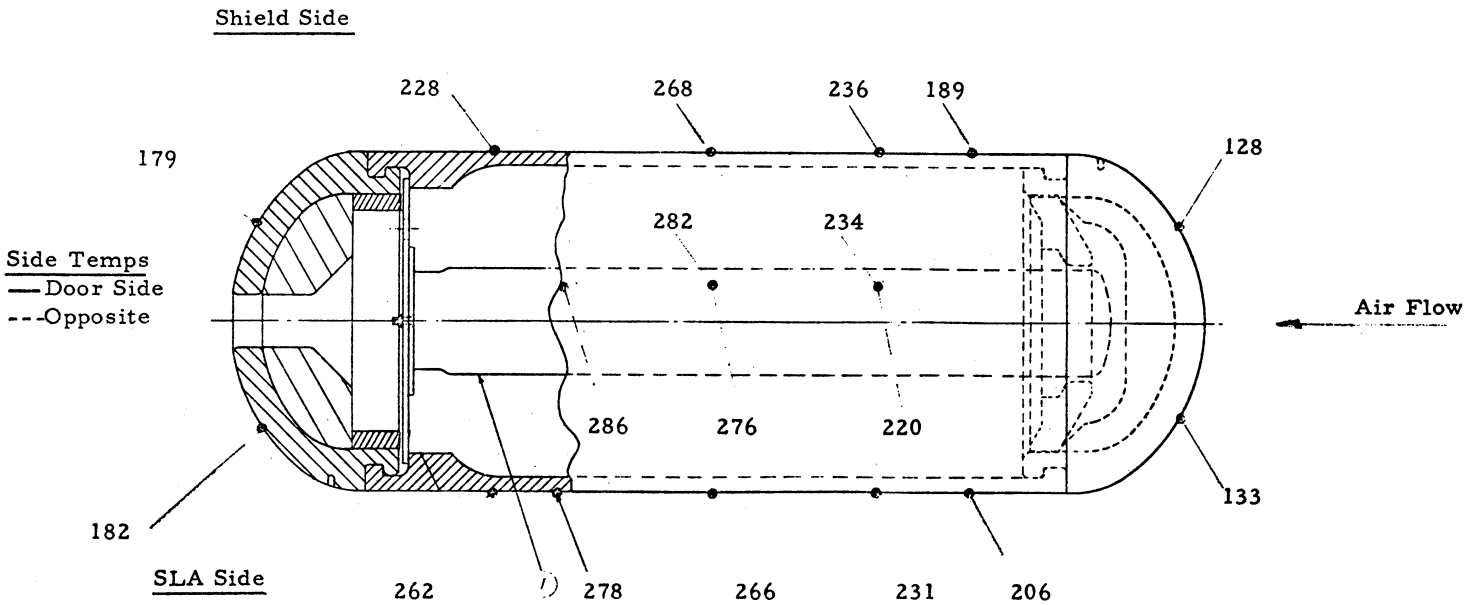

Surface Description	Test Results °F
1. Capsule Surface	1101 - 1262
2. Cask External Surface	
a. Center	182 - 286
b. Ends	189 - 262
3. Cask Domes	128 - 185
4. Thermal Shield	82 - 93
5. Astronaut Door	76 - 213
6. LM Panel	73 - 83
7. SLA	70 - 72
8. Air Supply	130

Figure 5.9. Cask surface temperature results.

Run No. 3
2.25 in. dia. Conical Nozzle
24 in. separation

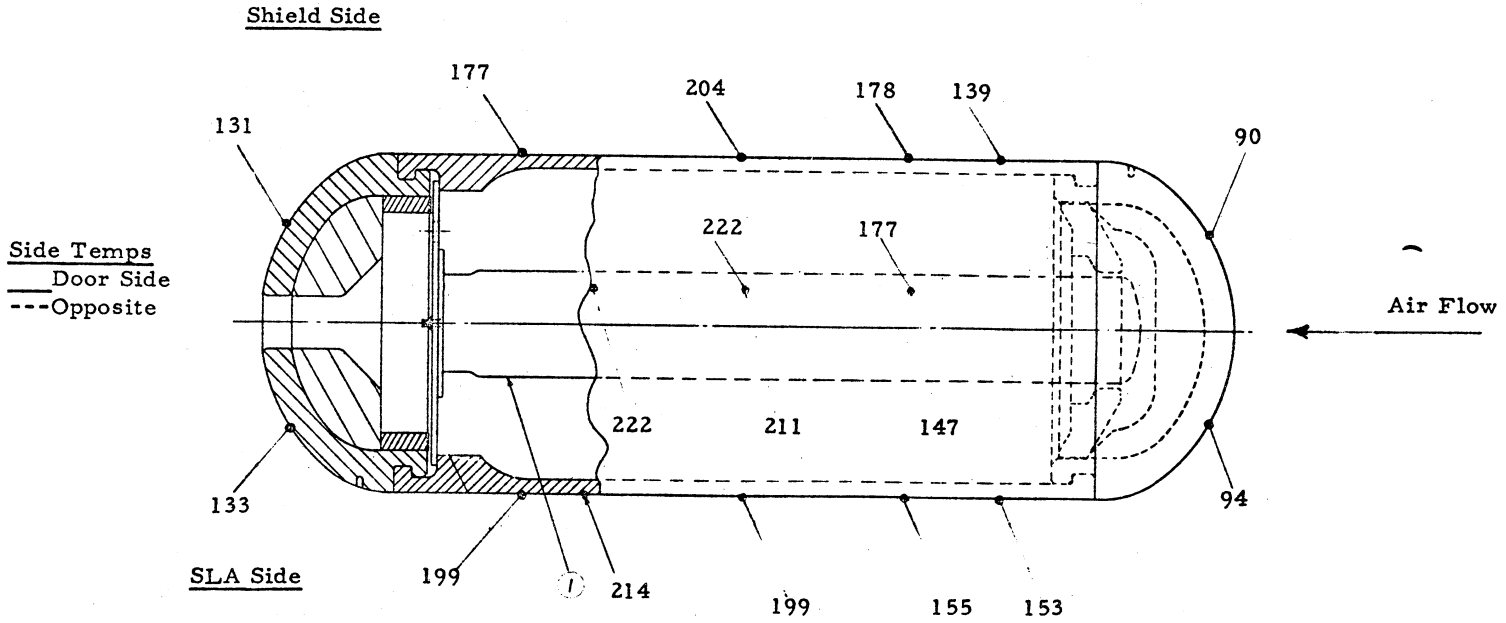

Surface Description	Test Results °F
1. Capsule Surface	1090 - 1256
2. Cask External Surface	
a. Center	131 - 222
b. Ends	139 - 199
3. Cask Domes	170 - 133
4. Thermal Shield	71 - 95
5. Astronaut Door	72 - 211
6. LM Panel	71 - 75
7. SLA	71 - 72
8. Air Supply	75

Figure 5.10. Cask surface temperature results.

considerable latitude in nozzle design was allowed. Therefore, additional factors were considered to determine the most satisfactory design compromise. Only two factors were found to be significant. One was the alignment problem between the nozzle and the cask, and the other was the resulting heated exhaust plume above the cask. From geometric considerations, a larger area (and, subsequently, a larger mass flow) nozzle would be less sensitive to misalignment. However, to reduce the effects of the heated exhaust plume, the flow rate should be minimized, which called for a smaller nozzle area. Therefore, a balance was sought, yielding finally a 2.5 in. diameter nozzle. In the final cooling system, the conical nozzle was positioned 24 in. from the bottom of the cask and a flow rate of 20 lb/hr was used.

After the above free and forced convection tests, further testing was done under the following simulated conditions: Earth orbit with and without heating. In general, the test results agreed within explicable error, and were well within the specified boundaries, as can be seen from Figure 5.11.

	Interface Specification	Specification Requirement	Test Results	Pretest Predicted Values
. MAXIMUM FUEL CASK SURFACE TEMPERATURE	BxA/GE	800°F	615°-798°F	672°-785°F
. MAXIMUM FUEL CASK CIRCUMFERENTIAL TEMP GRADIENT	BxA/GE	150°F	130°F	140°F
. MAXIMUM FUEL CAPSULE SURFACE TEMPERATURE	BxA/GE	1400°F	1210°-1320°F	1220°-1302°F
. MAXIMUM HEAT LEAK TO LM	BxA/GAEC	100 BTU/HR	50 BTU/HR	75 BTU/HR
. MAXIMUM LM SKIN SURFACE TEMPERATURE (EXCEPT ASTRONAUT THERMAL DOOR)	BxA/GAEC	270°F	238°F	240°F
. ASTRONAUT THERMAL DOOR	BxA/GAEC	400°F	388°F	400°F
.. MAXIMUM CASK THERMAL SHIELD TEMPERATURE	BxA	600°F	588°F	558°F

Figure 5.11. Test results vs. specifications.

6. CHRONOLOGICAL DEVELOPMENT

On January 9, 1967 BxA was notified by the MSC to begin work on the support structure for the graphite cask. During the first two months, BxA spent most of its time determining the interface points between the cask support assembly they were to build, the GE cask, and the GAEC LM. At this time BxA asked GE to put protrusions or grooves on the cask (Figure 6.1) for attachment of the cask to the support structure. GE, still in the early stages of developing the cask, agreed to look into the proposals. However, GAEC, being well under way in development of the LM, considered it impossible to alter their existing pick-up points for the cask support structure as BxA had proposed. Briefly, BxA had asked GAEC to run their interface members back directly to the LM outer surface (Figure 6.2). This would decrease the load on the support structure by 7 to 8 lbs. GAEC also established a weight limit for the cask and support structure at 65 lb, which included the weight of a heat shield also part of BxA's design. The heat shield was required to protect the exterior surface of the LM from the heat transfer of the cask. Meanwhile, MSC told BxA that they would have to design a protection device that would support the astronauts' weight and not destroy his suit if he fell into the cask assembly.

During March and April, the details of a cask rotator mechanism were completed. With this device the astronaut was able to lower the cask, at 15° intervals, to a desired height for removal of the Snap-27 capsule. Also at this time, from information on the dimensions and weight of the cask

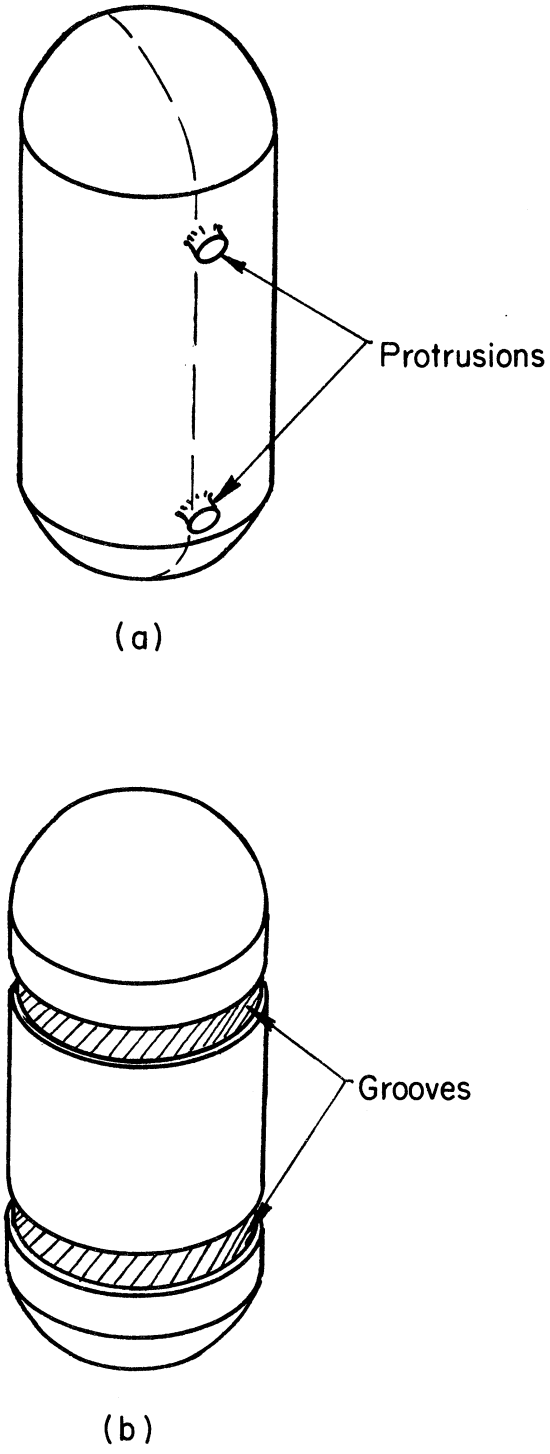

Figure 6.1. Early cask design proposals.

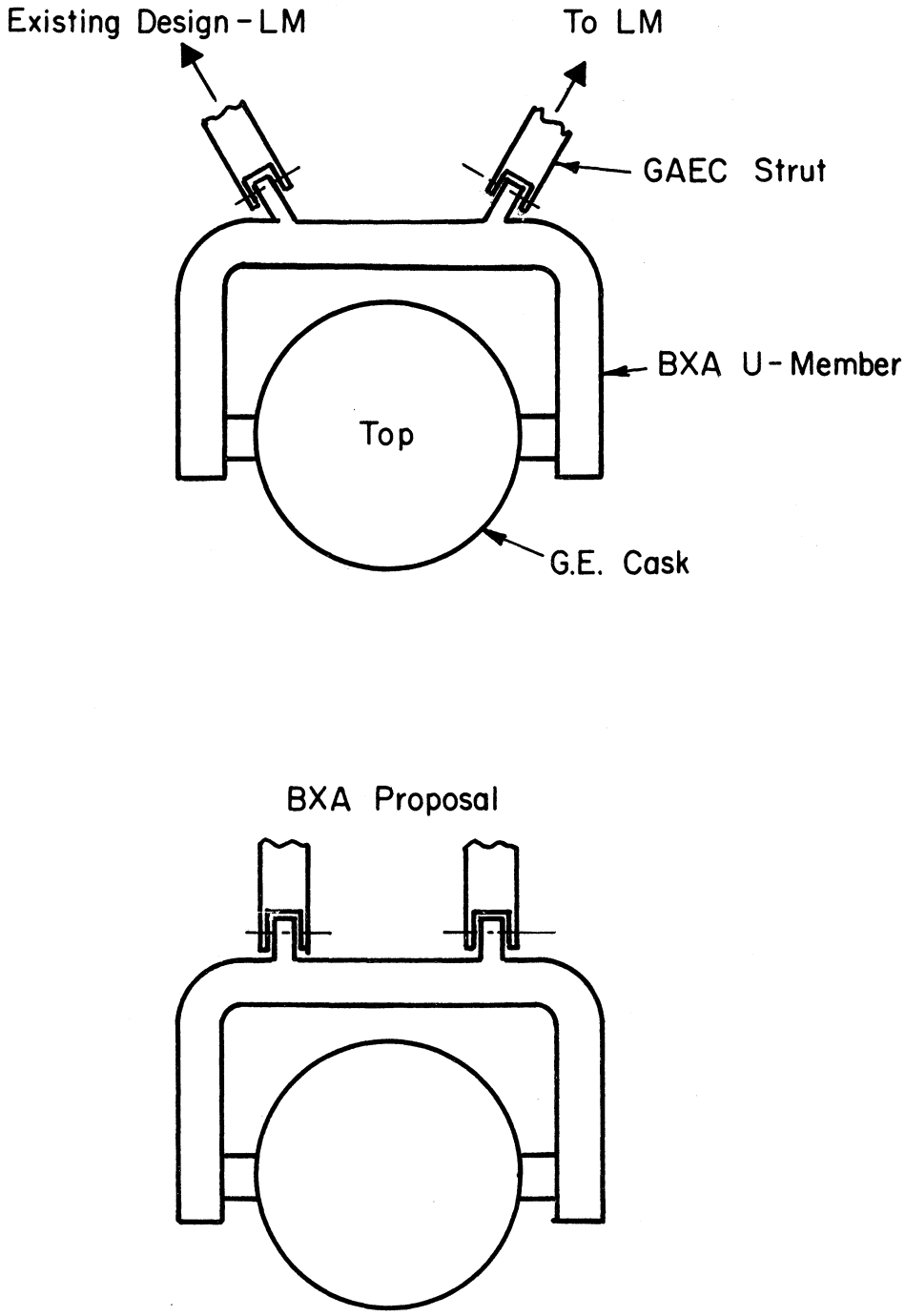

Figure 6.2. Early mounting proposal.

established by GE, BxA estimated the overall weight of the cask, support structure, heat shield, and protection guard to be 52.5 lb which was 12.5 lb under the maximum weight established by GAEC. The support structure had changed to a U-member type for added strength. The proposed heat shield was to be made of corrugated titanium sheet and Kapton-H (the same material used on the skin of the LM). The corrugated design was considered because it gave extra strength to the shield under the "g" loading. At this time the biggest setback in the development of the cask support structure occurred. That was, GE had decided against putting any holes, grooves, slots, or protrusions on the cask. The main reason for this decision was that any obstructions would lead to local stress concentrations and localized areas of high temperatures, thus jeopardizing a safe return of the cask and capsule should the mission be aborted. Therefore, in view of GE's decision, BxA decided to use a cradle-type arrangement to retain the smooth-surfaced cask.

From May to June, BxA built a simulated cask assembly. The assembly was sent to MSC for vibrations testing of the total LM vehicle. Also during this period, BxA was told by MSC that they did not want the astronauts near the cask assembly while they were lowering it on the lunar surface. Consequently work began on the worm, gear-type drive mechanism with a braided glass fiber cord which allowed the astronaut to lower the cask from a distance of 7 to 9 ft.

During the period from July to August a model of the cask assembly was built. Tests on the model indicated 11.8 lb pull was required to place the cask into position. This was under the 15 lb maximum pull requirement

established by MSC. Also at this time research was done on a ball-lock type trunnion release. In addition, the U-members were increased in size (cross sectional area) to handle 60 g loads, whereas the original calculations were based on 36 g loading. This was due to an error in the original specifications from NASA. To compensate for the increased weight the vertical members were changed from tubing to I-section beams.

From September to December a prototype assembly was built. The prototype employed worm drive lowering mechanism and a ball-lock trunnion release mechanism. The astronaut was required to pull two cords in order to release the cask from the upper trunnion supports. He then pulled a third cord to lower the cask. After the prototype was subjected to simulated flight conditions BxA discovered the ball-lock release arranagement was inadequate unless a truly axial pull was applied. At times the pins jammed. Consequently an analysis began to determine the causes of the erratic behavior. Also during this period a "walk through" demonstration (Photo 1 in Appendix I) of the cask release and rotation was conducted at MSC. The astronauts suggested to BxA that the release of the cask upper trunnions, the removal of the cask dome locking spline and the rotation of the cask to a suitable position should all be performed by one continuous pull on the gear box cord.

Starting in January, 1968, to the end of August, final drawings were made and a series of tests were agreed for the prototype cask assembly. Since most of the development on the assembly was completed, the available manpower for the project was reduced. The testing carried out during this

period were thermal-vacuum, vibrations, and band tensioning. Results of the vibration testing in August indicated that the ball-lock trunnion release mechanism was still unsatisfactory. Random "g" loading caused the mechanism to lock thereby making it impossible to release the cask. Therefore, three new methods of releasing the cask were under investigation. They were, a guillotine arrangement, a design based on the principle of the "collet," and a suitcase-type latch.

During the months of September and October, GAEC, who had moved their door hinge, discovered that the astronaut guard and gearbox interferred with the LM door. Two proposals were discussed to correct the interference. They were (1) BxA would move the gear box to the left side of the support structure and change the guard to suit this modification, or (2) GAEC would reduce the door movement from 105° to 100°. As a result of cost and time estimates proposal (1) was decided upon. Also at this time, the guillotine release mechanism was tested and adopted as the replacement for the ball-lock trunnion release mechanism.

This briefly summarizes the design and development of the cask support structure. Greater depth and detail of the structure is covered in the preceding sections of this review.

EPILOGUE

We have presented the design and development of a project carried out by BxA during 1967 and 1968. This epilogue contains our criticisms of what Bendix Aerospace did and what we feel we accomplished as far as a design experience.

When we were first introduced to this design many criticisms were raised. However during the course of our interviews with Mr. Durrant we learned that BxA had valid answers to our criticisms. Among these criticisms we asked BxA why a very extensive analytical dynamic development was made on the system when the actual vibrations test program was in itself very thorough. BxA explained that the cask and support structure was expensive, therefore they wanted to be assured that the system would survive the test program before it was performed. The cost of the dynamic analysis was much less than the costs which would have occurred as a result of a failure on the test stand. In addition, the dynamic analysis provided BxA with locations on the system where vibration loads might cause trouble. Another question we asked was why were expensive materials used, i.e., gold on the heat shield and titanium for the entire support structure? Also, since testing was expensive why were identical tests, such as vibrations, run at both BxA and GE? BxA explained that the major concern was to have a completely fail-safe mission. Therefore cost was secondary compared to reliability. Another question we asked was why did BxA decide on the complex manually operated lowering arrangement as opposed to a more automatic type system. BxA's reasons were

discussed in Section 2.1. Basically, the reason was that there were no proven automatic systems for a lunar-type environment.

This report is an indication of what we learned about an engineering design and development program. We feel that our experience would have been enhanced had there not been a time lapse between our study and the completion of the project. In this instance we could have interviewed more of the personnel that contributed to the development of the project. Because this review was written two years after the development some of the engineers are no longer at BxA. In addition, some of the details of the design have been misplaced or forgotten. It also would have been advantageous had we examined a working system and BxA's testing facilities. However, certain research projects prohibited our admission to these facilities. Although these elements would have helped our understanding of the cask support structure, they did not deter from the insight we gained in our approach to an engineering design problem.

APPENDIX I

PHOTOS

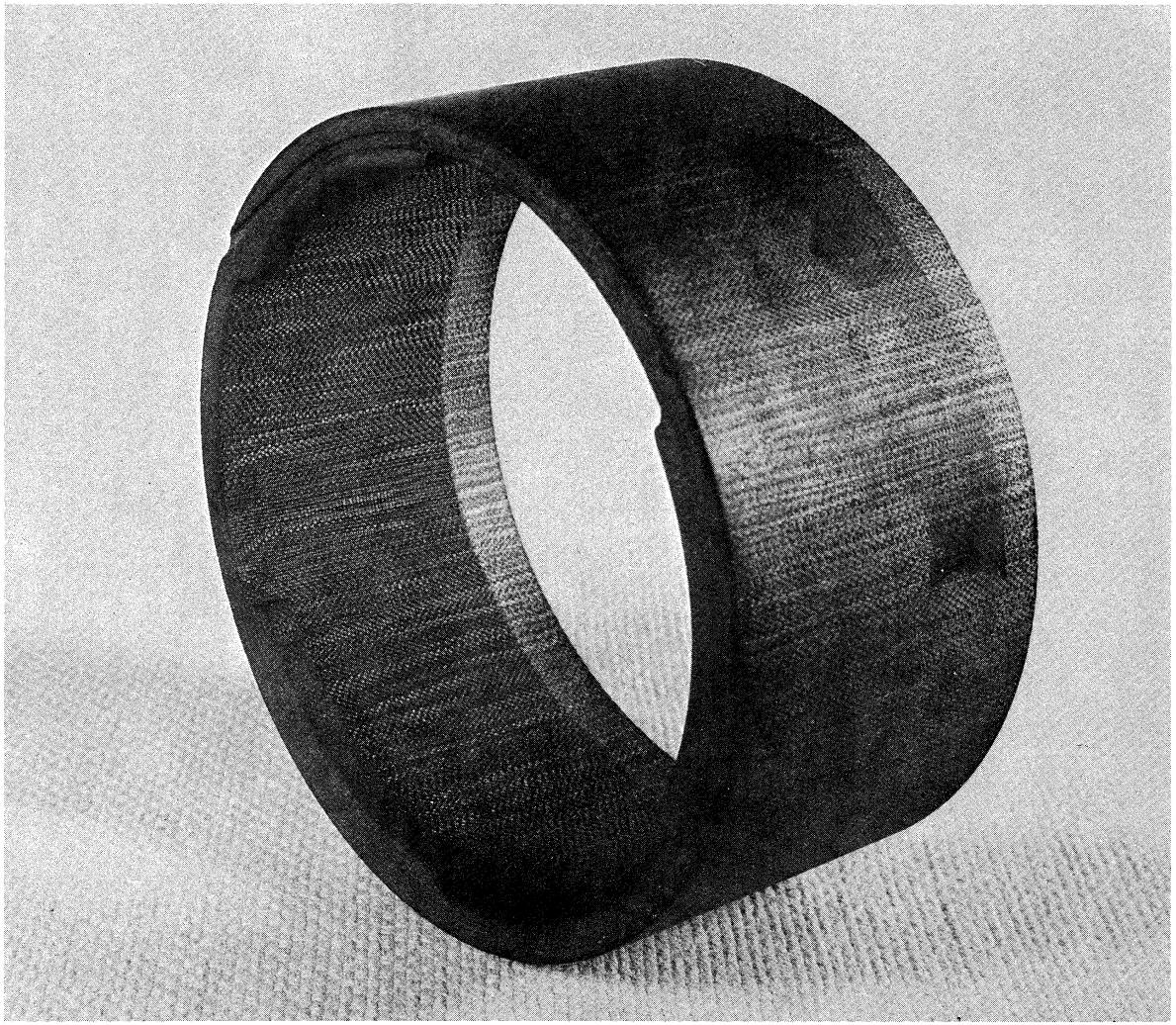

Photo O. Section of graphite cask.

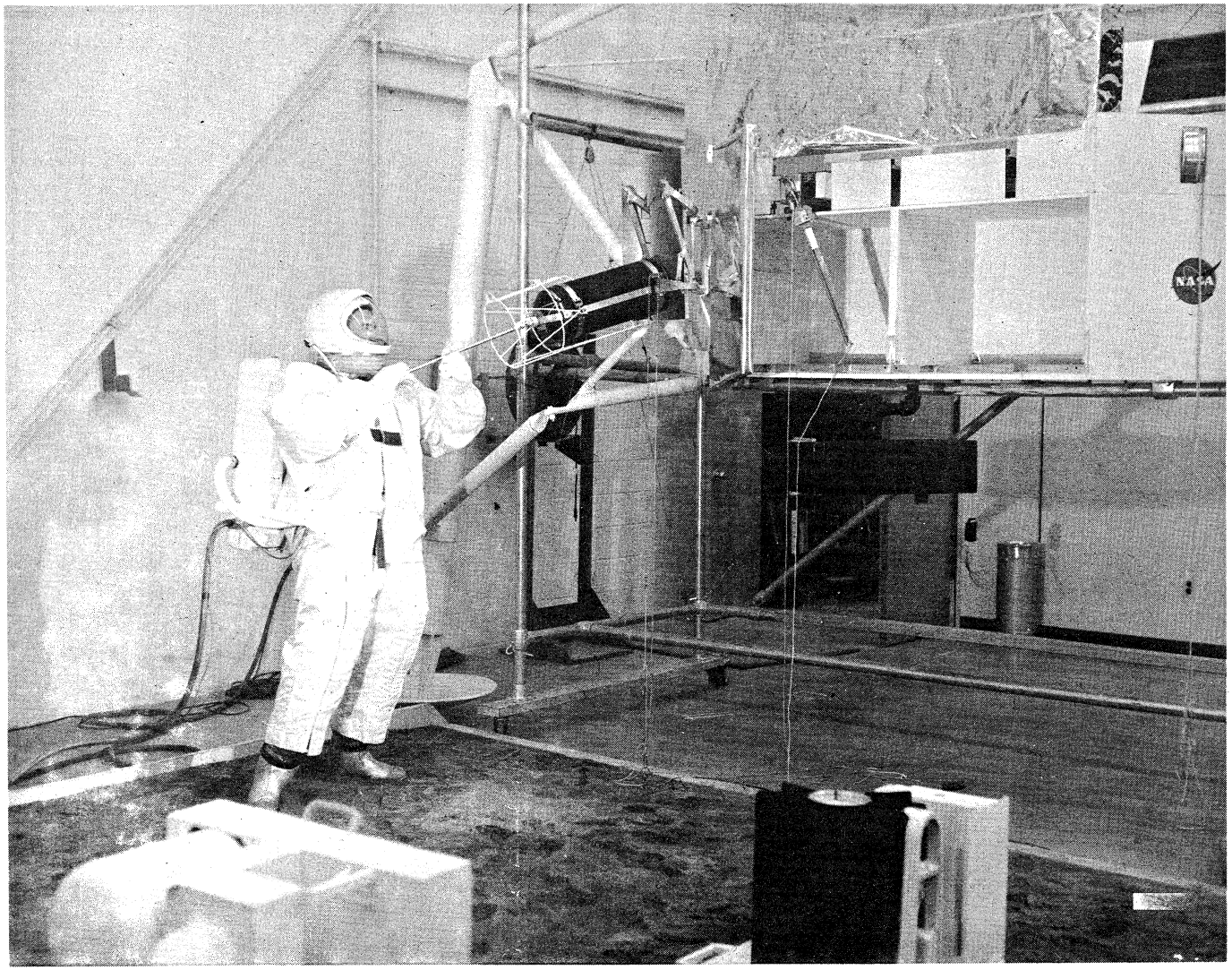

Photo 1. Demonstration of cask deployment procedure.

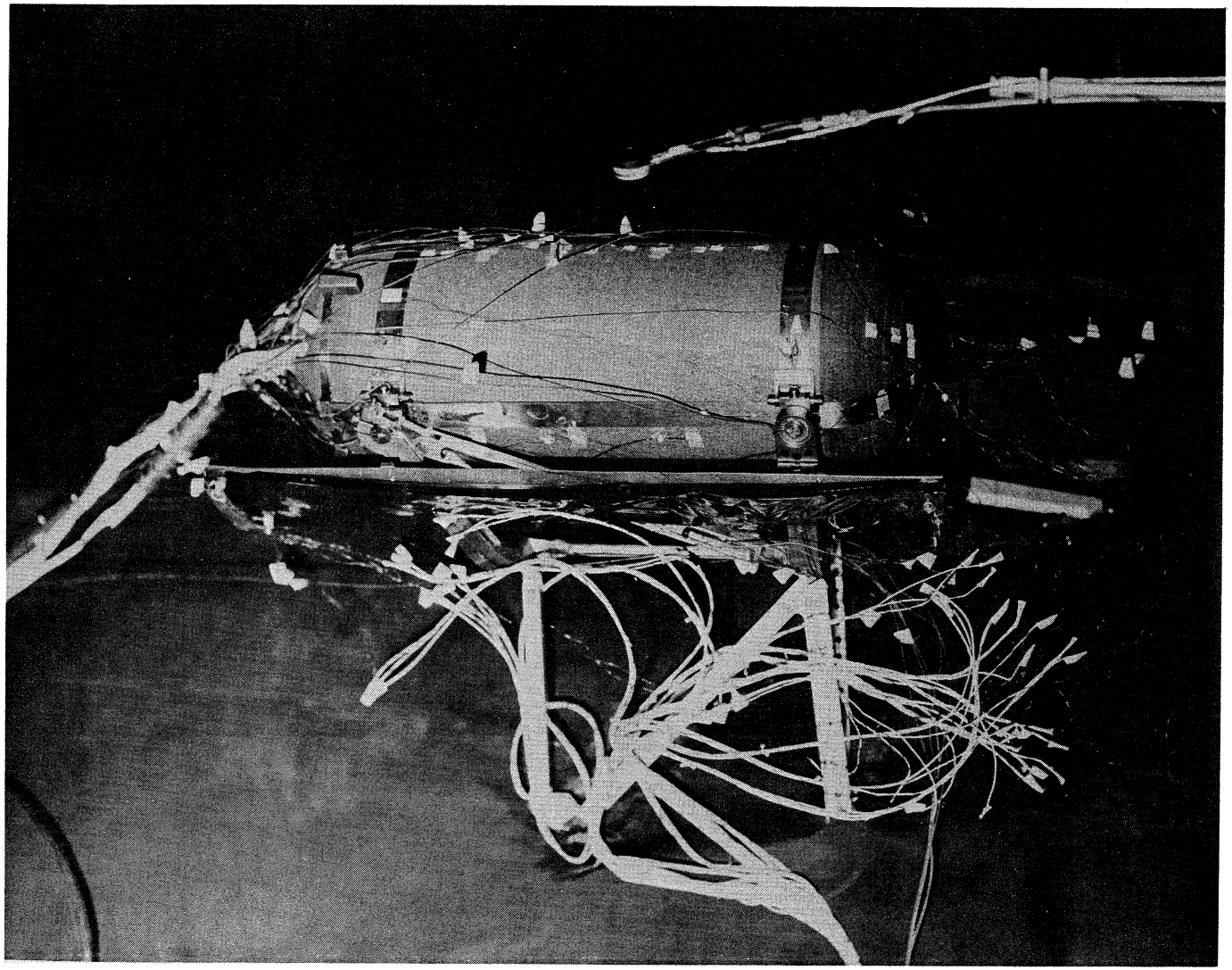

Photo 2. Thermal analysis test set up.

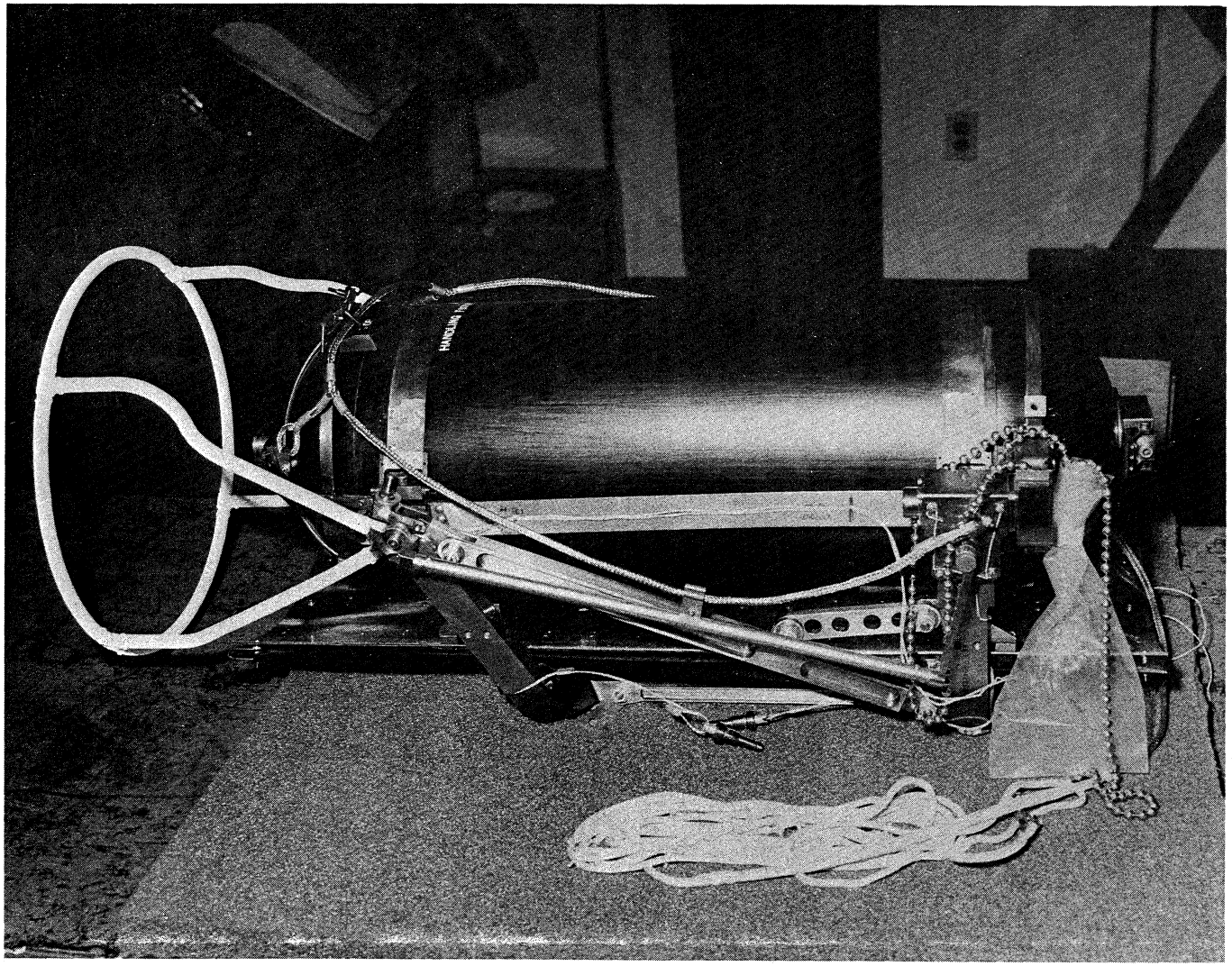

Photo 3. Final cask support assembly.

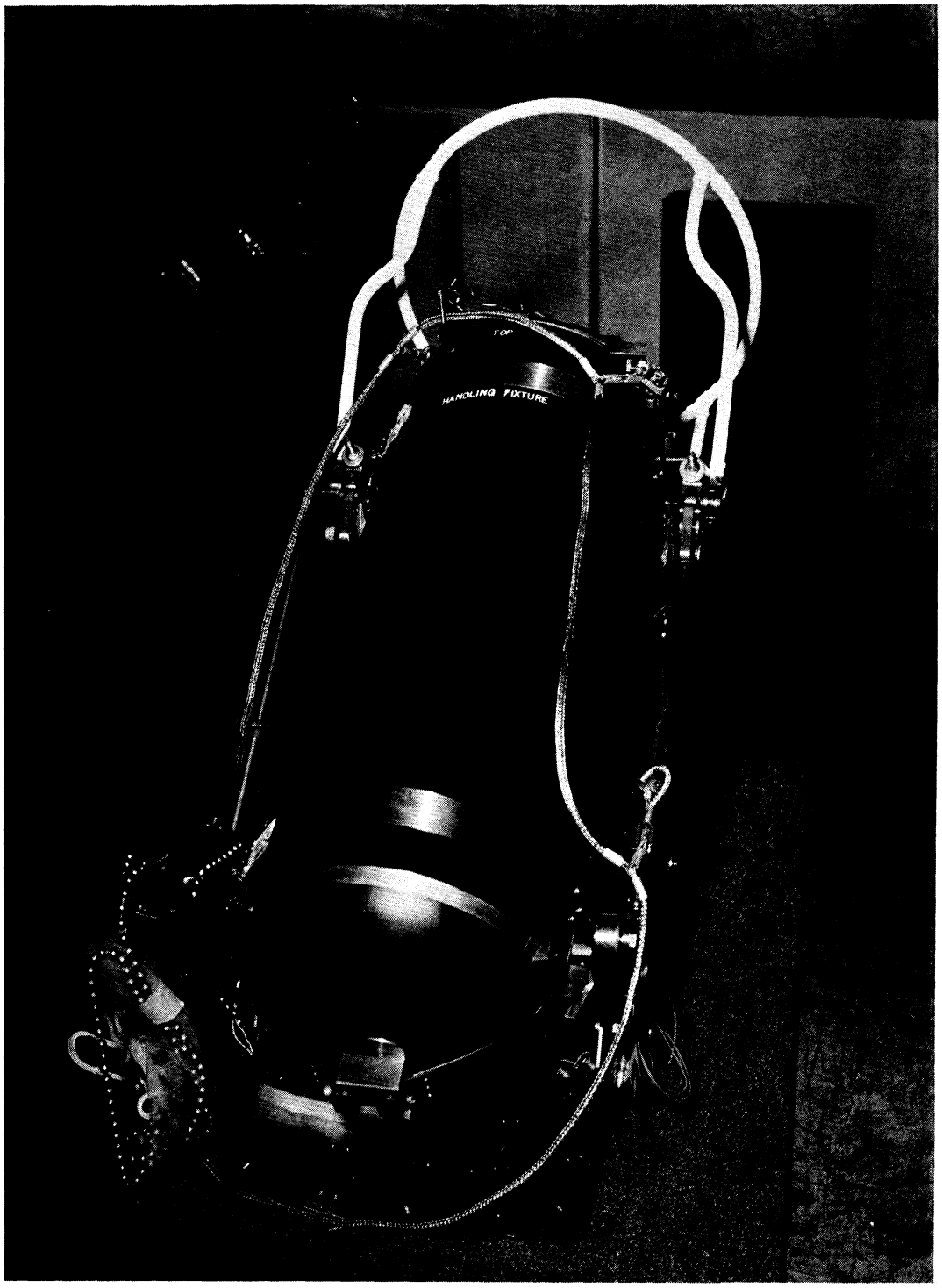

Photo 4. Final cask support assembly.

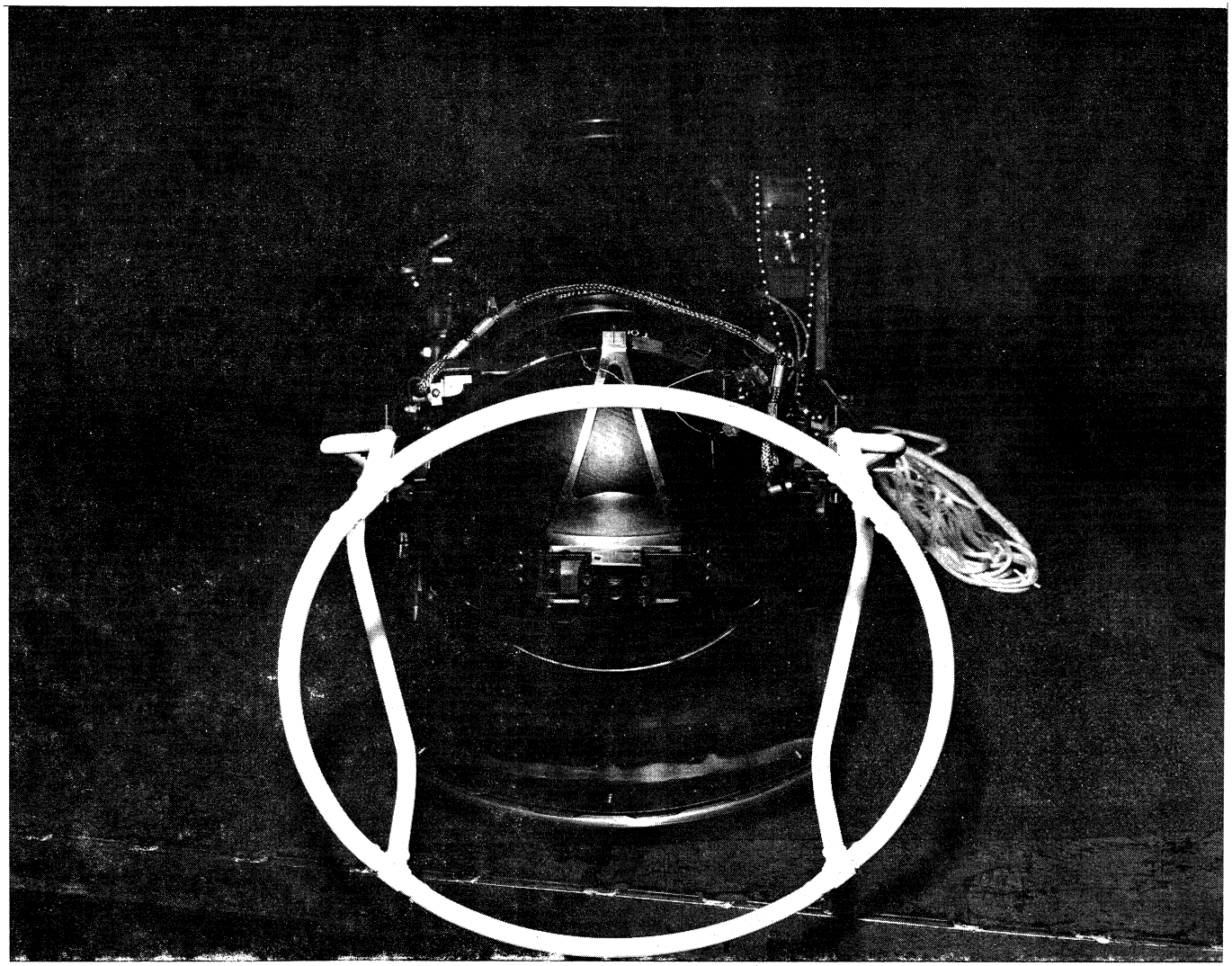

Photo 5. Final cask support assembly.

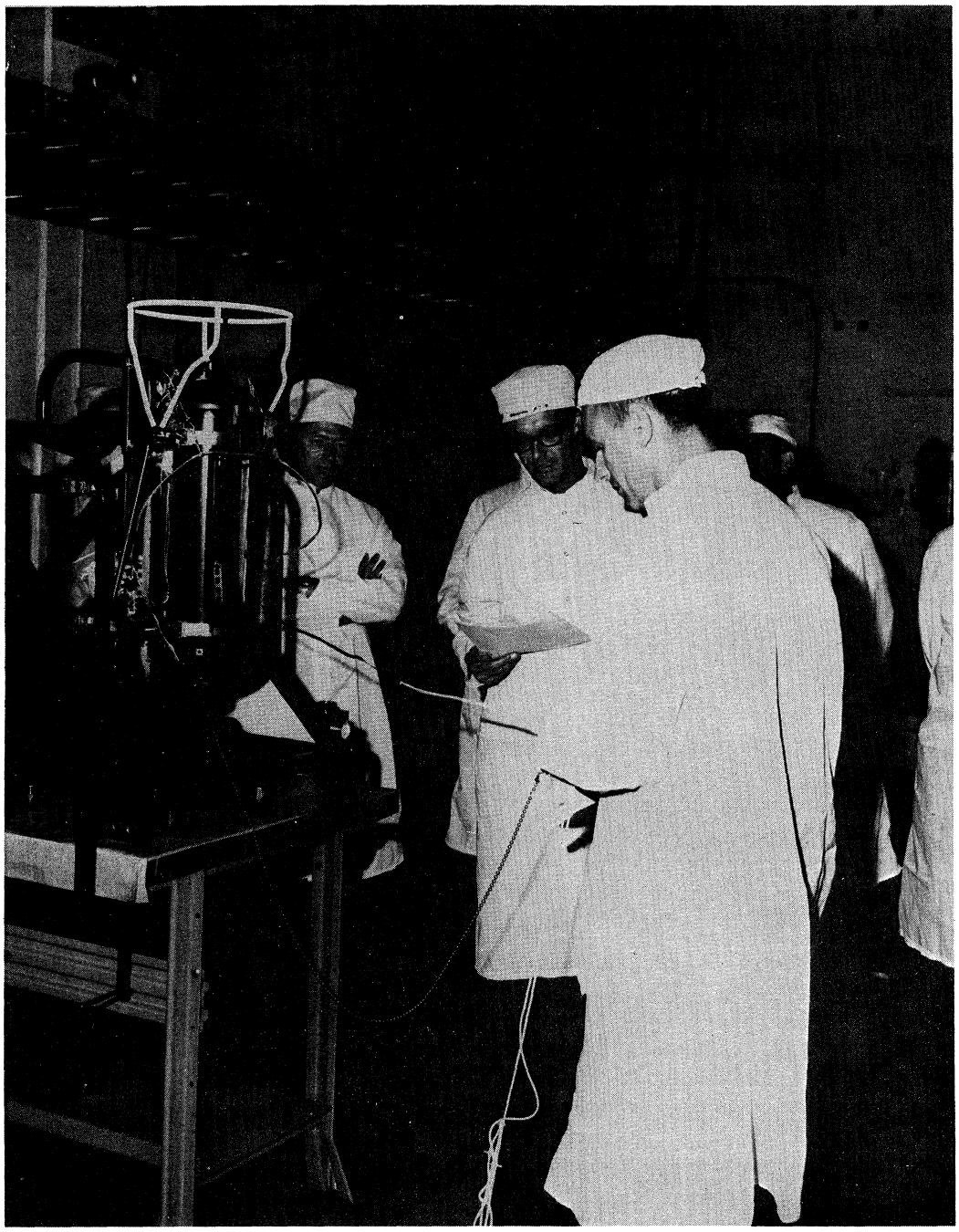

Photo 6. Technicians ready to attach cask to LM.

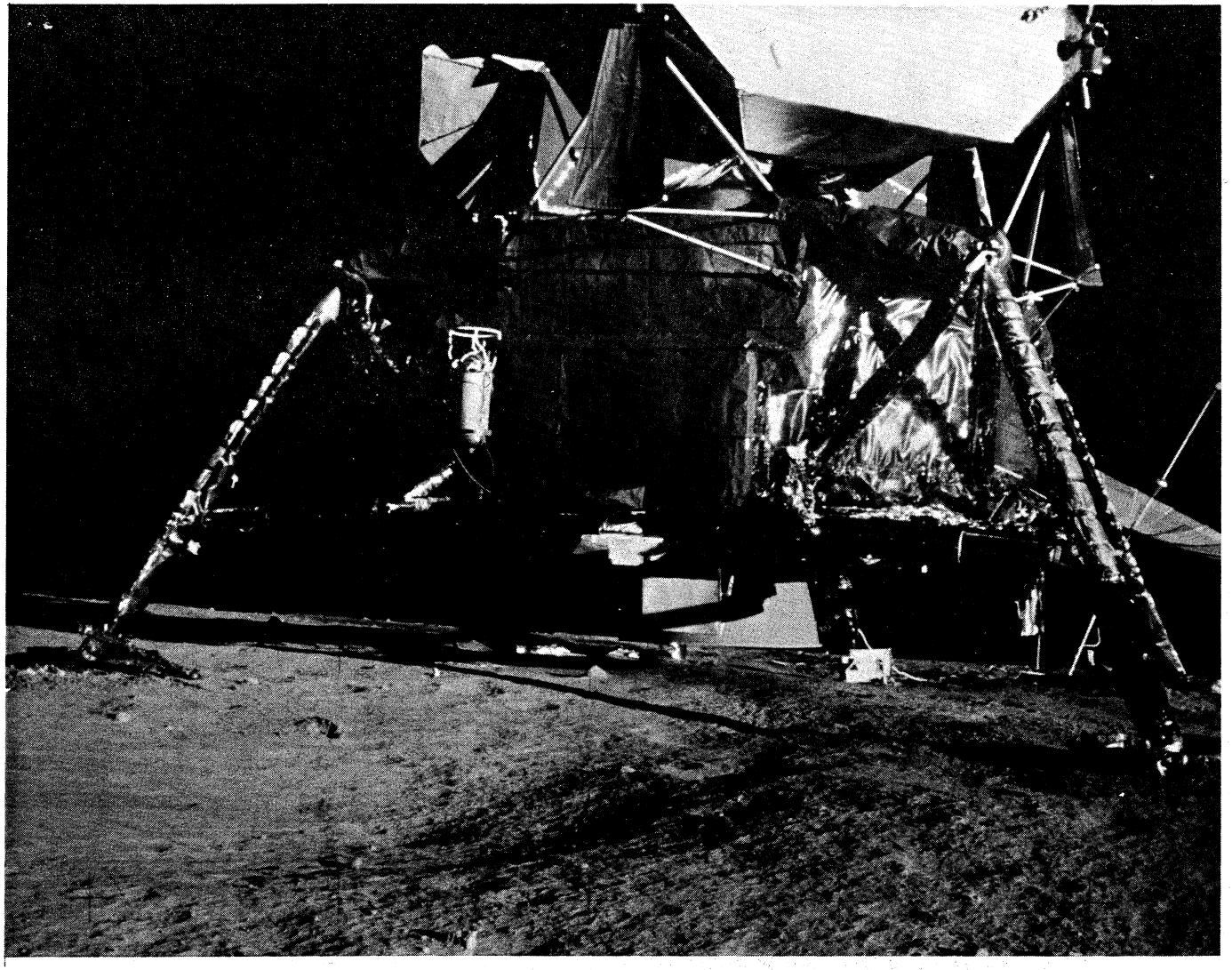

Photo 7. LM on lunar surface.

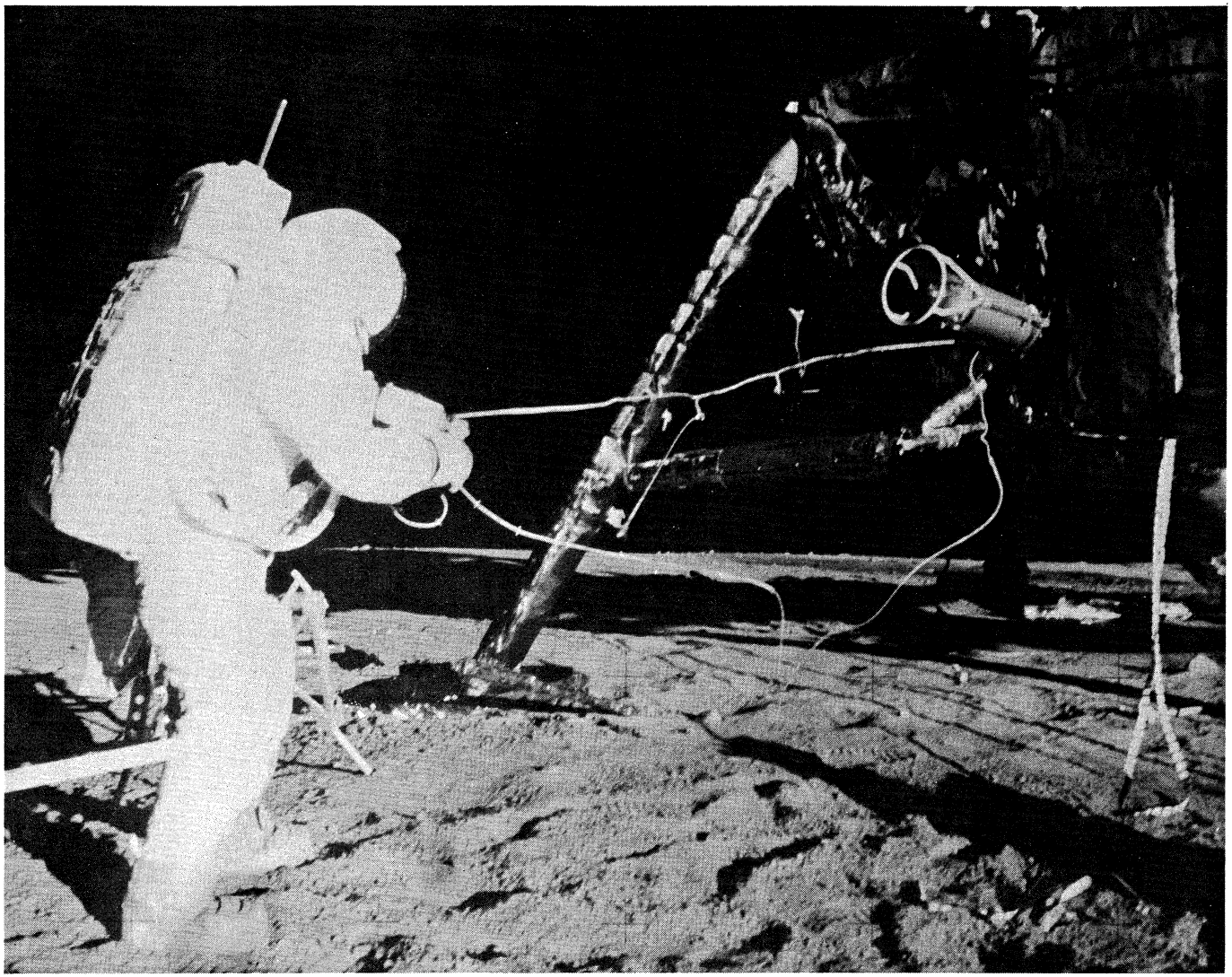

Photo 8. Astronaut lowering cask.

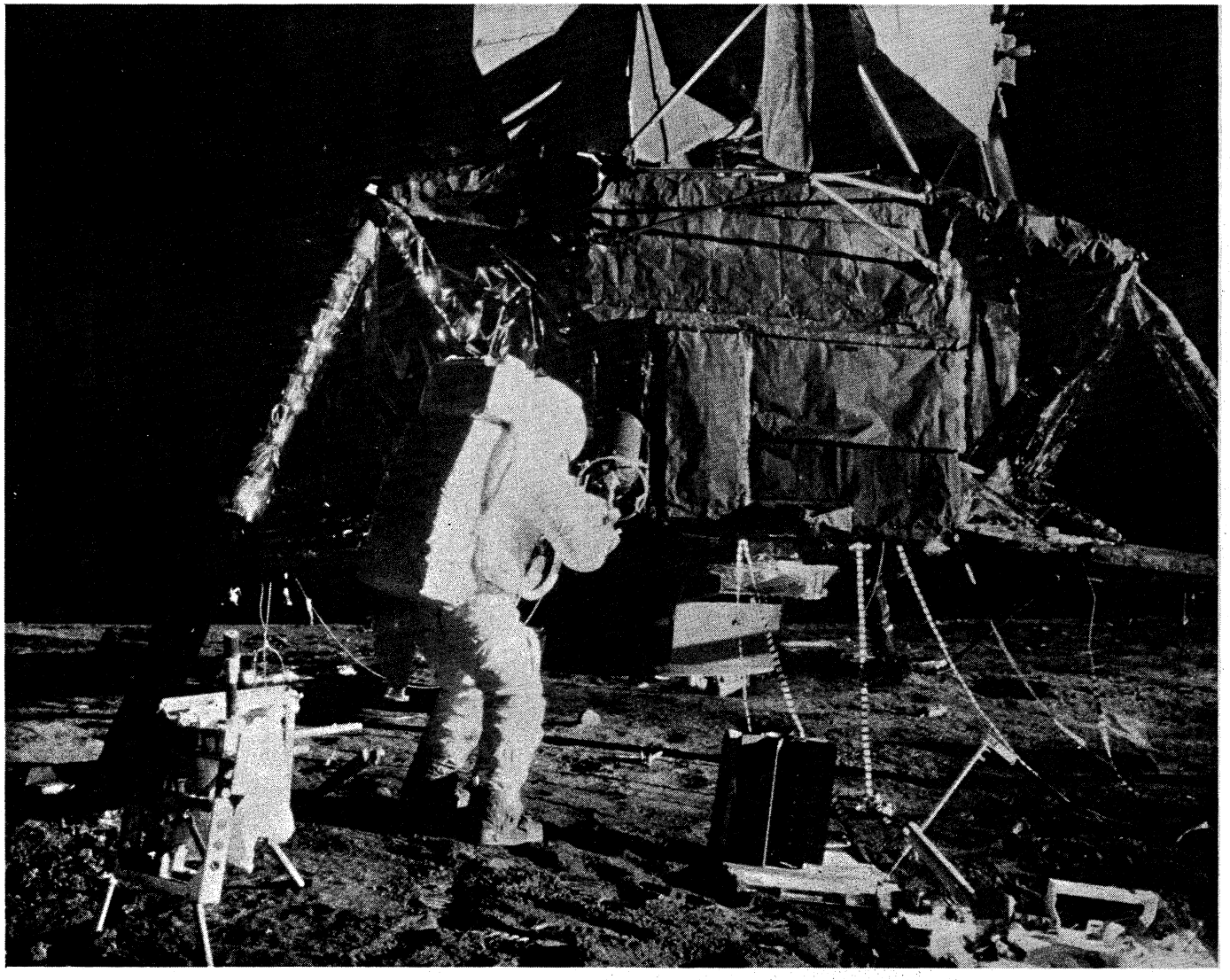

Photo 9. Astronaut removing dome.

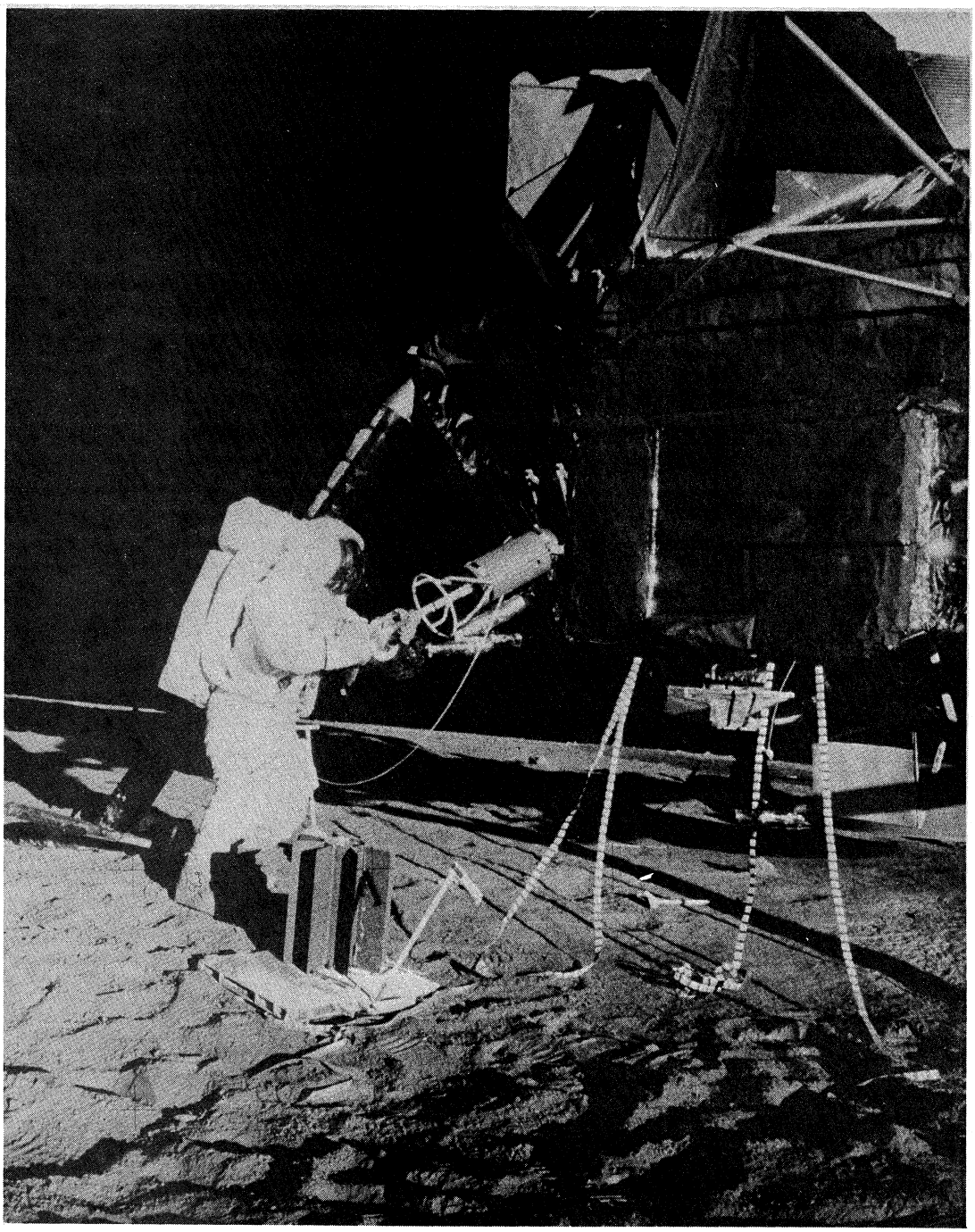

Photo 10. Astronaut removing fuel element.

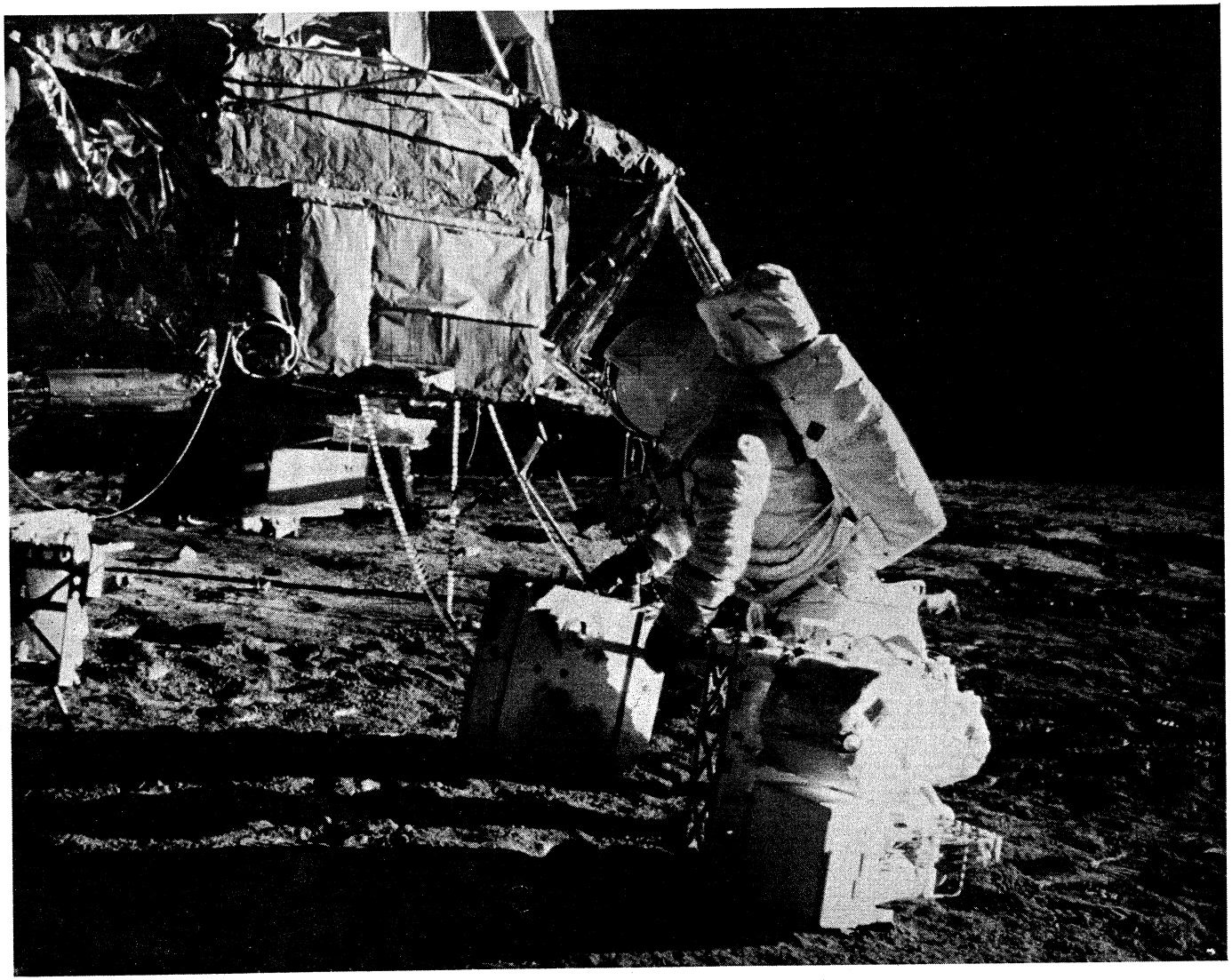

Photo 11. Astronaut assembling ALSEP.

APPENDIX II

DYNAMIC ENVIRONMENT/TEST SPECIFICATIONS

APPENDIX 1 - DYNAMIC ENVIRONMENT/TEST SPECIFICATIONS

1.0 GENERAL

The environments listed below represent design limit (or qualification) levels. Induced (or acceptance) levels can be calculated by dividing limit acceleration values by 1.3 and limit PSD (random vibration) values by $(1.3)^2$.

The shock, acceleration, and vibration environments may occur simultaneously with the following exceptions:

(a) shock loads will not be combined with vibration loads during lunar descent.

(b) acceleration loads will not be combined with vibration loads during launch and boost.

2.0 VIBRATION

2.1 Sinusoidal. -

2.1.1 Launch and Boost Phase. - (For definition of axes see page 15)

Axis	Frequency Range	Level
x	5 - 23 cps	0.5 in. d.a.
	23 - 100 cps	13.0 g - peak
y	5 - 30 cps	0.5 in. d.a.
	30 - 100 cps	23.0 g - peak
z	5 - 18 cps	0.3 in. d.a.
	18 - 100 cps	5.0 g - peak

NOTE:

(1) sweep rate : 3 octaves/min.
(2) tolerance : ± 10% (g - values)
(3) sweep : 5 - 100 - 5 cps (qual.)
5 - 100 cps (accept.)

2.1.2 Lunar Descent Phase. -

Axis	Frequency Range	Level
x, y, z	5 - 28 cps	0.15 in. d.a.
	28 - 100 cps	6.0 g - peak

NOTE:

(1) sweep rate : 1 octave/min.
(2) tolerance : ± 10% g - values
(3) sweep : 5 - 100 - 5 cps (qual.)
5 - 100 cps (accept.)

2.2 Random. -

2.2.1 Launch and Boost Phase. -

Axis	g_{RMS}	Frequency Range	Level
x	16.9	10 - 100 cps	+6 db/octave
		100 - 1000 cps	0.20 g^2/cps
		1000 - 2000 cps	-6 db/octave
y	14.6	10 - 100 cps	+6 db/octave
		100 - 1000 cps	0.15 g^2/cps
		1000 - 2000 cps	-6 db/octave
z	28.8	10 - 100 cps	+9 db/octave
		100 - 1500 cps	0.40 g^2/cps
		1500 - 2000 cps	-9 db/octave

NOTE:

(1) duration : 2.5 min. per axis
(2) tolerance : ± 3 db (PSD)
± 10% (g_{RMS})

2.2.2 Lunar Descent Phase. -

Axis	g_{RMS}	Frequency Range	Level
x, y	8.8	10 - 20 cps	+12 db/octave
		20 - 100 cps	0.10 g^2/cps
		100 - 120 cps	-12 db/octave
		120 - 1000 cps	0.05 g^2/cps
		1000 - 2000 cps	-6 db/octave
z	12.0	10 - 100 cps	+3 db/octave
		100 - 1000 cps	0.10 g^2/cps
		1000 - 2000 cps	-6 db/octave

NOTE:

(1) duration : 12.5 min.
(2) tolerance : ± 3 db (PSD)
± 10% (g_{RMS})

3.0 SHOCK

Level: 20 g@ 11 msec sawtooth as per MIL. STD. 810 B (see Figure 2)

Direction: +x, +y, -y, +z, -z

Duration: 3 shocks per direction (for a total of 15)

4.0 ACCELERATION

Level: 14 g ± 10%

Direction: +x, +y, -y, +z, -z

Duration: 1 min. per direction

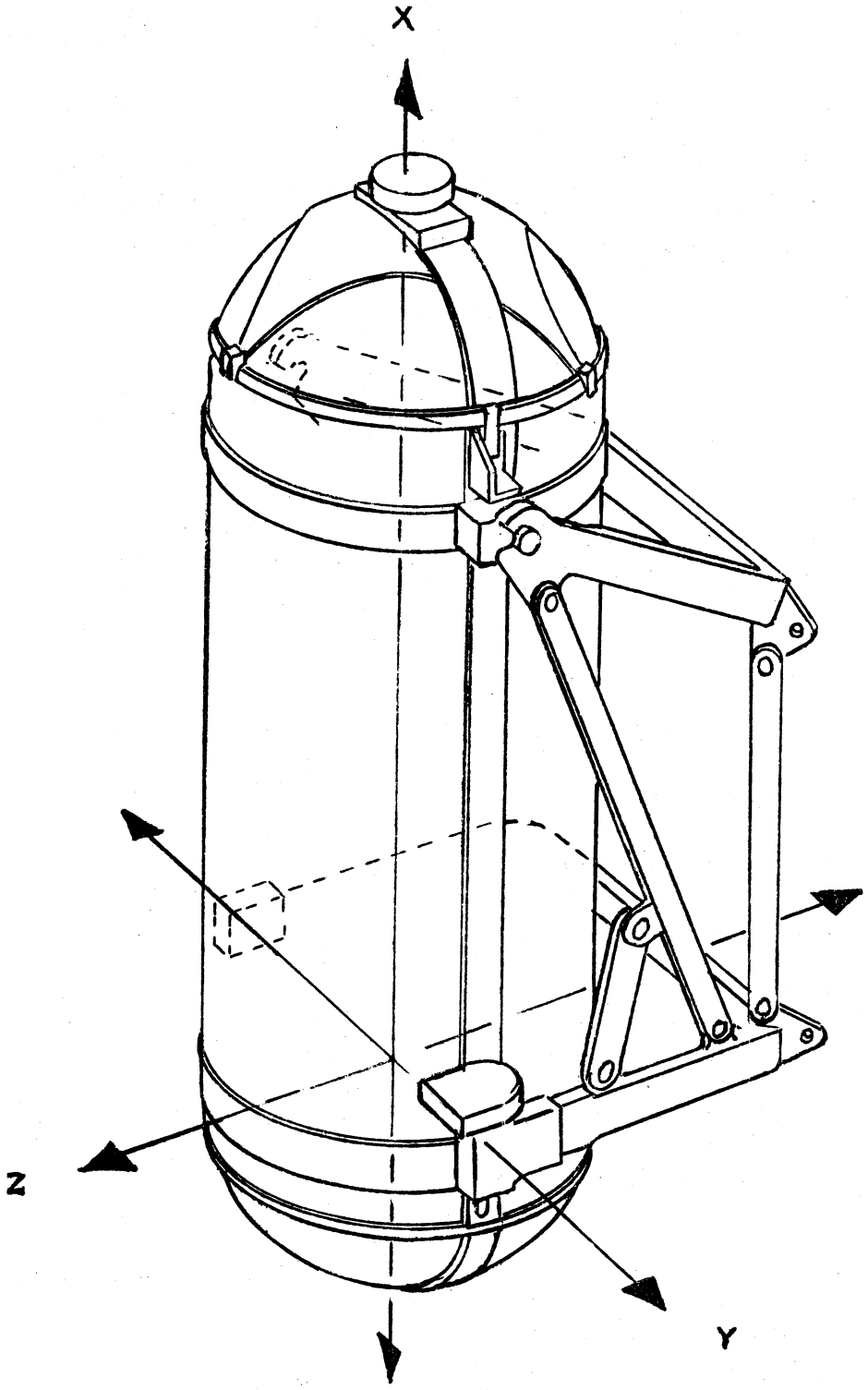
X
Z
Y

UNIVERSITY OF MICHIGAN
3 9015 02224 7400